FINITE ELEMENT NONLINEAR STABILITY ANALYSIS OF FRAMED STRUCTURES

by

R.L. McAdie

A thesis submitted in partial fulfillment of the requirements for the Degree of Master of Science (Engineering)

Department of Civil Engineering
University of Cape Town

August 1985

DECLARATION OF CANDIDATE

I hereby declare that this thesis is my own work and that it has not been submitted for a degree at any other University.

Signed by candidate

R L McAdie

August 1985

DEDICATION

I would like to dedicate this thesis to my Father, Mother and Sister who consistently supported and encouraged me throughout this work.

ACKNOWLEDGEMENTS

I would like to extend my appreciation to the following:-

Prof J B Martin, under whose supervision this thesis was conducted.

Dr Luis Resende for his enthusiastic help and guidance.

Gino Duffett for his helpful suggestions.

Cheryl Wright for her patience and immaculate typing of this thesis.

The Council of Scientific and Industrial Research for their financial assistance.

ABSTRACT

The development of efficient and accurate finite element modelling techniques for the routine analysis of elastic-plastic stability problems in frame structures is addressed. The necessary models, solution procedure and geometric algorithm used for nonlinear stability analysis of frames are presented.

An available finite element code, NOSTRUM, which had the basic algorithms necessary to carry out nonlinear analysis was used as the starting point. The Timoshenko beam/frame elements with a layered representation of the cross-section, uniaxial elastic-plastic constitutive models, different integration procedures and simplified large deformation geometric assumptions incorporated into NOSTRUM are discussed in detail.

Numerical examples are given to validate the algorithms implemented and to provide the experience necessary to give guidelines for the adequate choice of discretization and numerical schemes to be used in routine nonlinear stability analysis of frame structures.

CONTENTS

NOMENCLATURE

This is a list of symbols used in the main text of this thesis.

Special Symbols

'	the differential with respect to
~	a vector or matrix
[ ]	a matrix
| |	the absolute value of
|| ||	the norm of
T (superscript)	the transpose of a vector or matrix
-1 (superscript)	the inverse of a matrix
d	the differentiation with respect to
∂	the partial differentiation with respect to

Lower Case Characters

b	breadth
d	depth
d_n	depth of a layer
g	gravity acceleration constant
ℓ	length
m	distributed moment
n	number of sampling points
p	body force
q	distributed loading
s	surface traction
t	thickness
u	axial displacement
$\underset{\sim}{u}$	displacement vector
w	transverse displacement
x,y	local co-ordinates
w_i	weight of sampling point
z	depth co-ordinate of a section

Upper Case Characters

A	area of cross-section
$\hat{A}$	effective shear area
$\underset{\sim}{B}$	strain-displacement matrix
C	concentrated couple
D	material constant
$\underset{\sim}{D}$	constitutive matrix
E	Young's modulus
E_T	Tangential modulus
$\underset{\sim}{F}$	total load vector
G	shear modulus
H_α	internal parameter
I	second moment of area of the cross-section about the axis of bending
$J(\xi)$	Jacobian operator
K	curvature
$\underset{\sim}{K}$	stiffness matrix
M	bending moment
M_p	plastic (ultimate) bending moment
N	axial force
$\underset{\sim}{N}$	vector of Lagrangian Shape functions
P	concentrated load
P_o	elastic buckling load
P_p	plastic collapse load
Q	shear force
$\underset{\sim}{R}$	internal load vector
$\underset{\sim}{T}$	co-ordinate transformation matrix
$\underset{\sim}{V}$	volume of element
W_p	plastic work
X,Y	Global co-ordinates

Greek Characters

α	shear correction factor
γ_{xy}	shear strain
δ	transverse displacement
$\underset{\sim}{\delta}$	displacement vector
Δ	increment in
$\underset{\sim}{\varepsilon}$	strain vector
ε_x	axial strain

Greek Characters (continued)

θ	rotation or angle
λ	plastic multiplier
ν	Poisson's ratio
ξ	natural co-ordinate
Π	total potential energy
ρ	mass density
$\underset{\sim}{\sigma}$	stress vector
$\bar{\sigma}$	defined in eq. (3.25)
σ_p	current elastic-plastic stress
σ_x	axial stress
σ_y	yield stress
σ_z	transverse stress
ϕ	yield function
$\underset{\sim}{\psi}$	residual load vector

Subscripts

a	axial contribution
e	e-th element
ep	elastic-plastic
f	flexural contribution
i	i-th node or i-th sampling point
ℓ	layer
s	shear contribution
t	time (step)

Superscripts

e	element
e,p	elastic and plastic components (Chpt. 3)
i	i-th iteration
ep	elastic-plastic
*	pertaining to virtual system

CHAPTER 1

INTRODUCTION

The nonlinear stability analysis of frame structures is a well known problem. Steel designers, contractors and organisations promoting the use of structural steel have, for some time, expressed an interest in the development of efficient and accurate analysis methods for such stability calculations. In the South African context, it has been suggested that these analysis tools should become available on small desktop or micro computers. The main thrust of the present work is the first step in this process: it is intended to establish efficient and accurate modelling techniques (based on the finite element method) that can be later made available on small computers in the design environment for routine analysis purposes.

A large body of work on analysis procedures for the nonlinear stability of frames exists in the literature. It includes the use of design oriented interaction formulae, limit analysis techniques based on rigid-plastic assumptions and the more modern incremental/iterative elastic-plastic stability analyses techniques based on the finite element method.

The interaction formulae constitute an approximate method of predicting the stability failure load for a particular frame based on the plastic failure load and elastic buckling load of the frame or, in some cases, the ultimate load and elastic buckling load of the frame. Some of the widely used interaction formulae are the Merchant-Rankine formula [1, 2], its modification by Wood [3], and the design rule due to Lu [4]. The European Convention for Constructional Steelwork has proposed the inclusion of the modified Merchant-Rankine formula in the new British steel design code B20 [5]. However, more recent work by Scholz [6] indicates that these formulae are severely restricted in their scope of application and that the results obtained with the Merchant-Rankine rule are generally too conservative. Scholz proposes a new multi-curve interaction method which represents an improvement on the Merchant-Rankine formula. This inevitably results in increased complexity of the analysis procedure.

Limit analysis techniques based on a rigid-plastic moment-curvature assumption have also been used to analyse frame structures. Its application has been limited to individual beams and columns or to simple single-storey and two-storey frames. The reason for this lies in the fact that previous knowledge of the failure mechanism is generally necessary. For example, when using the kinematic approach, one has (or the computer has) to go through lengthy permutations of possible combinations of hinge positions in order to find the correct failure mechanism. Nevertheless, computer codes for this kind of analysis have been developed, for example Hansa [7].

Finally, finite element based incremental/iterative methods for elastic-plastic stability of frames have recently become very popular. These rely on the use of an elastic-plastic constitutive assumption for the material behaviour while the finite element spatial discretization framework provides a natural means of modelling the relatively large changes of geometry of the structure that occur prior to stability failure. In the finite element context, it is possible to record and take into account the changes in geometry of the structure in two ways [8]: one can use the original configuration as a reference configuration for the current stress and deformation fields - Total Lagrangian formulation (TL); or one can employ the current configuration of the structure at any given time of the loading process as the reference configuration - Updated Lagrangian formulation (UL). Cichoń [9] and Chebl et al [10] have used the TL approach whereas Saran [11] and Kang and Scordelis [12] opted for the UL approach. Although the choice of which approach is adopted depends, to an extent, on the finite element being used and the material constitutive law, the UL option is generally the most popular and a form of it is used in the present work.

This thesis is concerned with the development of efficient and accurate models for the routine analysis of elastic-plastic stability problems in framed structures. It is intended to provide guidelines for the adequate choice of discretization and numerical schemes to be used in the analysis of such problems. To achieve this, a finite element code developed by the Applied Mechanics Research Unit at the University of Cape Town, called NOSTRUM [13], was used as the starting point. NOSTRUM already had the basic algorithms necessary to carry out nonlinear analysis but some of the necessary models for the problem at hand had to be added. These

include the Timoshenko beam/frame elements with a layered representation of the cross-section necessary to model the progressive plastification of the member sections and the uniaxial elastic-plastic constitutive models to be used in conjunction with the layered Timoshenko elements. A number of elements, integration procedures and constitutive models were implemented in NOSTRUM; these are discussed in detail in later chapters. A simple form of the UL formulation was also implemented in order to take into account the changes in geometry of the structure.

The organisation of this thesis is as follows: Chapter Two gives the finite element formulation of the layered Timoshenko beam/frame elements and develops the basic equilibrium equations; Chapter Three deals with the elastic-plastic constitutive models for the layered elements; Chapter Four discusses the numerical algorithms implemented in NOSTRUM; and finally numerical examples are given in Chapter Five, not only to validate the algorithms implemented, but also to provide the experience necessary to give guidelines for routine analysis of nonlinear frame stability.

CHAPTER 2

BEAM/FRAME FINITE ELEMENT FORMULATION

2.1 Introduction

This chapter deals with the elastic formulation of the layered Timoshenko element. This element model is used because of the possibility of modelling shear effects and progressive plastification of the section with the use of layers. A realistic representation of the behaviour of the structure can thus be obtained. One disadvantage with using this element is that overstiff results can occur when modelling thin sections. This phenomenon, termed "locking", will be discussed later in the chapter.

The Timoshenko beam theory in terms of the small strain, small displacement concept is first presented. The basic linear equilibrium equations are developed in the context of the Lagrangian Isoparametric finite element formulation. The next section discusses the layered approximation and its associated assumptions. Finally, the numerical integration techniques to be employed are presented and discussed.

2.2 Timoshenko Beam Assumptions and Characteristics

2.2.1 Displacement Field

The main assumption in Timoshenko beam theory is that the plane sections remain plane but not necessarily normal to the neutral axis after deformation. This is depicted in Figure 2.1.

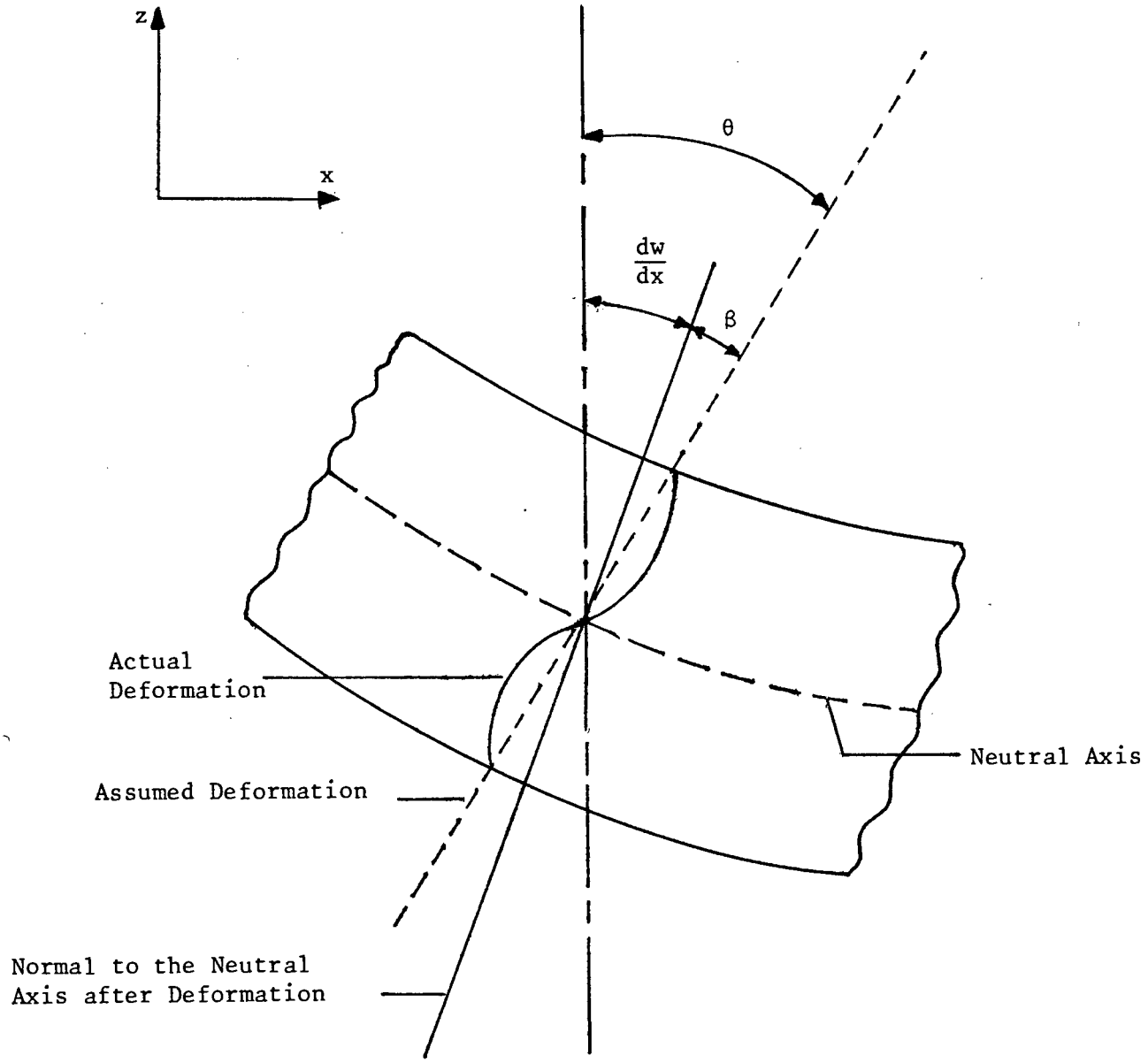

Figure 2.1 Assumed Deformation for Timoshenko Theory.

Hence we obtain

$$\theta(x) = \frac{dw}{dx} + \beta \,, \tag{2.1}$$

where: β - rotation due to transverse shear deformation,

$\frac{dw}{dx}$ - slope of the neutral axis,

θ - rotation of the normal.

The displacements in the x and z directions are respectively

$$\begin{aligned} \bar{u}\,(x, z) &= u\,(x) + z\theta\,(x), \\ \bar{w}\,(x, z) &= w\,(x), \end{aligned} \tag{2.2}$$

where $\bar{u}$ and $\bar{w}$ imply displacements at any point (x, z).

2.2.2 Strain-Displacement Relationships

For small displacement and small strain theory the axial strain is defined as

$$\begin{aligned} \varepsilon_x &= \frac{d\bar{u}}{dx} \\ &= \frac{du}{dx} + z\frac{d\theta}{dx} \,, \end{aligned} \tag{2.3}$$

and similarly, the shear strain is defined as

$$\begin{aligned} \gamma_{xz} &= \frac{\partial \bar{u}}{\partial z} + \frac{\partial \bar{w}}{\partial x} \\ &= \theta(x) - \frac{dw}{dx} \\ &= \beta \,. \end{aligned} \tag{2.4}$$

2.2.3 Elastic Stress-Strain Relationship

The beam is assumed to be in a state of plane stress. Thus for an isotropic material we get

$$\begin{bmatrix} \sigma_x \\ \sigma_z \\ \tau_{xz} \end{bmatrix} = \frac{E}{(1-\nu^2)} \begin{bmatrix} 1 & \nu & 0 \\ \nu & 1 & 0 \\ 0 & 0 & \frac{(1-\nu)}{2} \end{bmatrix} \begin{bmatrix} \varepsilon_x \\ \varepsilon_z \\ \gamma_{xz} \end{bmatrix} . \qquad (2.5)$$

It is assumed that there is no transverse stress. Therefore, $\sigma_z = 0$ and the transverse strain can be expressed as

$$\varepsilon_z = -\nu\varepsilon_x$$

Hence the stress-strain relationship becomes

$$\sigma_x = E\varepsilon_x \ , \qquad (2.6)$$

$$\tau_{xz} = G\gamma_{xz} \ ,$$

where $G = E/[2(1+\nu)]$ is the shear modulus of an isotropic material.

2.3 Basic Linear Equations

The governing equilibrium equations of the structural system are obtained by minimising the total potential energy.

Consider a beam of length ℓ, breadth b and depth d subject to body forces p per unit volume, applied surface tranctions s, concentrated axial loads P(x), concentrated transverse loads P(y) and concentrated couples C.

The total potential energy, Π, can be expressed as

$$\Pi = \tfrac{1}{2} \int_0^{\ell} \int_{-d/2}^{d/2} \int_{b(-d/2)}^{b(d/2)} \underset{\sim}{\sigma}^T \underset{\sim}{\varepsilon} \, dy \, dz \, dx \qquad (2.7)$$

$$- \int_0^{\ell} \int_{-d/2}^{d/2} \int_{b(-d/2)}^{b(d/2)} \underset{\sim}{\delta}^T p \, dy \, dz \, dx - \int_0^{\ell} \int_{b(-d/2)}^{b(d/2)} \underset{\sim}{\delta}^T s \, dy \, dx$$

$$- P(y)w - P(x)u - C\theta ,$$

where $\underset{\sim}{\sigma}$, $\underset{\sim}{\varepsilon}$ and $\underset{\sim}{\delta}$ are the total stress, strain and displacement vectors respectively.

We write $\underset{\sim}{\sigma}^T \underset{\sim}{\varepsilon} = (\sigma_x \varepsilon_x + \tau_{xz} \gamma_{xz})$ (2.8)

and from equation (2.6) we get

$$\Pi = \tfrac{1}{2} \int_v \varepsilon_x E \varepsilon_x \, dv + \tfrac{1}{2} \int_v \gamma_{xz} G \gamma_{xz} \, dv -$$

$$- \int_v \underset{\sim}{\delta}^T p \, dv - \int_s \underset{\sim}{\delta}^T s \, ds - P(y)w - P(x)u - C\theta$$

using equations (2.3) and (2.4) and integrating out the y and z terms, the total potential energy expression becomes

$$\Pi = \underbrace{\frac{EA}{2} \int_0^{\ell} \left(\frac{du}{dx}\right)^2 dx}_{\text{AXIAL}} + \underbrace{\frac{EI}{2} \int_0^{\ell} \left(\frac{d\theta}{dx}\right)^2 dx}_{\text{BENDING}} + \underbrace{\frac{GA}{2\alpha} \int_0^{\ell} \beta^2 \, dx}_{\text{SHEAR}}$$

$$\underbrace{- \int_0^{\ell} \delta^T pA \, dx}_{\text{BODY FORCE}} \underbrace{- \int_0^{\ell} \delta^T q \, dx}_{\text{DISTRIBUTED LOAD}} \qquad (2.9)$$

$$- P(y)w - P(x)u - C\theta .$$

POINT SOURCES

The term α is a shear correction factor, where $\alpha = 1.5$, Owen and Hinton [14].

From this expression it is observed that all the strain terms are of order 1 and hence only C(0) continuity is required. The strain terms are:

$$\text{axial strain,} \quad \varepsilon_a = \frac{du}{dx} \; ;$$

$$\text{bending strain,} \quad \varepsilon_f = \frac{d\theta}{dx} \; ; \qquad (2.10)$$

$$\text{shear strain,} \quad \varepsilon_s = \beta \; .$$

As only C(0) continuity is required, the Lagrangian finite element approximation is used. The structural system is discretized into a finite element mesh where the primary unknowns are the displacements u_i, w_i, θ_i, at the nodal points in the mesh. The displacement at any position in the structure is described in terms of these nodal displacements by Lagrangian Shape functions N_i. The displacement vector is written as

$$\underset{\sim}{\delta} = \underset{\sim}{N}\, \underset{\sim}{\delta}_i \; ,$$

where $\underset{\sim}{N}$ is the vector of Lagrangian Shape functions and $\underset{\sim}{\delta}_i$ is the vector of nodal displacements.

2.3.1 Isoparametric Element Definition

Three isoparametric Lagrangian elements are used; the two noded linear element, the three noded quadratic element and the four noded cubic element.

The natural co-ordinate system is used in the element definition, where ξ varies from -1 to $+1$. The elements

are illustrated in Figure 2.2 as:

, linear element;

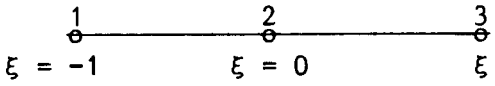

, quadratic element;

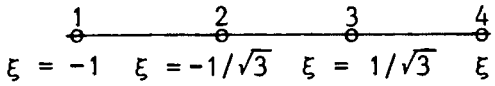

, cubic element.

Figure 2.2 Three one dimensional isoparametric Lagrangian elements.

The displacements at each node are given by

$$\delta_i = [u_i, w_i, \theta_i]^T ,$$

and the element displacement vectors are written as

$$\delta^e = [\delta_1 \ \ldots \ \delta_i]^T ,$$

where

i = 2 for the two noded element,
i = 3 for the three noded element,
i = 4 for the four noded element.

The Lagrangian shape functions associated with each element type are:

for the 2 noded element: $N_1 = \frac{1}{2}(1 - \xi)$

$N_2 = \frac{1}{2}(1 + \xi)$

for the 3 noded element:

$$N_1 = \xi/2\ (\xi - 1)$$
$$N_2 = (1 - \xi^2)$$
$$N_3 = \xi/2\ (\xi + 1) \qquad (2.12)$$

for the 4 noded element:

$$N_1 = -9/16\ (1/9 - \xi^2)(1 - \xi)$$
$$N_2 = 27/16\ (1 - \xi^2)\ (1/3 - \xi)$$
$$N_3 = 27/16\ (1 - \xi^2)\ (1/3 + \xi)$$
$$N_4 = -9/16\ (1/9 - \xi^2)(1 + \xi)$$

The element displacement field is then expressed as

$$\delta^e(\xi) = \sum_{i=1}^{N} N_i\ (\xi)\ \delta_i \ , \qquad (2.13)$$

where N = Total number of nodes in the element.

Similarly, the element geometry can be expressed in terms of the Lagrangian shape functions and the local element cartesian co-ordinate system,

$$x(\xi) = \sum_{i=1}^{N} N_i(\xi)\ x_i \ . \qquad (2.14)$$

The natural/element cartesian transformation is achieved by the use of the Jacobian Matrix, which in the one dimensional case is just a scalar operator, given by

$$J\ (\xi) = \frac{dx}{d\xi} = \sum_{i=1}^{N} \frac{dN_i}{d\xi}\ x_i \ . \qquad (2.15)$$

In equations (2.14) and (2.15) x_i defines the local cartesian co-ordinate.

The element strains can now be written in terms of the element nodal displacements as

$$\underset{\sim}{\varepsilon} = \underset{\sim}{B}\ \underset{\sim}{\delta}^e \ , \qquad (2.16)$$

where $\underset{\sim}{B}$ is generally called the strain matrix.

Both $\underset{\sim}{B}$ and $\underset{\sim}{\varepsilon}$ comprise the axial, flexural and shear terms and can be written as

$$\underset{\sim}{B} = [\underset{\sim}{B}_a, \underset{\sim}{B}_f, \underset{\sim}{B}_s]^T \quad ,$$

$$\underset{\sim}{\varepsilon} = [\varepsilon_a, \varepsilon_f, \varepsilon_s]^T \quad .$$

The strain-displacement formulation in terms of the Lagrangian shape functions is

$$\begin{bmatrix} \varepsilon_a \\ \varepsilon_f \\ \varepsilon_s \end{bmatrix} = \sum_{i=1}^{N} \begin{bmatrix} \frac{dN_i}{dx} & 0 & 0 \\ 0 & -\frac{dN_i}{dx} & 0 \\ 0 & \frac{dN_i}{dx} & -N_i \end{bmatrix} \begin{bmatrix} u_i \\ w_i \\ \theta_i \end{bmatrix} \quad ,$$

where N is the total number of nodes in the element and

$$\frac{dN_i}{dx} = \frac{dN_i}{d\xi} \cdot \frac{d\xi}{dx} = \frac{dN_i}{d\xi} \cdot J(\xi)^{-1} \quad .$$

Recalling the total potential energy equation for the system (eq. 2.9) we can now express the total potential energy of the structural system as the sum of the energy contributions of the individual elements. Thus,

$$\Pi = \sum_{e} \Pi_e \qquad (2.17)$$

where Π_e is the total potential of element e.

Equation (2.9), expressed in terms of an element, is

$$\Pi_e = \tfrac{1}{2} \int_o^{\ell} [\underset{\sim}{\delta}^e]^T [\underset{\sim}{B}_a]^T EA \, \underset{\sim}{B}_a \, \underset{\sim}{\delta}^e \, dx +$$

$$\tfrac{1}{2} \int_o^{\ell} [\underset{\sim}{\delta}^e]^T [\underset{\sim}{B}_f]^T EI \, \underset{\sim}{B}_f \, \underset{\sim}{\delta}^e \, dx +$$

$$\tfrac{1}{2} \int_o^{\ell} [\underset{\sim}{\delta}^e]^T [\underset{\sim}{B}_s]^T \frac{GA}{\alpha} \underset{\sim}{B}_s \, \underset{\sim}{\delta}^e \, dx - \qquad (2.18)$$

$$\int_o^{\ell} [\underset{\sim}{\delta}^e]^T [\underset{\sim}{N}]^T pA \, dx -$$

$$\int_o^{\ell} [\underset{\sim}{\delta}^e]^T [\underset{\sim}{N}]^T q \, dx -$$

$$P(y)w - P(x)u - C\theta ,$$

where $dx = \det J(\xi) d\xi = J(\xi) d\xi$.

The elastic material constitutive properties EA, EI, $\frac{GA}{\alpha}$ are expressed in terms of elasticity matrices $\underset{\sim}{D}_a$, $\underset{\sim}{D}_f$, $\underset{\sim}{D}_s$, respectively.

By minimising the element potential energy with respect to nodal displacements

$$\frac{\partial \Pi_e}{\partial \delta^e} = 0 ,$$

we get the characteristic linear equilibrium equation

$$\underset{\sim}{K}^e \, \underset{\sim}{\delta}^e = \underset{\sim}{F}^e \, , \tag{2.19}$$

where

$$\underset{\sim}{K}^e = \underset{\sim}{K}^e_a + \underset{\sim}{K}^e_f + \underset{\sim}{K}^e_s \quad \text{such that,}$$

$$\underset{\sim}{K}^e_a = \int_o^{\ell} \underset{\sim a}{B}^T \underset{\sim a}{D} \underset{\sim a}{B} \, dx \, ,$$

$$\underset{\sim}{K}^e_f = \int_o^{\ell} \underset{\sim f}{B}^T \underset{\sim f}{D} \underset{\sim f}{B} \, dx \, ,$$

$$\underset{\sim}{K}^e_s = \int_o^{\ell} \underset{\sim s}{B}^T \underset{\sim s}{D} \underset{\sim s}{B} \, dx \, ,$$

$$\underset{\sim}{F}^e = \int_o^{\ell} [\underset{\sim}{N}]^T pA \, dx + \int_o^{\ell} [\underset{\sim}{N}]^T q \, dx +$$

$$P(y)w + P(x)u + C\theta \, .$$

These matrices are all in the local element co-ordinate system. In order to assemble a global stiffness matrix for the whole structure, these element matrices have to be transformed to global co-ordinate system. The local and global co-ordinates systems are illustrated in Figure 2.3.

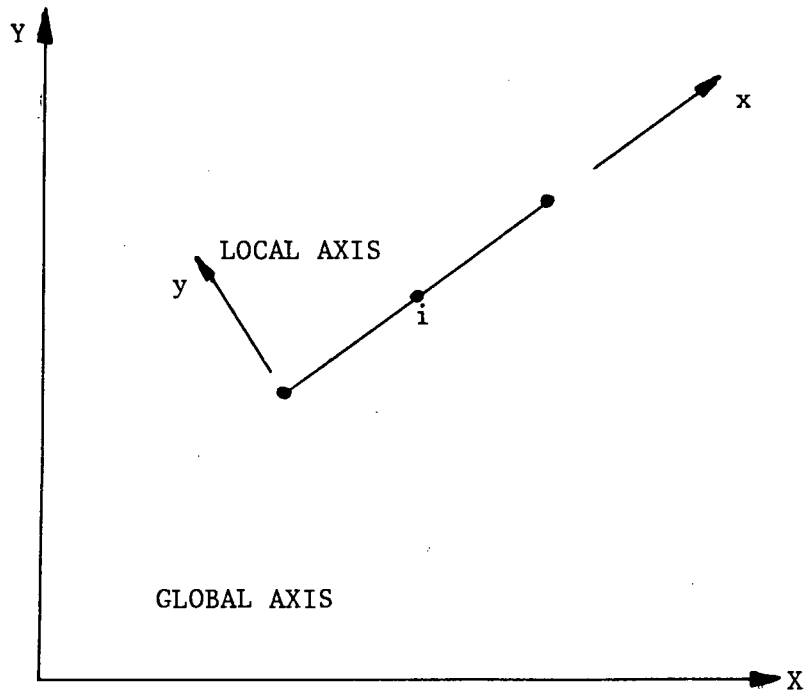

where node i of local co-ordinates $(x_i, 0)$ has global co-ordinates (X_i, Y_i)

Figure 2.3 Local and Global Co-ordinate Systems.

The transformation matrix used for an element is $\underset{\sim}{T}^e$ where

$$\underset{\sim}{T}^e = \begin{bmatrix} \underset{\sim}{T}^e_{11} & & & 0 \\ & \ddots & & \\ & & \underset{\sim}{T}^e_{ii} & \\ & & & \ddots \\ 0 & & & \underset{\sim}{T}^e_{NN} \end{bmatrix},$$

where: N = 2 for two noded element,
N = 3 for three noded element,
N = 4 for four noded element

and its submatrix $\underset{\sim}{T}^e_{ii}$ is expressed as

$$\underset{\sim}{T}^e_{ii} = \begin{bmatrix} \cos\theta & -\sin\theta & 0 \\ \sin\theta & \cos\theta & 0 \\ 0 & 0 & 1 \end{bmatrix}$$

where θ is the angle between the element local x axis and the global X axis.

Hence the element stiffness matrix expressed in the global co-ordinate system is

$$\underset{\sim}{K}^{s} = [\underset{\sim}{T}^{e}]^{T} \underset{\sim}{K}^{e} \underset{\sim}{T}^{e} \quad . \tag{2.20}$$

To assemble a global force vector, $\underset{\sim}{F}$, the terms in the element load vectors, $\underset{\sim}{F}^{e}$, have to be transformed to the global system. The sign convention for the nodal loads is given in Figure 2.4(a).

The calculation of distributed loading equivalent nodal loads for an element, in terms of the global system is given as

$$\begin{bmatrix} P_{xi} \\ P_{yi} \\ m_i \end{bmatrix} = \int_{-1}^{+1} \begin{bmatrix} -\cos\theta & \sin\theta & 0 \\ -\sin\theta & -\cos\theta & 0 \\ 0 & 0 & 1 \end{bmatrix} \begin{bmatrix} q_{xi} \\ q_{yi} \\ m_i \end{bmatrix} N_i(\xi) J(\xi) d\xi \ , \tag{2.21}$$

where q_{xi} , q_{yi} and m_i are the values of the intensity of the tangential, normal and moment distributed load components at each node in an element. The sign conventions for the components are given in Figure 2.4(b).

The calculation of mass proportional loading (body forces) equivalent nodal loads for an element, in terms of the global system, is given as

$$\begin{bmatrix} P_{xi} \\ P_{yi} \end{bmatrix} = \int_{-1}^{+1} \begin{bmatrix} -\sin\alpha \\ \cos\alpha \end{bmatrix} \rho g A \, N_i(\xi) \, J(\xi) \, d\xi \tag{2.22}$$

where g is an acceleration constant acting at an angle α measured anti-clockwise from the global Y axis and ρ is the mass density of the material.

For gravitational loading $g = 9.81\ m/s^2$ and $\alpha = 180°$.
Note $m_i = 0$ in this case.

The point loads and moments $P(x)_i$, $P(y)_i$ and C_i applied at the nodes are already expressed in the global system.

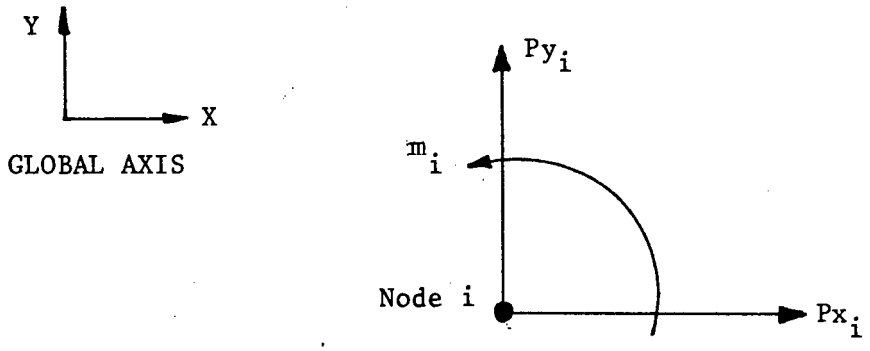

Figure 2.4(a) Positive Sign Convention for Nodal Loads in Global Load Vector.

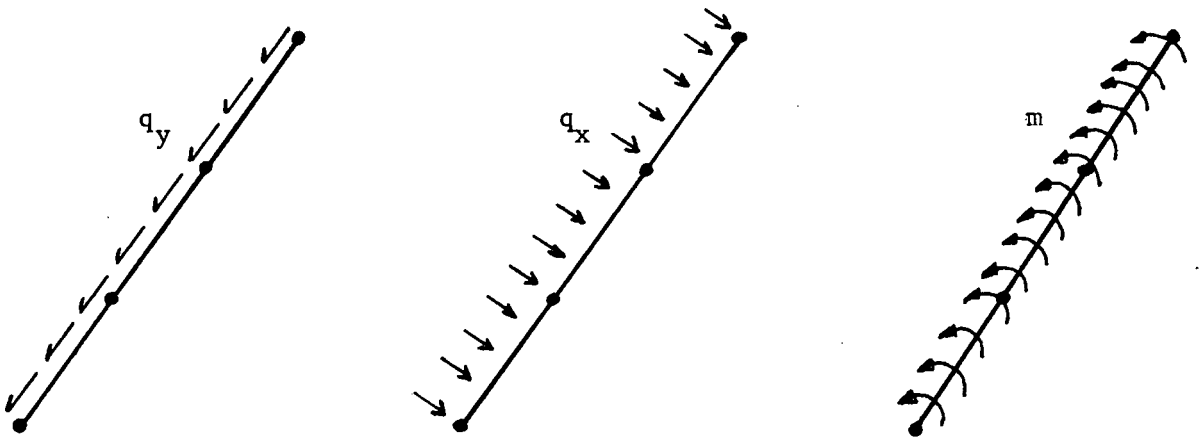

Positive Tangential Component

Positive Normal Component

Positive Moment Component

Figure 2.4(b) Positive Sign Convention for Element Distributed Loading.

Figure 2.4 Positive Sign Convention for Element Loading.

2.4 Layered Model

In the layered model the beam section is discretized into a number of layers. It is assumed that the stress at the centre of the layer is representative of the entire layer.

The actual stress distributed through the depth of the section is, therefore, modelled by a piecewise constant approximation. Consequently a more realistic solution is obtained as the numbers of layers are increased. This is illustrated in Figure 2.5 where the approximation to the linear elastic stress distribution for a rectangular section under pure bending is compared using two layers and six layers.

As depicted, the two layer approximation is far too crude, whereas a more refined solution is obtained using six layers.

The stresses in each layer are given by uniaxial stress $\sigma_{x\ell}$ and a shear stress $\tau_{xz\ell}$, where $\sigma_{x\ell}$ is comprised of contributions due to axial and bending strain. These stresses in the linear elastic case are expressed as

$$\sigma_{x\ell} = E_\ell \, (\varepsilon_a + \varepsilon_b \, z_\ell) \quad ,$$

$$\tau_{xz\ell} = G_\ell \, \varepsilon_s \quad . \tag{2.23}$$

The material constants EA, EI, $G\hat{A}$ and the stress resultants M, N, Q are calculated from the integration of the contributions from each layer over the depth of the section. The second moment of area of the cross-section about the axis of bending, I, and hence the resultant bending moment, M, are calculated by the mid-point rule integration scheme adopted for each layer.

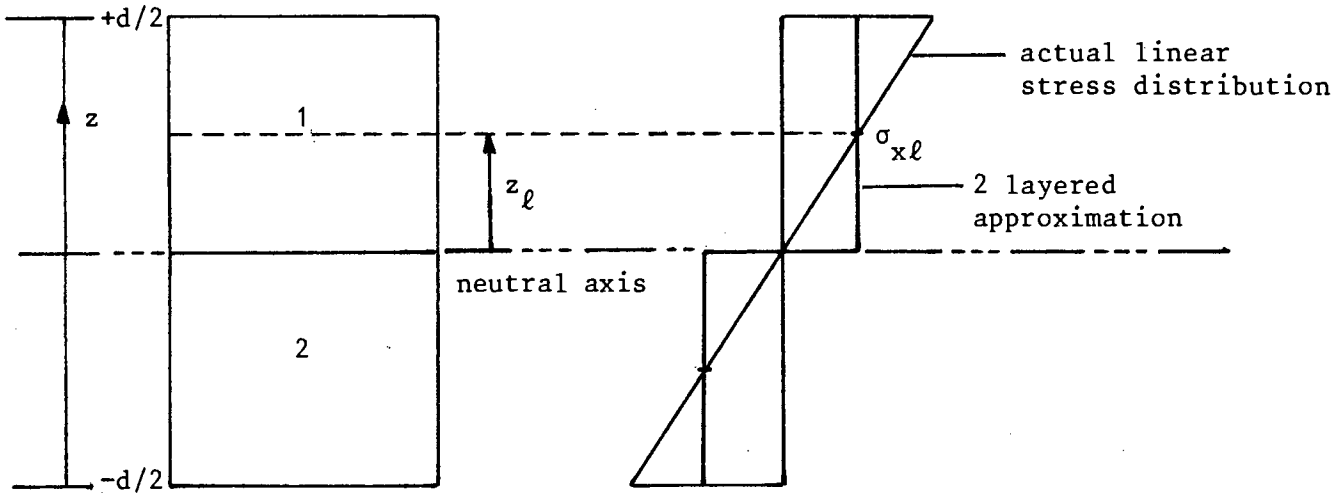

Stress Distribution Approximation using Two Layers to Model the Section

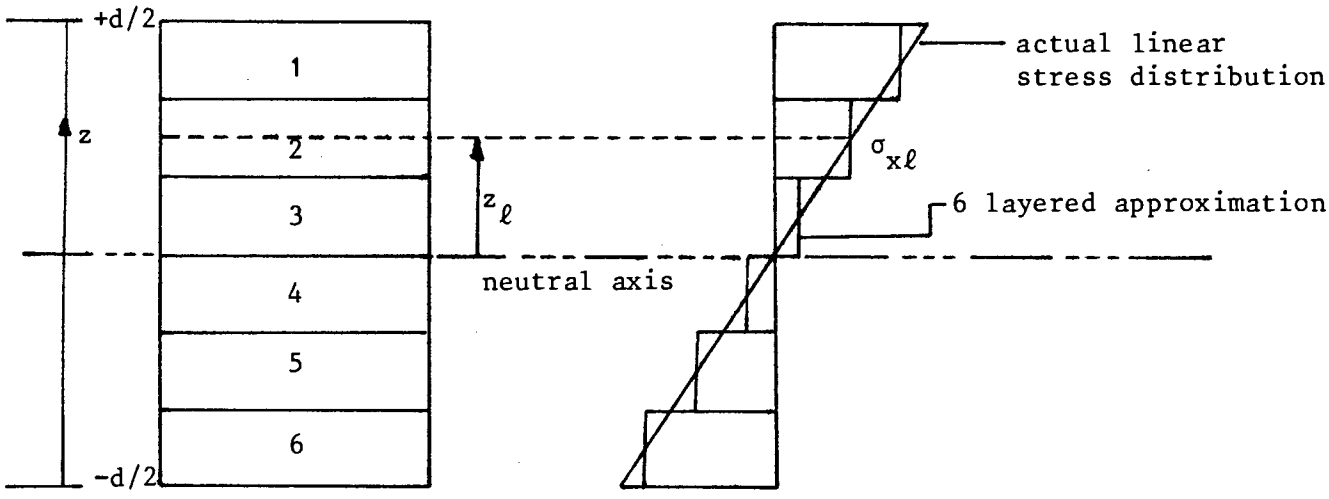

Stress Distribution Approximation using Six Layers to Model the Section

- z_ℓ is the z co-ordinate to the middle of a layer from the neutral axis
- $\sigma_{x\ell}$ is the representative stress of the layer

Figure 2.5 Approximation to the Linear Elastic Stress Distribution of the Section using the Layered Concept.

Using the fact that a realistic approximation is obtained using more layers, the exact formulation of I, which is given as

$$I = \sum_{\ell} \left(\frac{b_\ell t_\ell^3}{12} + b_\ell \, t_\ell \, z_\ell^2 \right)$$

is approximated by

$$I = \sum_{\ell} b_\ell \, t_\ell \, z_\ell^2 \, .$$

As with more layers, the layer thickness, t_ℓ, becomes small and hence the term

$$\frac{b_\ell t_\ell^3}{12}$$

tends to zero very fast.

Thus the material constants are expressed as

$$EI = \sum_{\ell} E_\ell \, b_\ell \, t_\ell \, z_\ell^2 \quad ,$$

$$EA = \sum_{\ell} E_\ell \, b_\ell \, t_\ell \quad , \qquad (2.24)$$

$$G\hat{A} = \frac{1}{\alpha} \sum_{\ell} G_\ell \, b_\ell \, t_\ell \quad .$$

The calculation of the stress resultants are given as follows:

- bending moments,

$$M = \int_{b(-d/2)}^{b\,(d/2)} \int_{-d/2}^{d/2} \sigma_x \, z \, dzdy = \sum_{\ell} \sigma_{x\ell} \, b_\ell \, t_\ell \, z_\ell$$

- normal/axial forces,

$$N = \int_{b(-d/2)}^{b\,(d/2)} \int_{-d/2}^{d/2} \sigma_x \, dzdy = \sum_{\ell} \sigma_{x\ell} \, b_\ell \, t_\ell \qquad (2.25)$$

- shear forces,

$$Q = \int_{b(-d/2)}^{b\,(d/2)} \int_{-d/2}^{d/2} \tau_{xz} \, dzdy = \sum_{\ell} \tau_{xz\ell} \, b_\ell \, t_\ell \, .$$

Layers of different thickness and material properties can be employed, as well as different numbers of layers per element. This enables the modelling of composite cross-sections and varying cross-sectional shapes.

2.5 Numercial Integration

Two types of numerical integration are used to calculate the elastic stiffness matrix and load vector: Gaussian Quadrature and Newton-Cotes Quadrature. Gaussian Quadrature is used due to its efficiency as a more accurate solution is obtained for less sampling points. The Newton-Cotes Quadrature is used as the sampling points are positioned at structurally important points, like nodes. The effects in terms of accuracy and efficiency of these two integration schemes are compared.

2.5.1 Gaussian Quadrature

The Gauss-Legendre rules are applied, Bathe [15]. A table of coefficients (sampling points and weights) for the interval -1 to +1 for the integration orders used in this work is given in Table 2.1.

n	ξ_i	w_i
1	0.000000	2.00000
2	± 0.577530	1.00000
3	0.000000	0.888888
	± 0.774597	0.555555
4	± 0.861136	0.347855
	± 0.339981	0.652145

where n - no of sampling points

ξ_i - natural co-ordinate of sampling point

w_i - weight of sampling point

Table 2.1

For this integration scheme a polynomial of order (2n - 1) will be integrated exactly using a n - point Gauss-Legendre rule.

2.5.2 Newton-Cotes Quadrature

For Newton-Cotes integration a similar table of coefficients for the interval -1 to +1 for the integration orders to be used in this work is given in Table 2.2.

n	ξ_i	w_i
2	± 1.000000	1.000000
3	0.000000	1.333333
	± 1.000000	0.333333
5	0.000000	0.2666667
	± 0.500000	0.711111
	± 1.000000	0.1555556
7	0.000000	0.647619
	± 0.333333	0.0642857
	± 0.6666667	0.5142857
	± 0.100000	0.0976190

Table 2.2

The four and six point Newton-Cotes integration rules have been omitted as the 3 and 5 point rules have the same order of accuracy respectively, Bathe [15]. For this scheme a polynomial of order (n - 1) will be integrated exactly using a n - point Newton-Cotes rule.

2.5.3 Reduced Integration

As mentioned at the beginning of this Chapter, the Timoshenko elements exhibit what is known as "locking" when used to model thin sections. As the depth of the section is decreased, the bending contribution to the stiffness tends to zero much more rapidly than the shear contribution, leaving the shear terms to dominate the behaviour. This usually results in overstiff responses. This problem may be alleviated by using reduced integration schemes to integrate the stiffness matrix, Hughes et al [16]. This technique is used for the two integration schemes and its effect on the solutions is investigated.

A table showing the orders of the polynomial appearing in the elastic stiffness matrix and its corresponding full and reduced integration rules for the two schemes are given in Table 2.3.

ELEMENT TYPE	HIGHEST ORDER TERM IN ELASTIC STIFFNESS MATRIX	FULL INTEGRATION	REDUCED INTEGRATION
Two Noded (Linear)	2	2 GP 3 NCP	1 GP 2 NCP
Three Noded (Quadratic)	4	3 GP 5 NCP	2 GP 3 NCP
Four Noded (Cubic)	6	4 GP 7 NCP	3 GP 5 NCP

where: GP - Gauss-Legendre sampling points
NCP - Newton-Cotes sampling points

Table 2.3

2.5.4 Integration of Stiffness Matrix and Consistent Load Vector Terms

Using a n-point integration rule the integration of the element stiffness matrix, $\underset{\sim}{K}^e$, is given as

$$\underset{\sim}{K}^e = \sum_{i=1}^{n} [\underset{\sim}{B}(\xi_i)]^T \underset{\sim}{D}\, \underset{\sim}{B}(\xi_i)\, w_i \det J(\xi_i) \,. \qquad (2.26)$$

Similarly, the distributed loading contribution to the load vector is calculated as

$$\int_o^{\ell} [\underset{\sim}{N}]^T q\, dx = \sum_{i=1}^{n} \sum_{j=1}^{N} N_j(\xi_i)\, q\, w_i \det J(\xi_i) \,, \qquad (2.27)$$

where N is the total number of nodes in the element.

The mass proportional loading contribution to the load vector is given as

$$\int_o^{\ell} [\underset{\sim}{N}]^T \rho g A\, dx = \sum_{i=1}^{n} \sum_{j=1}^{N} N_j(\xi_i)\, \rho g A\, w_i \det J(\xi_i) \,. \qquad (2.28)$$

In equations (2.26), (2.27) and (2.28) the terms ξ_i and w_i are obtained from tables 2.1 or 2.2 for Gaussian Quadrature or Newton-Cotes Quadrature, respectively.

CHAPTER 3

ELASTIC-PLASTIC CONSTITUTIVE MODEL FOR THE LAYERED ELEMENT

3.1 Introduction

Uniaxial elastic-plastic constitutive relations are used to model the material behaviour in the layered beam/frame element. In each layer the uniaxial contribution of the axial and flexural stresses must satisfy the yield condition for plasticity to occur. The shear stress-strain relation is assumed to be elastic. It is assumed that the entire layer becomes plastic once the yield value is attained at the centre of the layer.

In this chapter, the basic equations of plasticity for the one dimensional case are discussed (Martin [17]) and the progressive plastification of the section is illustrated using the layered concept.

3.2 Uniaxial Elastic-Plastic Behaviour

The uniaxial behaviour of a layer under monotonic loading is illustrated in Figure 3.1 by an idealised linear strain hardening stress-strain curve. The behaviour is divided up into three parts as indicated on the curve. These are described as follows:

1. The material initially exhibits a linear elastic behaviour with the slope of the curve equal to the elastic modulus E_ℓ. At the point $\sigma_{x\ell} = \sigma_y$ the material yields and undergoes linear strain hardening. The slope of the response is now described by the tangential modulus $E_{T\ell}$.

2. The material is loaded up to a stress $\sigma_{x\ell} = \sigma_{*_1}$, where $\sigma_{*_1} > \sigma_y$. The load is removed and the stress is reduced to zero with a elastic response of slope E_ℓ. Permanent deformation will have occurred. This gives a residual strain called plastic strain, $\varepsilon^P_{x\ell}$. With reloading the material responds elastically until $\sigma_{x\ell} = \sigma_{*_1}$, where σ_{*_1} is now the current yield stress. Reyielding occurs and the curve follows its original elasto-plastic path with slope $E_{T\ell}$.

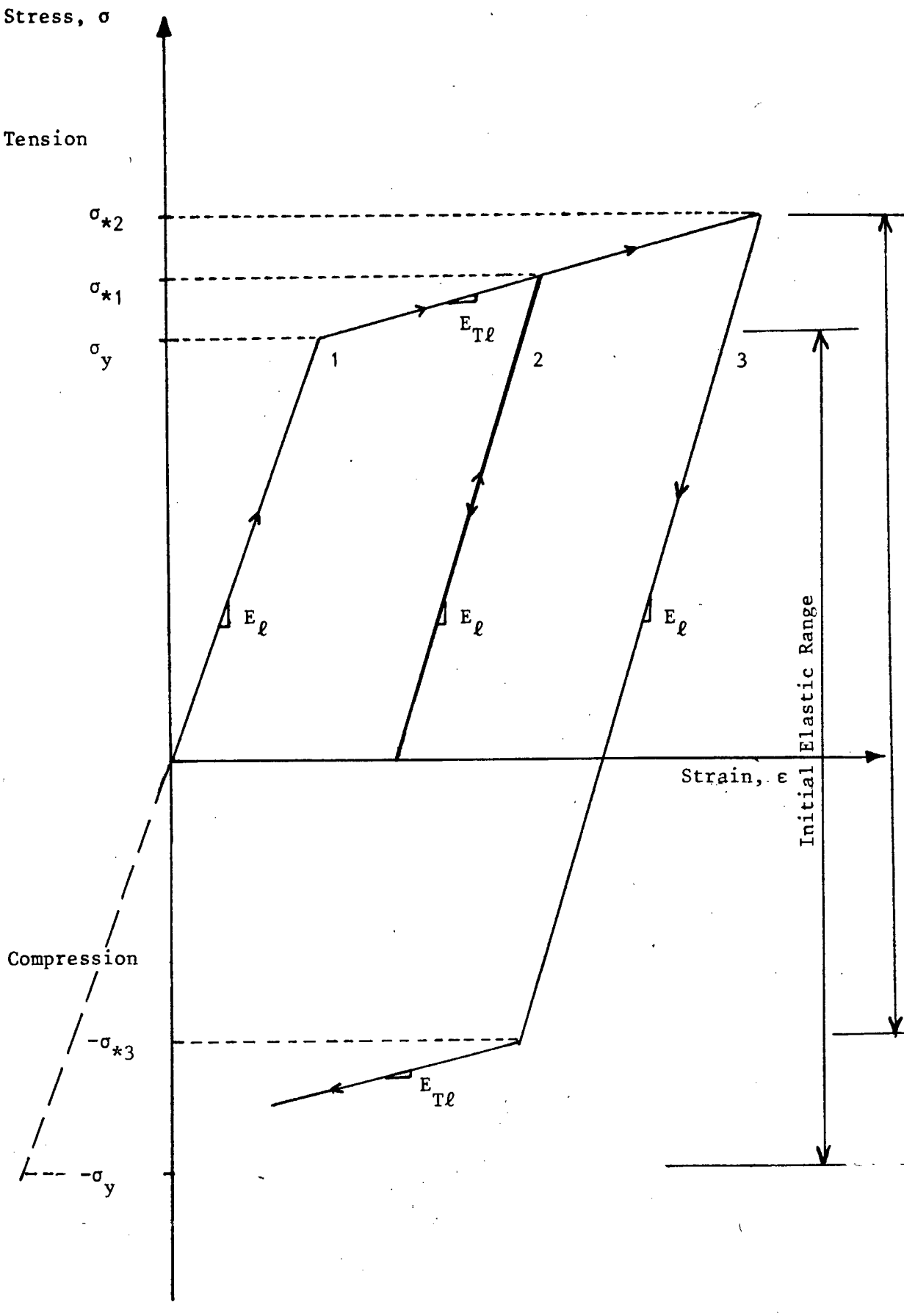

Figure 3.1 Idealised Elastic-Plastic Uniaxial Stress-Strain Behaviour.

3. The stress is increased to $\sigma_{x\ell} = \sigma_{*_2}$, where $\sigma_{*_2} > \sigma_{*_1} > \sigma_y$. At this point the load is reduced to zero and increased in the opposite sense until a negative (compressive) yield stress σ_{*_3} is reached. The material then undergoes compressive inelastic deformation with further increase in stress. From the curve we can see that the linear elastic behaviour is bounded by a positive tensile and negative compressive yield stress. If the stress moves out of the linear range, inelastic deformation occurs and the yield range changes.

3.3 Yield Condition

The yield range can be represented by a yield function

$$\phi = \phi (\sigma_{x\ell}, H_\alpha) \tag{3.1}$$

where H_α ($\alpha = 1 \ldots n$) denotes the internal parameters which constitute the recorded history of the material behaviour. In this model we include kinematic and isotropic hardening as special cases. Therefore, we have two parameters $H_1 = \varepsilon^P_{x\ell}$ and $H_2 = W_p$. $\varepsilon^P_{x\ell}$ is the plastic strain and W_p is the plastic work given by

$$W_p = \int \sigma_{x\ell} \, d\varepsilon^P_{x\ell} \tag{3.2}$$

Thus the yield function is expressed to include the kinematic and isotropic models as

$$\phi = \phi (\sigma_{x\ell} , \varepsilon^P_{x\ell} , W_p) \tag{3.3}$$

Note: $\phi < 0$ implies linear elastic behaviour,
$\phi = 0$ means yielding is possible,
$\phi > 0$ cannot be achieved.

The yield condition is thus defined as

$$\phi (\sigma_{x\ell} , \varepsilon^P_{x\ell} , W^P) = 0 \, . \tag{3.4}$$

There are two possibilities when $\phi = 0$:

i) $\dot{\phi} < 0$, the material is being unloaded and no change in plastic strain occurs.

ii) $\dot{\phi} = 0$, the material is being loaded and increments in plastic strain occur.

3.3.1 Yield Condition for Perfect Plasticity

For the perfectly plastic case the yield function is

$$\phi = \phi(\sigma_{x\ell}) \ , \tag{3.5}$$

where

$$\phi = \sigma_{x\ell}^{\ 2} - \sigma_y^{\ 2} \tag{3.6}$$

and yielding occurs when

$$\sigma_{x\ell} = \pm \sigma_y \ . \tag{3.7}$$

3.4 Constitutive Relations

During yielding, the total strain increment $d\varepsilon_{x\ell}$ is decomposed in classical plasticity fashion as

$$d\varepsilon_{x\ell} = d\varepsilon_{x\ell}^{e} + d\varepsilon_{x\ell}^{P} \ , \tag{3.8}$$

where the elastic strain increment is defined as

$$d\varepsilon_{x\ell}^{e} = d\sigma_{x\ell}/E_{\ell} \ , \tag{3.9}$$

and the plastic strain increment is proportional to the gradient of the yield function. Thus

$$d\varepsilon^{P}_{x\ell} = \lambda \frac{\partial \phi}{\partial \sigma_{x\ell}} \quad , \quad \lambda \geqq 0 \quad , \tag{3.10}$$

where λ is the proportionality factor. Equation (3.10) is normally referred to as the flow rule.

The equations for total strain are then expressed as

$$d\varepsilon_{x\ell} = \frac{d\sigma_{x\ell}}{E_{\ell}} \quad , \quad \text{for } \phi < 0 \text{ and } \phi = 0, \dot{\phi} < 0 \tag{3.11a}$$

and

$$d\varepsilon_{x\ell} = \frac{d\sigma_{x\ell}}{E_{\ell}} + \lambda \frac{\partial \phi}{\partial \sigma_{x\ell}} \quad , \text{ for } \phi = 0, \dot{\phi} = 0 \ . \tag{3.11b}$$

3.4.1 Perfect Plasticity

For the perfectly plastic case

$$\dot{\phi} = \frac{\partial \phi}{\partial \sigma_{x\ell}} d\sigma_{x\ell} \tag{3.12}$$

$$= 0$$

and by multiplying equation (3.11b) by $\frac{\partial \phi}{\partial \sigma_{x\ell}}$, we get

$$\lambda = \frac{(\partial \phi / \partial \sigma_{x\ell})}{(\partial \phi / \partial \sigma_{x\ell})^2} d\varepsilon_{x\ell} \ . \tag{3.13}$$

Eliminating λ from equation (3.11b) gives the constitutive equations

$$d\sigma_{x\ell} = E_{\ell} d\varepsilon_{x\ell} \quad , \text{ for } \phi < 0 \text{ or } \phi = 0 \text{ and } (\partial \phi / \partial \sigma_{x\ell}) d\varepsilon_{x\ell} \leqq 0$$

and (3.14)

$$d\sigma_{x\ell} = 0 \quad , \text{ for } \phi = 0 \text{ and } (\partial \phi / \partial \sigma_{x\ell}) d\varepsilon_{x\ell} > 0 \ .$$

3.4.2 Hardening

For the hardening case

$$\dot{\phi} = \frac{\partial \phi}{\partial \sigma_{x\ell}} d\sigma_{x\ell} + \frac{\partial \phi}{\partial \varepsilon^{P}_{x\ell}} d\varepsilon^{P}_{x\ell} + \frac{\partial \phi}{\partial W_p} dW_p$$

$$= \frac{\partial \phi}{\partial \sigma_{x\ell}} d\sigma_{x\ell} + \frac{\partial \phi}{\partial \varepsilon^{P}_{x\ell}} (\lambda \frac{\partial \phi}{\partial \sigma_{x\ell}}) + \frac{\partial \phi}{\partial W_p} dW_p \ .$$

however, from equation (3.9) (3.15)

$$dW_p = \sigma_{x\ell} \, d\varepsilon^{P}_{x\ell} \ ,$$

therefore

$$\dot{\phi} = \frac{\partial \phi}{\partial \sigma_{x\ell}} d\sigma_{x\ell} + \frac{\partial \phi}{\partial \varepsilon^{P}_{x\ell}} (\lambda \frac{\partial \phi}{\partial \sigma_{x\ell}}) + \frac{\partial \phi}{\partial W_p} \sigma_{x\ell} (\lambda \frac{\partial \phi}{\partial \sigma_{x\ell}})$$

$$= 0 \ .$$

Hence

$$\lambda = - \frac{1}{(\frac{\partial \phi}{\partial \varepsilon^{P}_{x\ell}} + \frac{\partial \phi}{\partial W_p} \sigma_{x\ell}) \frac{\partial \phi}{\partial \sigma_{x\ell}}} (\frac{\partial \phi}{\partial \sigma_{x\ell}} d\sigma_{x\ell})$$

$$= + G (\frac{\partial \phi}{\partial \sigma_{x\ell}} d\sigma_{x\ell}) \qquad (3.16)$$

then $d\varepsilon^{P}_{x\ell} = G (\frac{\partial \phi}{\partial \sigma_{x\ell}} d\sigma_{x\ell}) \frac{\partial \phi}{\partial \sigma_{x\ell}}$,

with $\frac{1}{G} = - (\frac{\partial \phi}{\partial \varepsilon^{P}_{x\ell}} + \frac{\partial \phi}{\partial W_p} \sigma_{x\ell}) \frac{\partial \phi}{\partial \sigma_{x\ell}} > 0$.

The incremental stress-strain relation is then evaluated as

$$d\sigma_{x\ell} = E_\ell d\epsilon^e_{x\ell}$$

$$= E_\ell \, (d\epsilon_{x\ell} - d\epsilon^P_{x\ell})$$

$$= E_\ell d\epsilon_{x\ell} - E_\ell G \, (\frac{\partial \phi}{\partial \sigma_{x\ell}})^2 \, d\sigma_{x\ell} \qquad (3.17)$$

or

$$d\sigma_{x\ell} = \frac{E_\ell d\epsilon_{x\ell}}{1 + E_\ell G \, (\frac{\partial \phi}{\partial \sigma_{x\ell}})^2} \qquad (3.18)$$

This is more generally written as

$$d\sigma_{x\ell} = E_\ell \left[1 - \frac{E_\ell \, (\partial \phi / \partial \sigma_{x\ell})^2}{1/G + E_\ell \, (\partial \phi / \partial \sigma_{x\ell})^2} \right] d\epsilon_{x\ell} \qquad (3.19)$$

or

$$d\sigma_{x\ell} = E_{T\ell} \, d\epsilon_{x\ell} \qquad (3.20)$$

where $E_{T\ell}$ is the tangent modulus.

The full set of constitutive relations is given as

$$d\sigma_{x\ell} = E_\ell d\epsilon_{x\ell} \text{ , for } \phi < 0 \text{ or } \phi = 0 \text{ and } (\frac{\partial \phi}{\partial \sigma_{x\ell}}) \, d\epsilon_{x\ell} \leq 0$$

and (3.21)

$$d\sigma_{x\ell} = E_{T\ell} \, d\epsilon_{x\ell} \text{ for } \phi = 0 \text{ and } (\frac{\partial \phi}{\partial \sigma_{x\ell}}) \, d\epsilon_{x\ell} > 0 \, .$$

3.5 Hardening Rules

The hardening rules incorporated in this elastic-plastic formulation include the linear kinematic and linear isotropic hardening rules.

3.5.1 Linear Kinematic Hardening

In the case of linear kinematic hardening the magnitude of the elastic range remains fixed but translates up and down the $\sigma_{x\ell}$ axis. This is illustrated in Figure 3.2. The yield function is defined as

$$\phi = (\sigma_{x\ell} - H'_\ell \, \varepsilon^P_{x\ell})^2 - \sigma_y^2 \tag{3.22}$$

where H'_ℓ is a linear strain hardening parameter.

This yield function is independent of W_p hence equation (3.15) is satisfied since $\frac{\partial \phi}{\partial W_p} = 0$.

During loading

$$\frac{1}{G} = - \frac{\partial \phi}{\partial \sigma_{x\ell}} \frac{\partial \phi}{\partial \varepsilon^P_{x\ell}} > 0$$

$$= 4H'_\ell \, (\sigma_{x\ell} - H'_\ell \, \varepsilon^P_{x\ell})^2 \tag{3.23}$$

$$= 4H'_\ell \, \sigma_y^2$$

Hence equation (3.19) becomes

$$d\sigma_{x\ell} = E_\ell \left(1 - \frac{E_\ell}{E_\ell + H'_\ell}\right) d\varepsilon_{x\ell} \, . \tag{3.24}$$

$$= E_{T\ell} \, d\varepsilon_{x\ell}$$

where the tangent modulus $E_{T\ell}$ is constant.

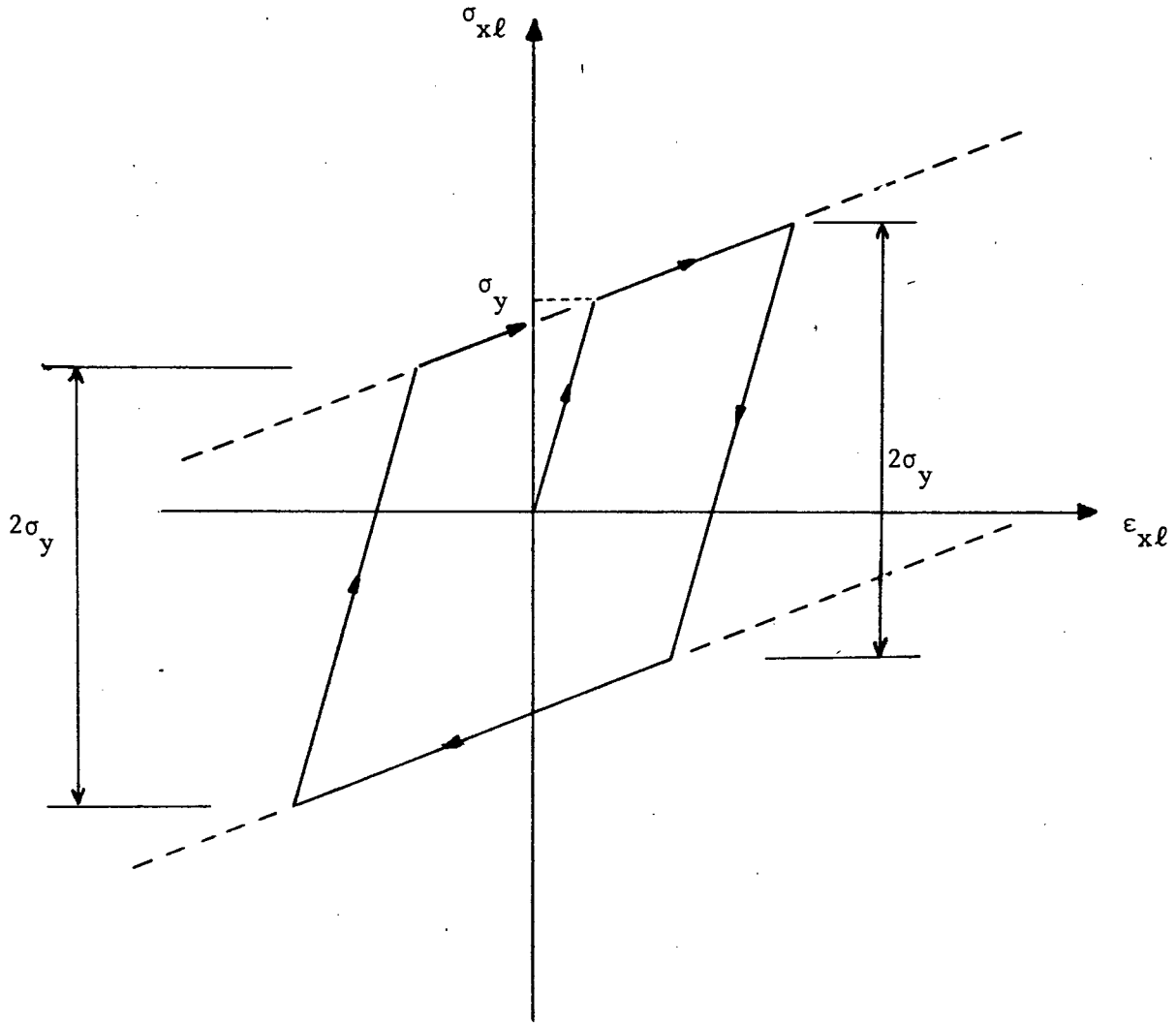

Figure 3.2 Linear Kinematic Hardening.

3.5.2 Linear Isotropic Hardening

In the case of linear isotropic hardening the elastic range expands uniformly without translation on the $\sigma_{x\ell}$ axis. This is illustrated in Figure 3.3. The yield function is defined as

$$\phi = \sigma_{x\ell}^2 - \bar{\sigma}^2 \tag{3.25}$$

where $\bar{\sigma} = \sigma_y^2 \ (1 + c \ W_p)$

with c same constant and W_p expressed in equation (3.2).

This yield function is independent of $\varepsilon^P_{x\ell}$ hence equation (3.15) is satisfied since $\left(\frac{\partial \phi}{\partial \varepsilon_{x\ell}}\right)_P = 0$.

During loading

$$\frac{1}{G} = -\left(\frac{\partial \phi}{\partial W_p} \sigma_{x\ell}\right) \frac{\partial \phi}{\partial \sigma_{x\ell}} > 0 \tag{3.26}$$

$$= 2c \ \sigma_{x\ell}^2 \ \sigma_y^2$$

Hence equation (3.19) becomes

$$d\sigma_{x\ell} = E_\ell \left[1 - \frac{E_\ell}{\frac{1}{2}c\sigma_y^2 + E_\ell}\right] d\varepsilon_{x\ell} \tag{3.27}$$

$$= E_{T\ell} \ d\varepsilon_{x\ell}$$

where the tangent modulus $E_{T\ell}$ is constant.

For this model $c = \frac{2H'_\ell}{\sigma_y^2}$ where we obtain the same value of the tangent modulus given in equation (3.24).

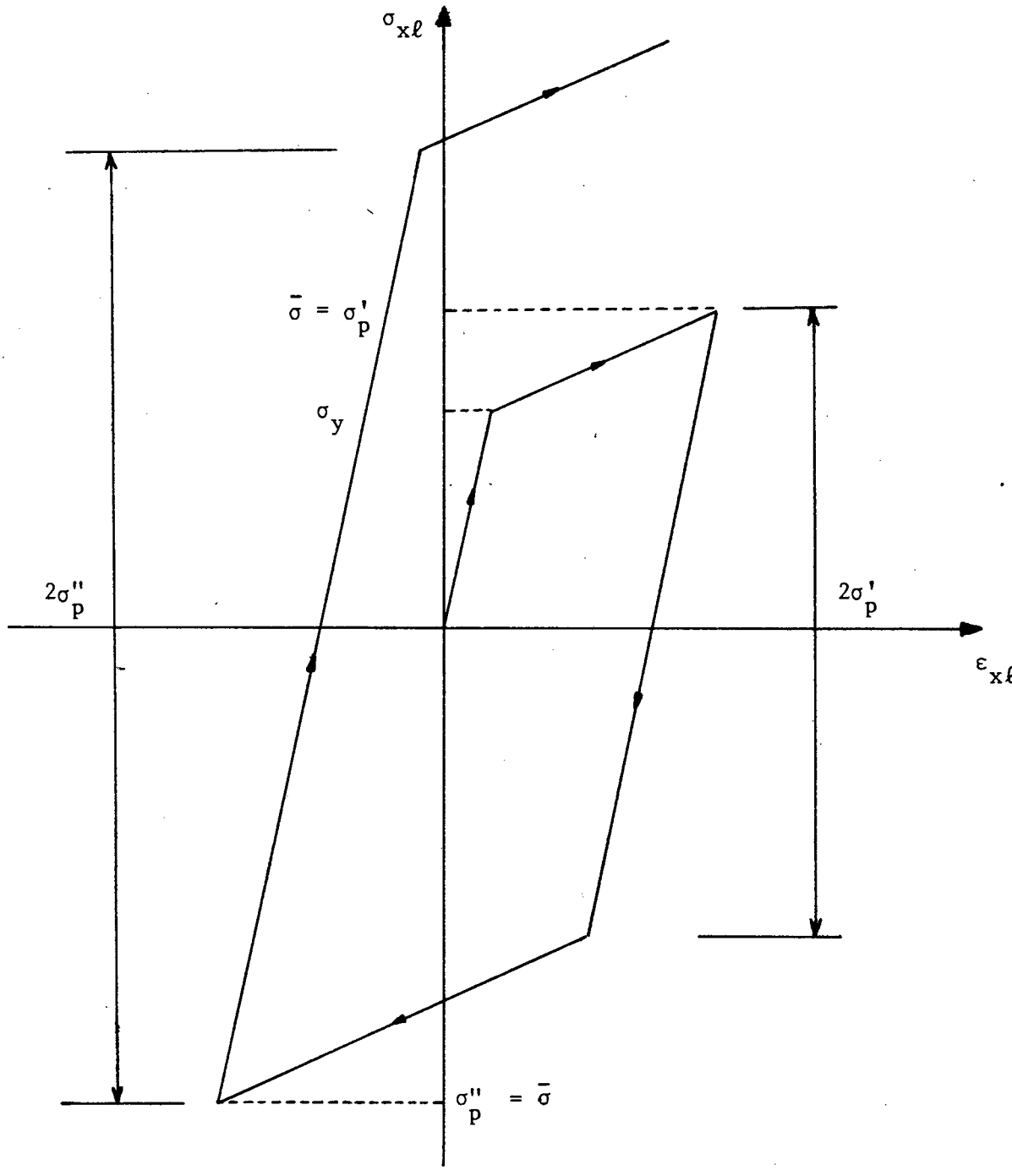

Figure 3.3 Linear Isotropic Hardening.

3.6 Elastic-Plastic Matrix

The elastic-plastic matrix $\underset{\sim}{Dep}$ of an element whose terms were derived for the elastic case in Chapter Two section four, is given as

$$\underset{\sim}{Dep} = \begin{bmatrix} \bar{E}A & 0 & 0 \\ 0 & \bar{E}I & 0 \\ 0 & 0 & G\hat{A} \end{bmatrix} \qquad (3.25)$$

where $\bar{E}$ is a resultant elastic-plastic modulus for the layered section. It is obtained from the integration through the depth of the section of $E_{T\ell}$ values for those layers which are actively yielding and E_{ℓ} values for those which remain elastic.

3.7 Modelling of the Propagation of Plasticity through a Section

The modelling of the propagation of plasticity through the section is made possible by the use of the layered section concept. In order to model this satisfactorily, a number of layers must be used in the section. The whole section is said to have yielded once all the layers have yielded. This spread of plasticity through the section is illustrated in Figure 3.4 for the pure bending case.

The effect of axial force on the stress distribution and the yielding of layers is illustrated in Figure 3.5. As the flexural and axial stresses contribute to the uniaxial stress in each layer, the stress distribution is shifted by a constant, $\sigma_{xa\ell}$. The neutral axis is shifted below the position corresponding to pure bending for added compressive axial stress and above this position for added tensile axial stress.

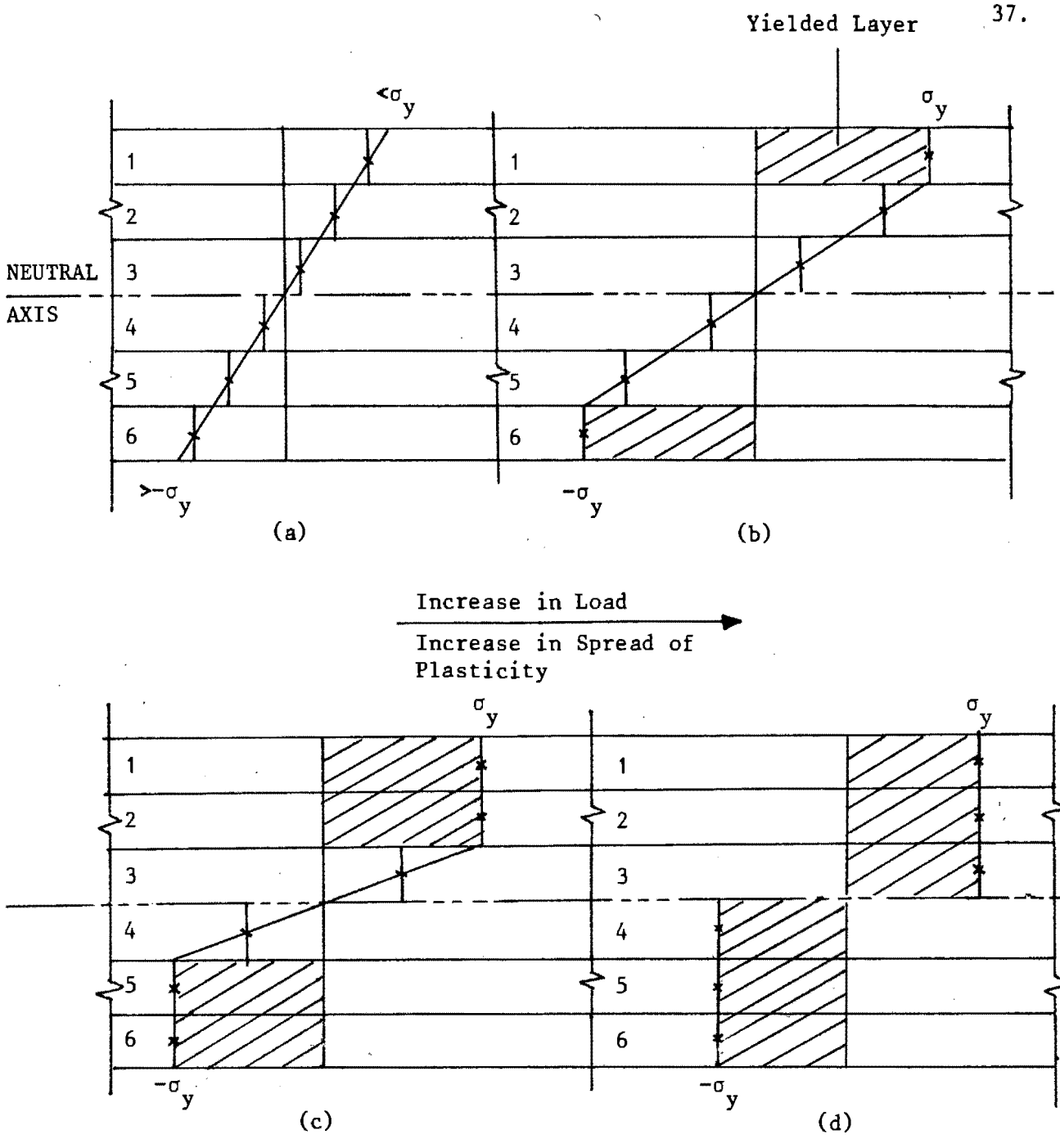

a) The highest stresses occur in the outermost layers but they are still elastic, $\sigma_{x\ell} < \sigma_y$

b) The outermost layers yield first, $\sigma_{x\ell 1} = \sigma_{x\ell 6} = \sigma_y$

c) Plastification progresses towards the centre of the section

d) The whole section has yielded

Figure 3.4 Yielding of Layered Beam under Pure Bending.

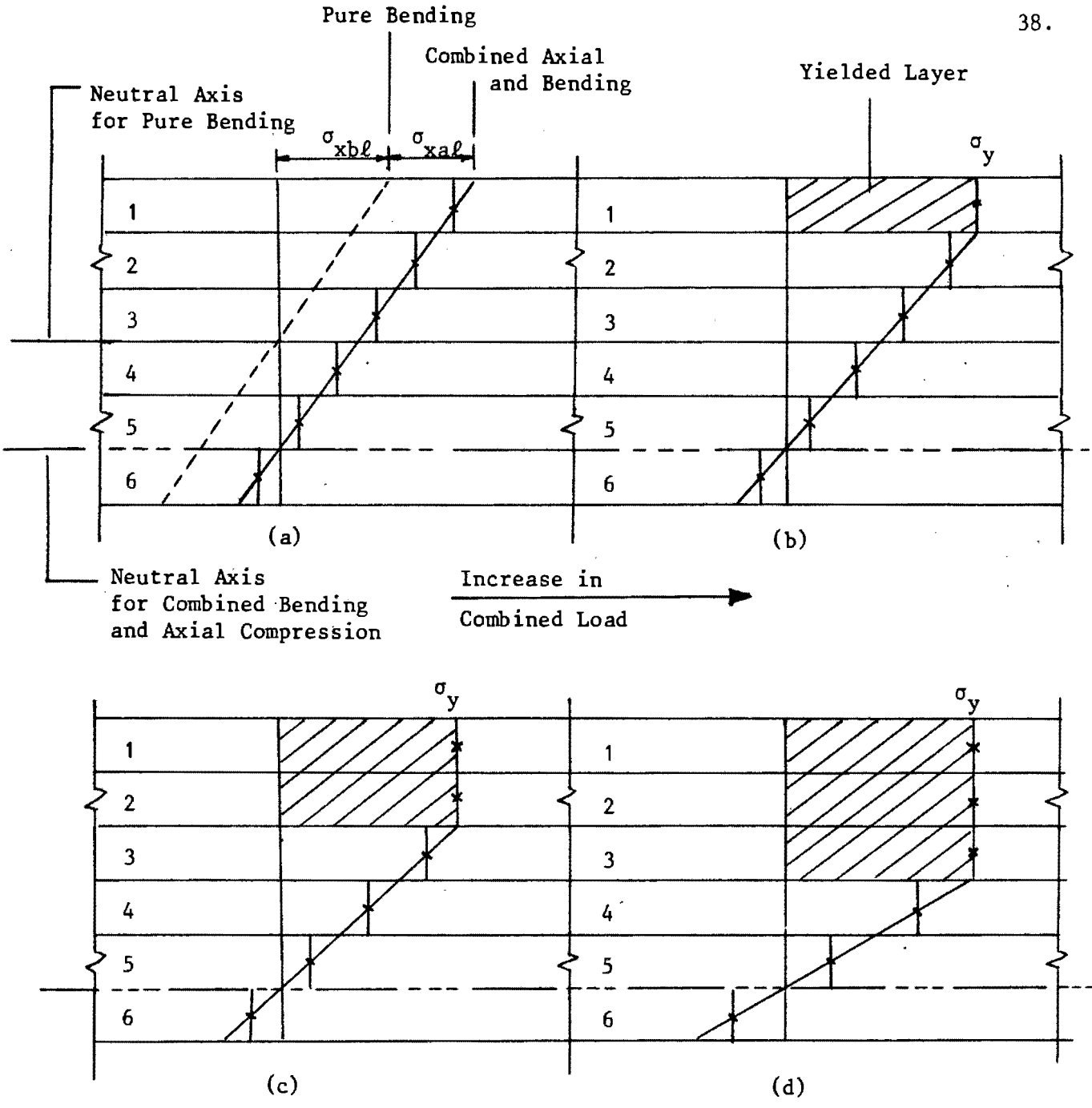

The uniaxial stress in each layer is

$$\sigma_{x\ell} = \sigma_{xa\ell} + \sigma_{xb\ell}$$

a) The highest stresses occur on the one side of the section but they are still elastic, $\sigma_{x\ell} < \sigma_y$.

b) The outermost layer on the side with the highest uniaxial stress yields first, $\sigma_{x\ell 1} = \sigma_y$.

c) & d) Plastification propagates towards the neutral axis from one side.

Figure 3.5 Yielding of Layered Frame under Combined Bending and Compressive Axial Loads.

CHAPTER 4

NUMERICAL IMPLEMENTATION

4.1 Introduction

The software necessary to carry out the nonlinear stability analysis of beams and frames was developed within the framework of NOSTRUM [13], an existing finite element program for the static and dynamic nonlinear analysis of plane continua and structures. NOSTRUM was used as the starting basis as it has the required equation solving routines and the basic algorithms necessary to carry out nonlinear analysis and to model nonlinear geometric behaviour. The additional routines needed for the present problem were added. These additions incorporate the layered Timoshenko beam/frame elements, the uniaxial elastic-plastic constitutive models and the associated loading, numerical integration and co-ordinate transformation sub-routines.

This chapter starts with a brief description of NOSTRUM. The incremental/iterative solution procedure used and the assumptions made in conjunction with the geometric algorithm are then discussed. Finally, the program structure developed for the solution of the stability problem is described to illustrate the changes and additions made to the basic NOSTRUM code.

4.2 Overview of NOSTRUM

The features of NOSTRUM relevant to the present work are briefly summarised in this section.

The fundamental framework upon which NOSTRUM is built is a general incremental solution strategy employing a tangent stiffness approach which allows both linear and nonlinear analysis to be performed. Incorporated into the incremental solution is an equilibrium iteration procedure of sufficient generality to allow a number of nonlinear solution techniques such as the initial stiffness method and the Newton Raphson and modified Newton Raphson methods to be employed [13].

For static analysis the equations of equilibrium are solved using an out-of-core frontal solver.

The original structural element library included truss, spring and beam elements. The beam elements were two node Hermitian straight line elements based on classical Euler-Bernoiulli bending theory. The only constitutive option available for these elements is linear elasticity.

The Updated Lagrangian formulation is used to describe the nonlinear geometric behaviour of the finite element model.

Different types of loading associated with the various element types are available. In addition, prescribed displacements may be applied at any node to give in effect a strain controlled loading program. Each load is governed by a continuous time function which specifies the relative magnitude of the load at a given time step in the analysis.

The procedures used for the solution of the nonlinear equations and modelling of the nonlinear geometric effects are discussed in more detail in the following sections.

4.3 Solution of Nonlinear Equilibrium Equations

This procedure uses an equilibrium iteration scheme based on the Newton Raphson method. The load is applied incrementally and two successive values of the total load are identified as $\underset{\sim}{F}_t$ and $\underset{\sim}{F}_{t+\Delta t}$ so that the load increment is

$$\underset{\sim}{\Delta F} = \underset{\sim}{F}_{t+\Delta t} - \underset{\sim}{F}_t \,. \tag{4.1}$$

It is assumed that an acceptably accurate set of displacements is known for the loading $\underset{\sim}{F}_t$. By this we mean the displacements $\underset{\sim}{u}_t$, together with the previous history, lead to internal forces $\underset{\sim}{R}_t$ such that a norm of the residual $(\underset{\sim}{F}_t - \underset{\sim}{R}_t)$ is within a specified tolerance.

Assume now that the i-th estimate of displacements for load $\underset{\sim}{F}_{t+\Delta t}$ is $\underset{\sim}{u}^{i}_{t+\Delta t}$. This leads to internal forces $\underset{\sim}{R}^{i}_{t+\Delta t}$ which are not equal to the loads $\underset{\sim}{F}_{t+\Delta t}$. In order to improve the displacement estimates, we compute a tangent stiffness matrix $\underset{\sim}{K}^{i}_{t+\Delta t}$ and put

$$\underset{\sim}{u}^{i+1}_{t+\Delta t} = \underset{\sim}{u}^{i}_{t+\Delta t} + \Delta\underset{\sim}{u}^{i} \tag{4.2}$$

where $\Delta\underset{\sim}{u}^{i}$ is calculated from the equilibrium equations as

$$\begin{aligned} \Delta\underset{\sim}{u}^{i} &= (\underset{\sim}{K}^{i}_{t+\Delta t})^{-1} (\underset{\sim}{F}_{t+\Delta t} - \underset{\sim}{R}^{i}_{t+\Delta t}) \\ &= (\underset{\sim}{K}^{i}_{t+\Delta t})^{-1} \underset{\sim}{\psi}^{i} . \end{aligned} \tag{4.3}$$

This iterative process is continued until a norm of the residual $\underset{\sim}{\psi}^{i} = (\underset{\sim}{F}_{t+\Delta t} - \underset{\sim}{R}^{i}_{t+\Delta t})$ is reduced to an acceptable tolerance. At this point, the solution moves to the next load step.

There are a number of options in the program regarding the choice of the stiffness matrix $\underset{\sim}{K}^{i}_{t+\Delta t}$. The full Newton Raphson option is used, where $\underset{\sim}{K}^{i}_{t+\Delta t}$ is updated at each iteration, in order to include the improved estimate of displacement $\underset{\sim}{u}^{i}_{t+\Delta t}$. It is used in this work as geometrical nonlinearity is involved, but is expensive in computer time in that the stiffness matrix must be reformulated and re-inverted at each iteration.

4.4 Integration of the Constitutive Equations

To complete the procedure established in the previous section, the calculation of $\underset{\sim}{R}^{i}_{t+\Delta t}$ has to be dealt with. $\underset{\sim}{R}^{i}_{t+\Delta t}$ is calculated from the stresses $\underset{\sim}{\sigma}^{i}_{t+\Delta t}$ at each integration point as

$$\overset{e}{\underset{\sim}{R}}{}^{i}_{t+\Delta t} = \int_{Ve} \underset{\sim}{B}^{T} \underset{\sim}{\sigma}^{i}_{t+\Delta t} \, dV_e \tag{4.4}$$

where the superscript e denotes element e with volume V_e and $\underset{\sim}{B}$ is the strain displacement matrix.

For the uniaxial layered model ${}^{e}\underset{\sim}{R}^{i}_{t+\Delta t}$ is expressed as

$$
\begin{aligned}
{}^{e}\underset{\sim}{R}^{i}_{t+\Delta t} = & \int_{o}^{\ell} [\underset{\sim}{B}_{a}]^{T} N \, dx + \int_{o}^{\ell} [\underset{\sim}{B}_{f}]^{T} M \, dx \\
& + \int_{o}^{\ell} [\underset{\sim}{B}_{s}]^{T} Q \, dx
\end{aligned}
\tag{4.5}
$$

where N, M and Q are the axial, flexural and shear stress resultants calculated from the integration through the depth and breadth of the section of the uniaxial stresses $\sigma_{x\ell}$ and shear stresses $\tau_{x\ell}$ of each layer, respectively. This is given in equation (2.25).

For the purpose of this section $\sigma_{x\ell}$ and $\varepsilon_{x\ell}$ will be simply written as σ and ε.

The calculation of the internal forces $\underset{\sim}{R}^{i}_{t+\Delta t}$ requires that we be able to integrate the constitutive equations through the incremental iterative process of analysis. For this, at each integration point, one has to satisfy the incremental relations

$$
\begin{aligned}
d\sigma &= D^{ep} \, d\varepsilon \\
\text{where} \quad D^{ep} &= E_{\ell} \quad \text{for elastic states} \\
\text{or} \quad D^{ep} &= E_{T\ell} \quad \text{for elastic-plastic states,}
\end{aligned}
\tag{4.6}
$$

for each increment in load. In a displacement based formulation the strain changes are known for every load increment and the corresponding changes in stress have to be evaluated according to equation (4.6), together with the changes in internal variables.

The stresses at the increment $t+\Delta t$ for the i-th equilibrium iteration can be calculated as follows:

$$\sigma^{i}_{t+\Delta t} = \sigma_t + \int_{\underset{\sim}{\varepsilon}_t}^{\underset{\sim}{\varepsilon}^{i}} {}_{t+\Delta t}D^{ep}\, d\varepsilon \qquad (4.7)$$

where σ_t represents the equilibrated stresses at increment t. Bathe [15] emphasises that the integration should be done from an equilibrated state which has previously been obtained, for instance the previous step as indicated in equation (4.7). However, in quasi-static problems where relatively small changes in stress are likely to occur in each increment, equation (4.7) can be relaxed for ease of computation. Owen and Hinton [14] suggests

$$\sigma^{i}_{t+\Delta t} = \sigma^{i-1}_{t+\Delta t} + \int_{\varepsilon^{i-1}_{t+\Delta t}}^{\varepsilon^{i}_{t+\Delta t}} D^{ep}\, d\varepsilon \qquad (4.8)$$

$$= \sigma^{i-1}_{t+\Delta t} + \Delta\sigma^{i-1} \quad .$$

Equation (4.8) is used in the present calculations.

The integration of equation (4.8) can be performed explicitly in the uniaxial model. This procedure is explained in detail in Owen and Hinton [14] and will not be repeated here.

4.5 Nonlinear Geometric Formulation and Assumptions

An Updated Lagrangian formulation is used to model the non-linear geometric behaviour. At step t we use as a reference configuration of the configuration at the previous step $t-\Delta t$; this is in contrast to the total Lagrangian formulation where the reference configuration is the initial configuration at step t=0. Certain assumptions on the element geometry are made in conjunction with this formulation. It is assumed that the elements remain straight and the internal element

nodes maintain their relative positions during and after spatial displacement. Thus the local reference axis always passes through the end nodes of the element. There are no added geometric terms in the stiffness matrix. Consequently, small increments are used to capture the changes in the tangential stiffness matrix. To assess the ability to model nonlinear geometric behaviour, large displacement pure bending, buckling and post-buckling analysis of a cantilever were carried out. These results, presented in Chapter 5, are compared to published results obtained for the same problems.

4.6 Software Structure

As stated in the introduction to this chapter, the program structure for the solution of the stability problems is built into the NOSTRUM framework. NOSTRUM has a modular structure in that it is broken down into a large number of subroutines each of which perform a well defined task. These subroutines may be graded according to the level of generality of the task they perform. This lends itself to a well-defined overlay structure in which each primary subroutine constitutes the basis of its own functional module. New features are thus added effectively by simply adding on separate subroutines via a single CALL statement in the code.

The parts of the NOSTRUM structure relevant to the solution of the nonlinear stability problem are illustrated in Figure 4.1. The additional subroutines incorporate the layered Timoshenko elements, together with the associated loading, geometric and constitutive models. A description of the program is given in the following paragraphs.

The highest level subroutines perform primary functions such as directing the order of calculations, controlling the iterative solution procedure, solving the equilibrium equation, reading in of data and printing out of results.

The order of element calculations and calculation of residual vector are controlled by LOADS, STIFFN and RESIDU:

LOADS controls the calculation of the element load vector, ${}^{e}\underset{\sim}{F}_{t+\Delta t}$;

STIFFN controls the calculation of the element tangential stiffness matrix, ${}^{e}\underset{\sim}{K}^{i}_{t+\Delta t}$;

RESIDU controls the formulation of the residual load vector, $\underset{\sim}{R}^{i}_{t+\Delta t}$.

The incremental iterative solution procedure is controlled by INCREM, UPDAT and CONVER:

INCREM sets up the current load increment, $\Delta\underset{\sim}{F}$ and updates the total load vector $\underset{\sim}{F}_{t+\Delta t} = \underset{\sim}{F}_{t} + \Delta\underset{\sim}{F}$.

Similarly for prescribed displacements the current increment in displacement and the total displacements are set up.

UPDAT updates the total displacements and geometry,

$$\underset{\sim}{u}^{i+1}_{t+\Delta t} = \underset{\sim}{u}^{i}_{t+\Delta t} + \Delta\underset{\sim}{u}^{i} \quad .$$

CONVER checks the convergence of the iterative process. Convergence is reached when the following condition is satisfied:

$$\frac{\| \underset{\sim}{F}_{t+\Delta t} - \underset{\sim}{R}^{i}_{t+\Delta t} \|_2}{\| \underset{\sim}{R}_{t+\Delta t} \|_2} \times 100 \leq \text{FTOL}$$

where FTOL is a force tolerance and $\| x_n \|$ is the Euclidean vector norm defined as

$$\| x_n \| = \left(\sum_{n=1}^{N} |x_n|^2 \right)^{\frac{1}{2}} \quad .$$

The solution of the incremental equilibrium equation $\underset{\sim}{K}\ \Delta\underset{\sim}{u} = \underset{\sim}{\psi}$ is carried out by subroutine FRONT:

FRONT is a symmetric, out-of-core frontal solution procedure. Its function is to assemble the contributions from each element to form the global stiffness matrix and global load vector and to solve the resulting set of simultaneous equations by Gaussian elimination.

The reading in of the necessary data, initialising of arrays and printing out of results is carried out by subroutines INPUT, ZERO and OUTPUT respectively.

The second level subroutines control the calculations relating to each element class such as the present structural elements. These subroutines are CHEC1D, GRAV1D, EDGE1D, STIF1D, RESD1D and SOUT1D:

CHEC1D checks the validity of the input data;

GRAV1D controls the mass proportional loading calculations;

EDGE1D controls the distributed loading calculations;

STIF1D controls the formulation of element stiffness matrices;

RESD1D controls the calculation of the internal load vector;

SOUT1D prints out the corresponding stress resultants, stresses and strains.

The third level of subroutines relate to a specific element type within the element class. The subroutines ISOGRV, ISOEDG, SBEAMN, GLOBNL and TSBEMN which were added in the present work relate specifically to the Layered Timoshenko Lagrangian element family. The task of each subroutine is described as follows:

ISOGRV calculates for each element the equivalent nodal loads for mass proportional loading. The loading is divided into each node using the Lagrangian shape functions, $N_i\ (\xi)$, according to equations (2.22) and (2.28).

ISOEDG calculates the equivalent nodal loads for a constant or linearly varying distributed load or moment. The distributed loading is divided into each node as described by equations (2.21) and (2.27).

SBEAMN calculates the elastic-plastic tangential stiffness matrix of the element.

GLOBNL calculates the associated element space transformation matrix.

TSBEMN calculates the layered elastic-plastic constitutive relation and residual vector.

The fourth level of subroutines are used in the calculations of the element load vectors, tangential stiffness matrix and residual load vector. The subroutines COTE, GAUSS, SHAP1D, JACOB1, MODP, LAYER, BMATB and DBE which were added in the present work are used specifically in these calculations of the Layered Timoshenko, Lagrangian elements. The task of each routine is described as follows:

COTE sets up the Newton Cotes quadrature integration coefficients given in Table 2.2.

GAUSS sets up the Gauss Legendre integration coefficients given in Table 2.1.

SHAP1D defines the Lagrangian element shape functions, $N_i(\xi)$, given in equation (2.12).

JACOB1 calculates the element Jacobian operator, det J (ξ).

MODP sets up the element elastic-plastic matrix $\underset{\sim}{D}_{ep}$.

LAYER calculates the terms EA, EI and $G\hat{A}$ in the elastic-plastic matrix, $\underset{\sim}{D}_{ep}$, by integrating the values corresponding to each layer over the depth of the section.

BMATB calculates the associated element strain displacement matrix given in equation (2.16).

DBE carries out the matrix multiplication $\underset{\sim}{D}_{ep}\underset{\sim}{B}$ needed as part of the element stiffness matrix calculation.

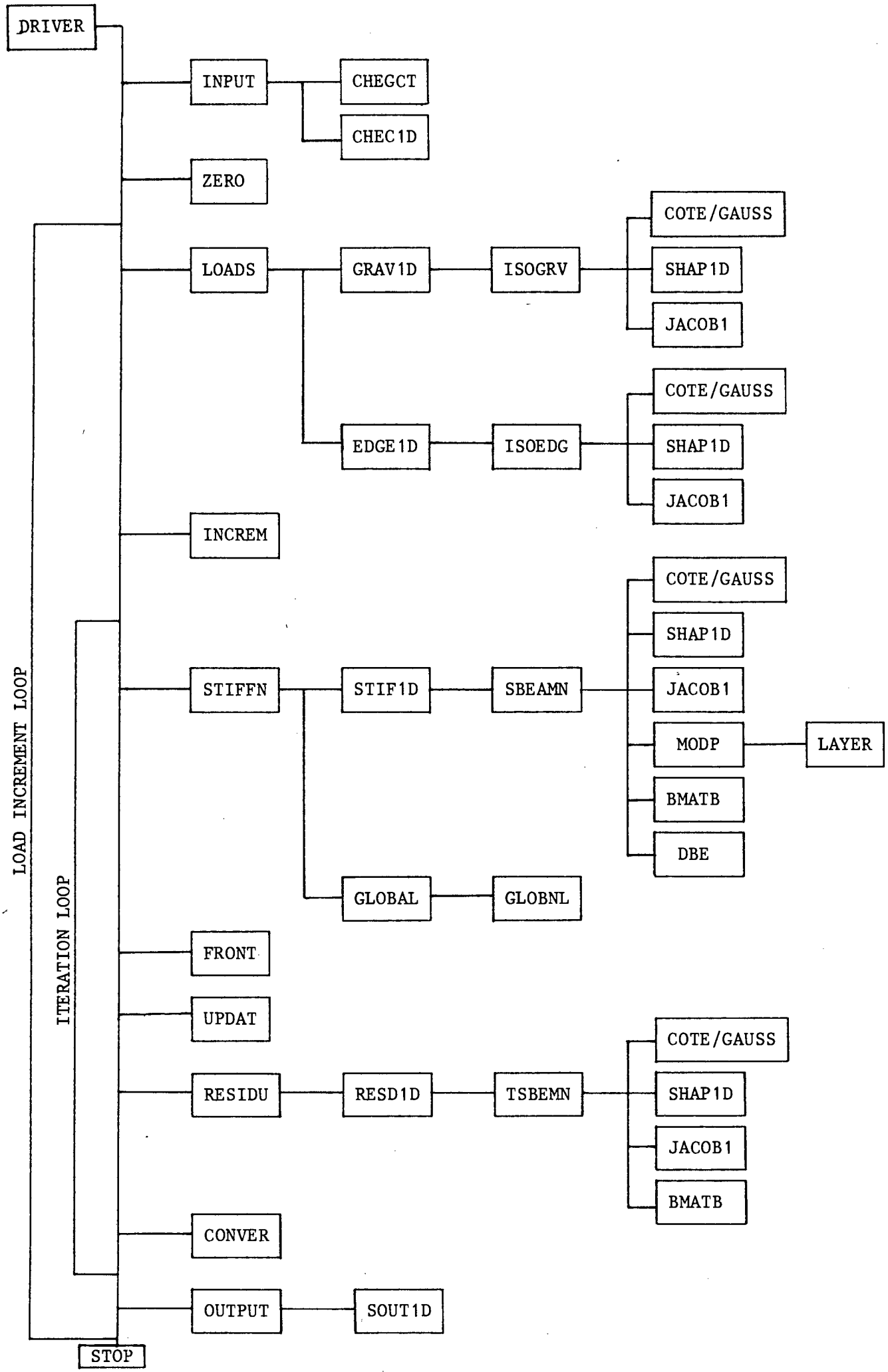

Figure 4.1 Modified NOSTRUM Call-Chart for Nonlinear Stability Analysis.

CHAPTER 5

NUMERICAL EXAMPLES

5.1 Introduction

The numerical examples are aimed at providing the experience necessary to give guidelines for routine analysis of nonlinear frame stability problems as well as to validate the algorithms implemented.

This chapter is divided into four sections. The first section deals with the investigation of the influence of element discretization and numerical integration on the elastic and elastic-plastic finite element solutions. The second section examines the results of small strain, small displacement beam examples with different loading conditions, boundary conditions and cross-sectional shapes. In the third section the ability to simulate elastic and elastic-plastic large deflection bending and buckling problems is considered. The nonlinear geometric behaviour of a cantilever beam-column is compared to results published by Tang et al [18]. Finally, in the fourth section, the nonlinear stability of a two storey frame is modelled. The elastic buckling and the plastic failure loads obtained for the frame are compared to the experimental results of Scholz [6].

5.2 Influence of Element Discretization and Numerical Integration

The effect that the number of elements, the different integration rules and the different Lagrangian element types have on the accuracy of the finite element solution is investigated in this section. The full and reduced Gauss Legendre and Newton Cotes integration rules given in Table 2.3 are used for each element type. The element types employed are the linear (two noded), the quadratic (three noded) and the cubic (four noded) Lagrangian elements.

The numerical results are compared to analytical solutions for the elastic case as well as for the elastic-perfectly plastic case.

The analytical solutions for the elastic problems are obtained from the Principle of Virtual Work. The compatability equation from which the elastic displacements are calculated is given as

$$1.\delta^* = \int_o^{\ell} m^* K \, dx + \int_o^{\ell} s^* \gamma \, dx \quad ,$$

where:

$K = M/EI$;

$\gamma = S/G\hat{A}$, $\hat{A} = A/1.5$;

m^* , s^* , γ^* are the bending moment, shear force and deflection of the virtual system respectively.

The analytical solutions for the plastic limit load are based on a rigid-perfectly plastic moment curvature relationship which neglected the effect of shear.

The structure used in this study is a rectangular cross-section cantilever beam subject to a point load at its end. The geometrical and material properties for this model are given in Figure 5.1(a).

5.2.1 Comparison of the Elastic Solutions

A comparison of the percentage error obtained for the elastic tip displacement is illustrated in Figures 5.2 and 5.3. This percentage error is defined as

$$\% \text{ Error} = \frac{\delta \text{ analytical} - \delta \text{ numerical}}{\delta \text{ analytical}} \times 100 \quad ,$$

where δ is the transverse tip displacement.

The analytical solution will be termed the exact solution for the purposes of this chapter.

For all the element models the solution converged on a displacement result which is within 2.6% of the exact. This discrepancy is related to the insufficient number of layers in the section (six layers in this case). The error is reduced to 0.9% when ten layers are used to model the section. It must be remembered that the layered model is only an approximation discussed in section 2.4.

From Figure 5.2 it is clear that the percentage error for the linear element solutions reduces with an increase in element discretization density. The reduced Gauss Legendre integration rule (1GP) yields results with the lowest errors showing comparatively rapid discretization convergence for six elements to within 2% of the exact. With further elements the solution converges to a value within 2.6% of the exact. The largest errors are obtained using the reduced Newton Cotes integration rule (2NCP) and discretization convergence is slow.

Figure 5.3 shows the results obtained with the quadratic and cubic elements where similar accuracy and convergence trends are evident. The decrease in error with an increasing number of elements, for all integration rules, is more rapid for these two higher order elements. The solutions obtained converge on a result which is within 2.6% of the exact.

In conclusion it can be said that for all elements the most accurate elastic results are achieved with reduced Gauss Legendre integration.

5.2.2 Influence of Element Discretization on the Plastic Limit Load

In the load versus deflection responses for the elastic-perfectly plastic problems presented in this section and throughout the rest of this chapter, plastic collapse is indicated as a horizontal line of constant load with increasing displacement. Numerically, this occurs when the whole section becomes plastic (zero stiffness in the perfectly plastic case) at a specific number of Gauss points which make the structure a mechanism. No further numerical solutions can then be obtained for further increase in load.

As the trends in the solutions using the three different elements are similar only the two noded element with reduced Gauss Legendre integration rule (1GP) is used to study the effect of element discretization on the plastic limit load.

The percentage error in the plastic limit load is defined as

$$\% \text{ error} = \frac{P \text{ numerical} - P \text{ analytical}}{P \text{ analytical}} \times 100 \ ,$$

where P is the value of the plastic limit load.

The elastic-plastic solutions obtained with a number of different discretizations are illustrated in Figure 5.4 where it becomes clear that increasing the number of elements from two to six decreases the error in limit load from 105% to 9%. It is evident that with an increase in the number of elements the element size decreases and thus Gauss points are positioned closer to the support. This permits a more accurate monitoring of the inelastic behaviour in the support zone resulting in better estimates of the limit load.

Using this idea the cantilever beam is modelled using a small four noded element next to the support and one three noded element for the rest of the beam. This model is illustrated in Figure 5.1(b). The corresponding elastic-perfectly plastic load-deflection response is plotted in Figure 5.4. The error in the limit load solution for this mesh is 1.3%.

In conclusion, an efficient model of the structure can be set up by using small elements to model the inelastic zones and large elements for the remaining parts of the model. The small elements mean Gauss points close enough to the plastic 'hinge' positions which permit the accurate modelling of the plastification process. Prior knowledge of the expected areas of plastification is thus helpful.

This can be established by initially modelling the structure with a crude mesh and identifying the zones of highest stress.

5.2.3 Influence of Numerical Integration on the Plastic Limit Load

In this section the effect on the plastic limit load due to the different integration schemes for the three types of elements is investigated. A seven noded finite element mesh is chosen to model the cantilever beam. Thus for the linear, quadratic and cubic elements the model is discretized using six, three and two elements respectively. The elastic-perfectly plastic load-deflection responses for each element type are illustrated in Figures 5.5, 5.6 and 5.7.

The lowest errors in limit load are obtained for each element type using reduced Gauss Legendre integration rules. For this integration scheme the error in limit load decreases from 10.3% for the linear element model to 5.4% for the cubic element model. The largest errors in limit load are obtained using the reduced Newton Cotes rules where the error decreases from 89% for the linear element model to 18.6% for the cubic element model.

In conclusion, it can be said that the best results are obtained for each element type using reduced Gauss Legendre integration. In addition, there is reduction in error with an increase in the order of the element used in the model (from a linear to a cubic element).

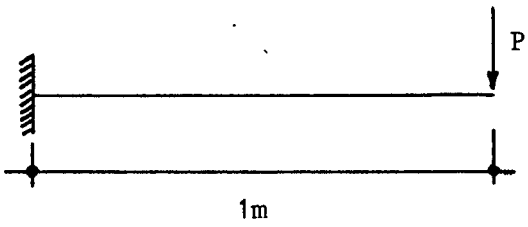

1. Material Properties

$E = 210 \times 10^6$ MPa

$G = 80.769 \times 10^6$ MPa

$I = 337.5 \times 10^{-6}$ m4

$\nu = 0.3$

$\sigma_y = 250 \times 10^3$ MPa

$A = 0.045\ m^2$

$\hat{A} = A/1.5$

$\ell/d = 3^1/_3$

2. Cross-Section

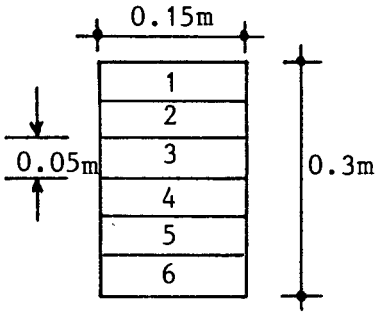

Cross-section modelled using 6 equal layers of 0.05 x 0.15

Figure 5.1(a) Geometric and Material Properties of Cantilever Test Model.

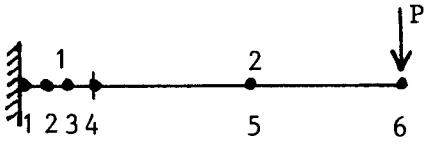

Node	x(m)
1	0.000
2	0.033
3	0.066
4	0.100
5	0.550
6	1.000

Figure 5.1(b) Refined Finite Element Model using One Four Noded Element and One Three Noded Element.

Figure 5.1 Cantilever Test Model.

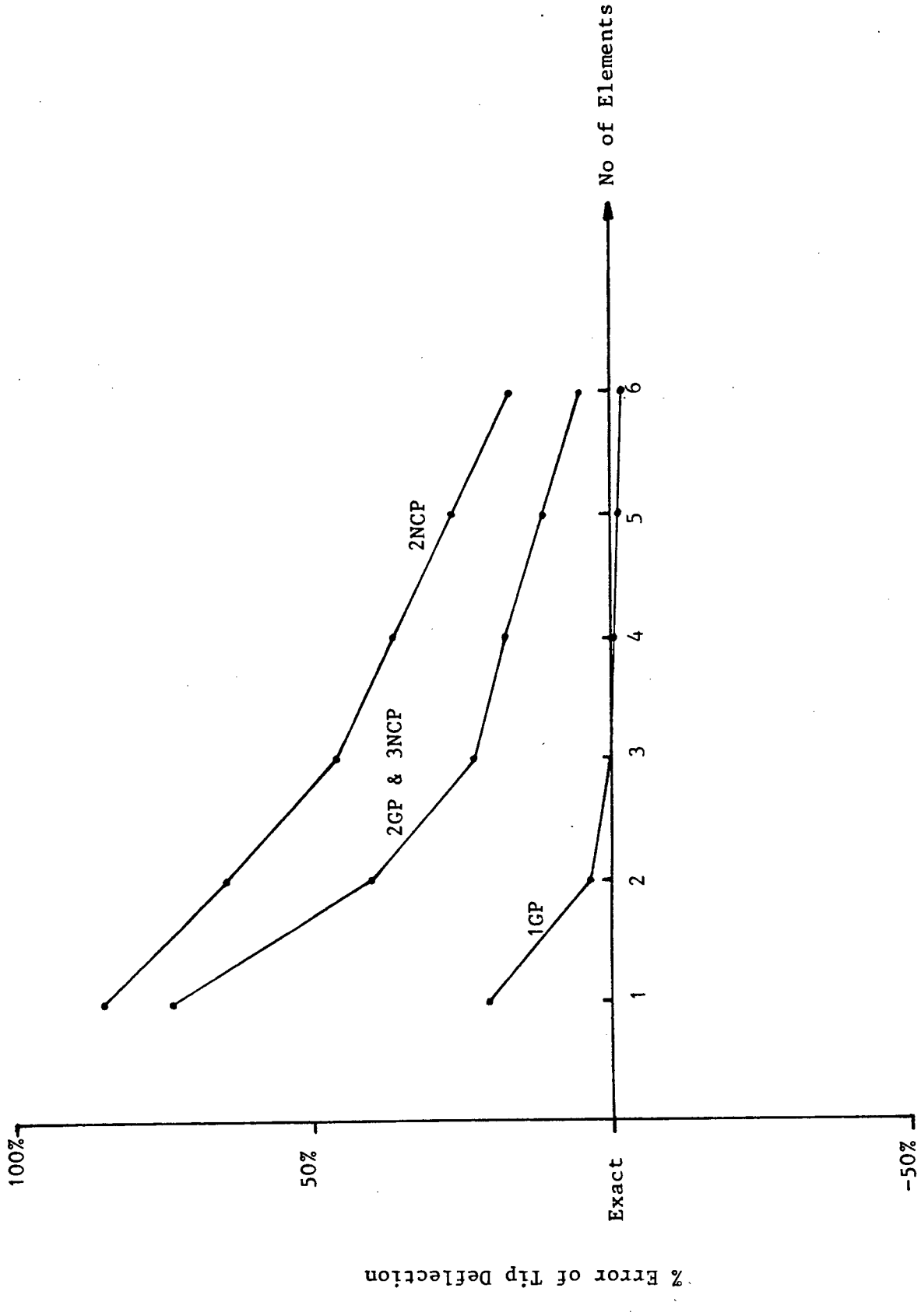

Figure 5.2 Error Analysis for the Two Noded Element Model in the Elastic Range.

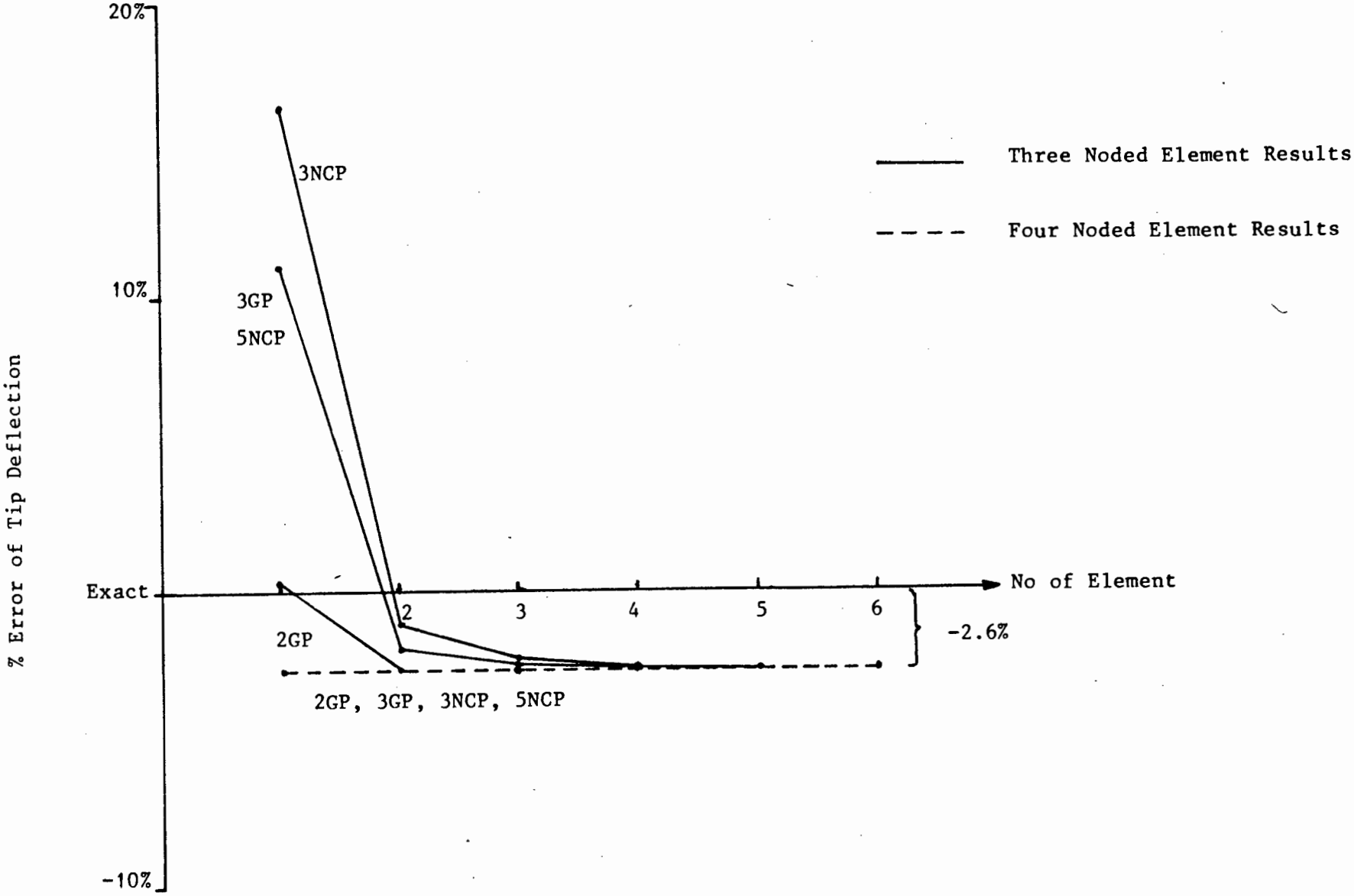

Figure 5.3 Error Analysis for the Three and Four Noded Element Models in the Elastic Range.

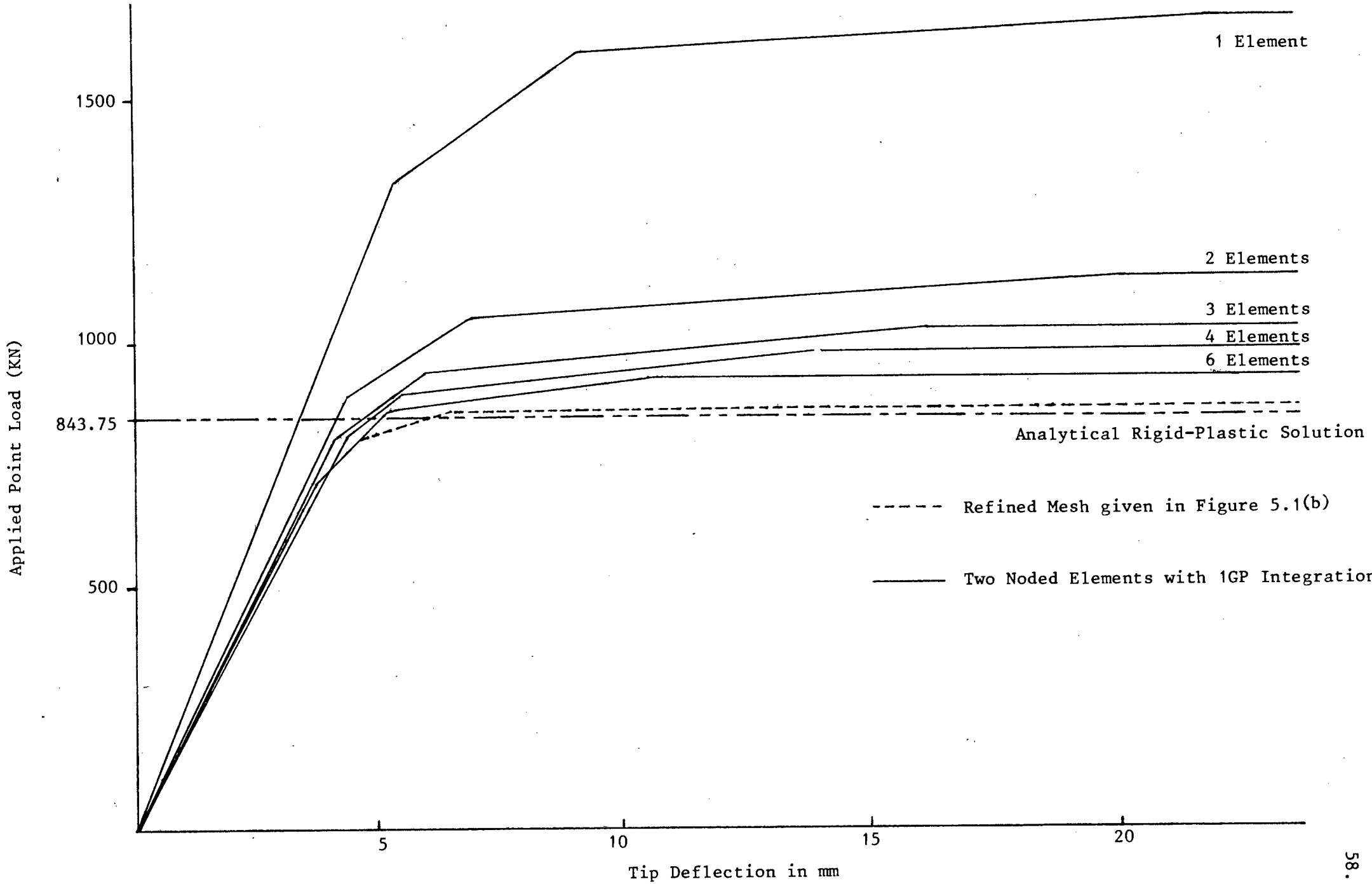

Figure 5.4 Effect of Element Discretization on Plastic Limit Load.

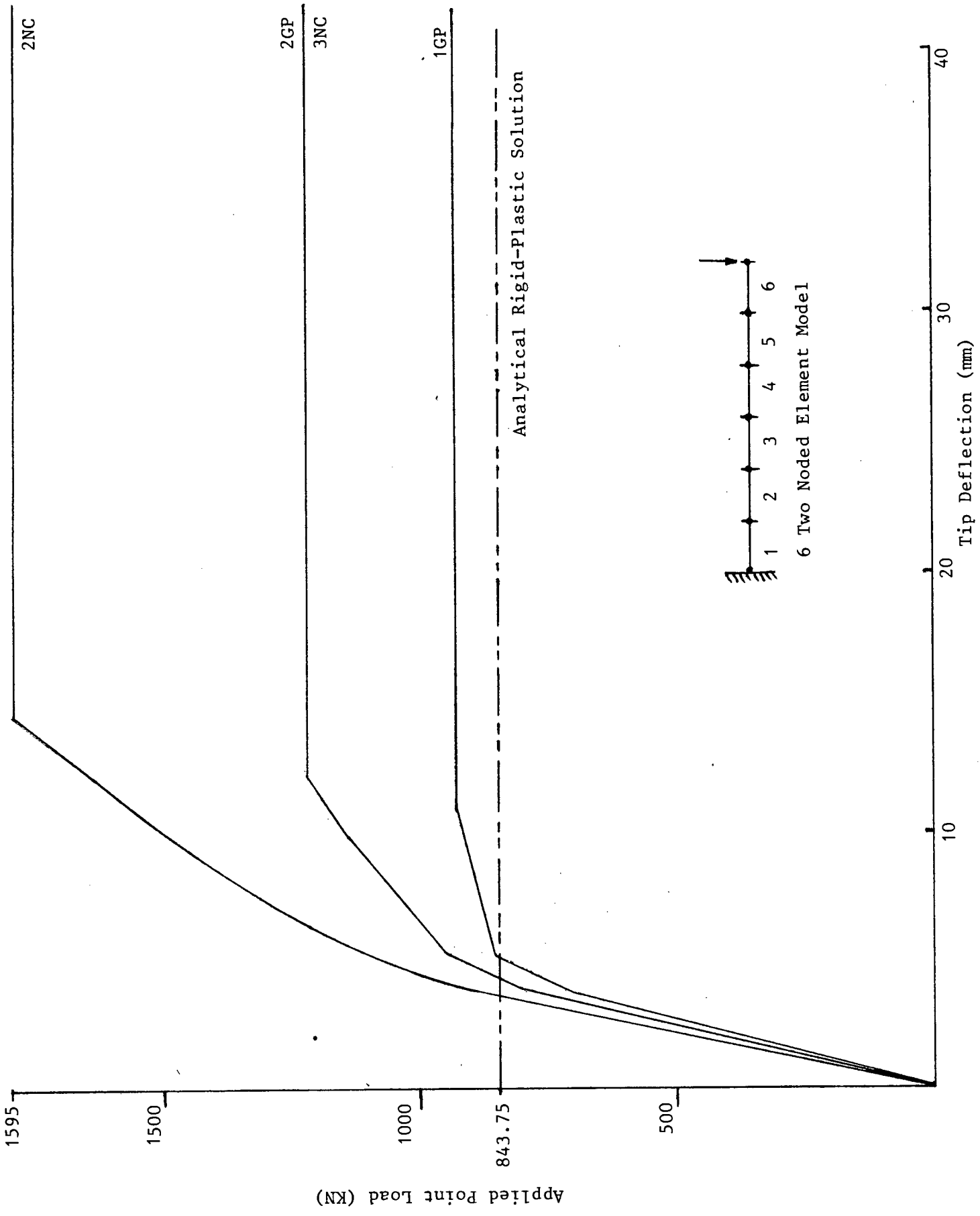

Figure 5.5 Effect of Numerical Integration on Plastic Limit Load for the Two Noded Element Model.

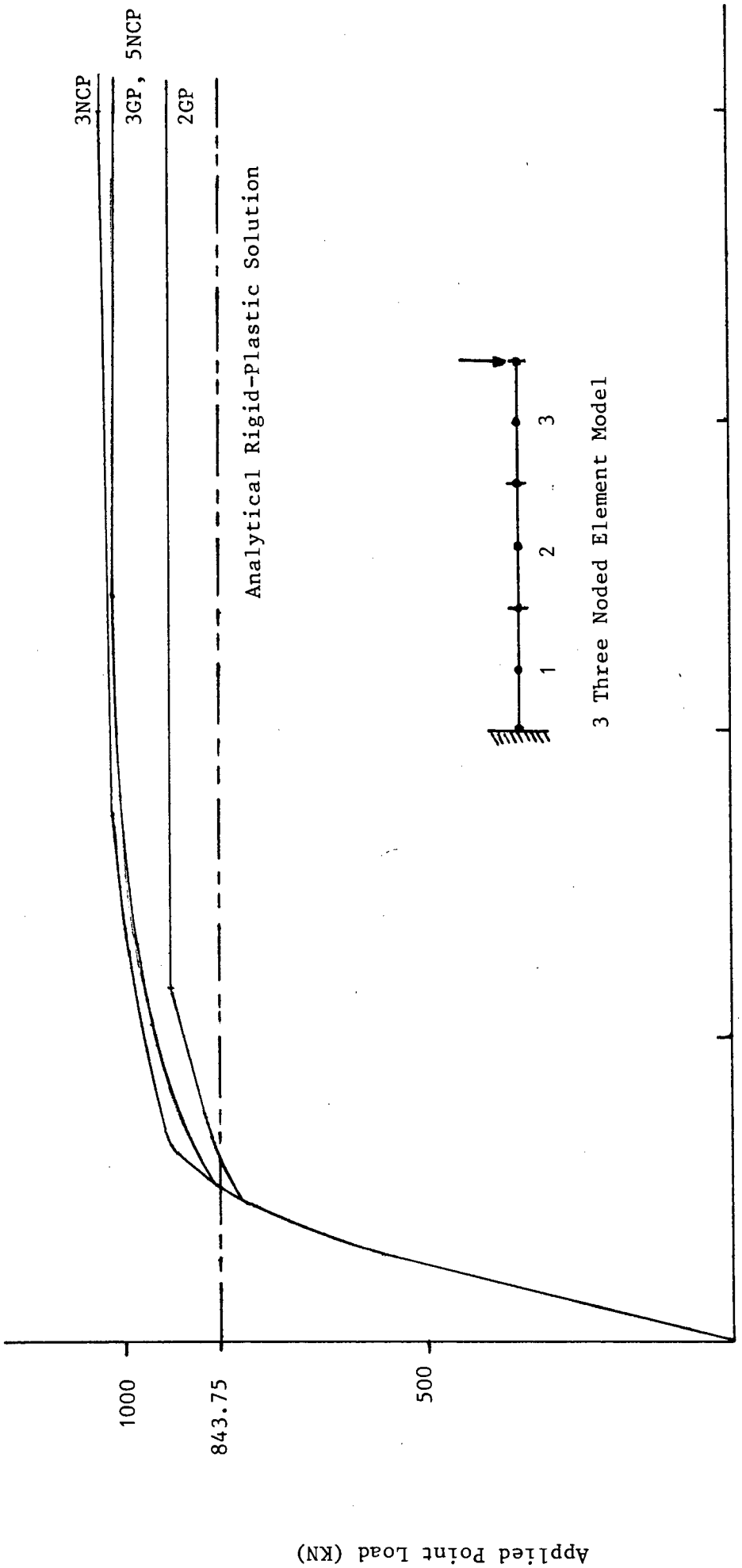

Figure 5.6 Effect of Numerical Integration on Plastic Limit Load for the Three Noded Element.

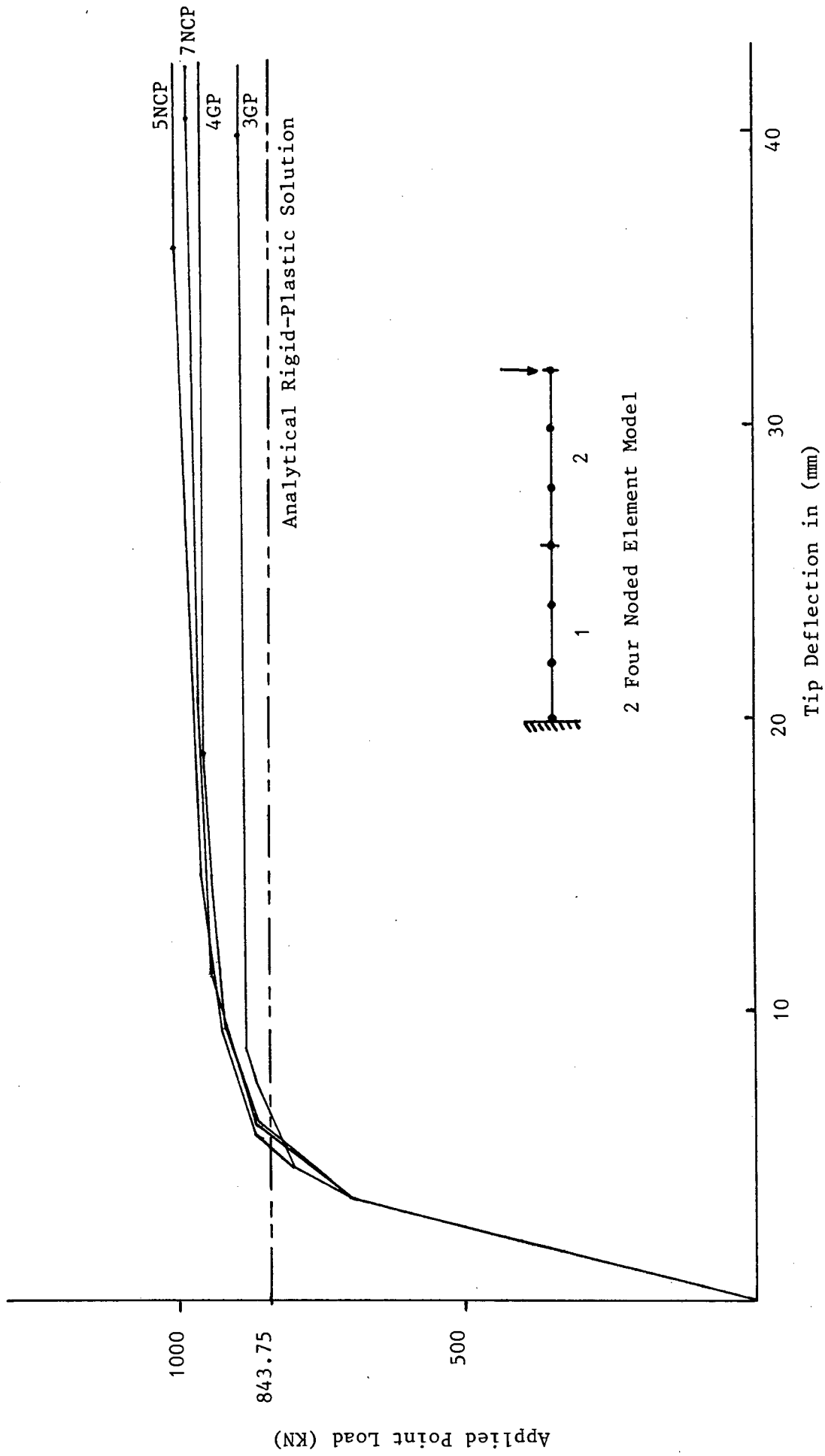

Figure 5.7 Effect of Numerical Integration on the Plastic Limit Load for the Four Noded Element.

5.3 Small Strain, Small Displacement Beam Examples

Three examples are chosen to investigate the effect different loading conditions, boundary conditions and cross-sectional properties have on the finite element solutions. For each example a three meter beam is modelled using ten linear elements with reduced Gauss Legendre integration (1GP).

5.3.1 Simply Supported Rectangular Cross-Section Beam Subject To a Point Load at Midspan

The geometric and material properties for this example are given in Figure 5.8. The elastic solution for this problem is within 1.8% of the analytical value. In Figure 5.9(a) a plot of the elastic-perfectly plastic load-deflection response is shown. The error in the plastic limit load is 12%. The bending moment diagram at plastic collapse for the numerical and analytical solutions is given in Figure 5.9(b). The peak moment in Figure 5.9(b) is equal to the ultimate moment of the section, 843.75KNm, which is calculated from the material and geometric properties of the section. From this value the analytical limit load of the structure can be calculated. The numerical solution limit load is greater than the analytical value as no Gauss points are situated at the peak moment position. Hence the load has to be increased until the moment at the Gauss points closest to midspan reaches the value of the ultimate moment of the section. It is evident that a more accurate approximation to the limit load could be obtained using smaller elements in the midspan region.

Figure 5.10 shows the effect of modelling the section with different numbers of layers on the quality of the elastic deflection. The elastic-perfectly plastic response for the two layered, six layered and ten layered models are shown in Figure 5.9(a). It becomes clear in this case that six to ten layers are necessary to model the section adequately (i.e. $d_n/d \leqq 0.175$).

5.3.2 Clamped I Beam with Uniformly Distributed Loading

The geometric and material properties for this example are given in Figure 5.11. The elastic solution is within 2.9% of the analytical value. A plot of the elastic-perfectly plastic response is given in Figure 5.12(a). The error in the plastic limit load is 26.4%. The bending moment diagram at plastic collapse for the numerical and analytical solutions is given in Figure 5.12(b). As described in the previous example, the peak moments in the bending moment diagram at plastic collapse are equal to the ultimate moment of the section, 196KNm. As the degree of mesh refinement is crude in the vicinity of the peak moment locations, especially where $\frac{dM}{dx}$ is large, the value of the limit load is higher than that calculated from the ultimate sectional moment.

In this example a study of the accuracy of the stress resultants calculated numerically for the different integration rules was carried out. It was found that the least errors were obtained using the reduced Gauss Legendre integration rule.

5.3.3 Simply Supported I Beam with Uniformly Distributed Loading

The geometric properties, material properties and loading conditions for this example are the same as those given in section 5.3.2. The elastic solution is within 0.9% of the analytical value. A plot of the elastic-perfectly plastic load-deflection response is given in Figure 5.13(a). The error in the plastic limit load is 2.8%. From Figure 5.13(b) it is clear that the bending moment values at the gauss points are very close to the analytical values with the highest errors being 1%. At the position of highest moment $\frac{dM}{dx}$ tends to zero and hence a relatively crude mesh can provide an accurate approximation of the plastic limit load.

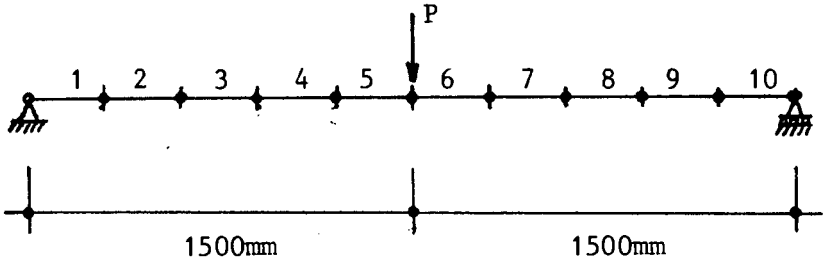

1. Ten, Two Noded Elements

2. 1 GP Integration Rule used per Element

3. Material Properties

$E = 210 \times 10^6$ MPa

$G = 80.769 \times 10^6$ MPa

$I = 337.5 \times 10^{-6}$ m^4

$\nu = 0.3$

$\sigma_y = 250 \times 10^3$ MPa

$A = 0.045$

$\hat{A} = A/1.5$

$\ell/d = 10$

4. Cross-Section

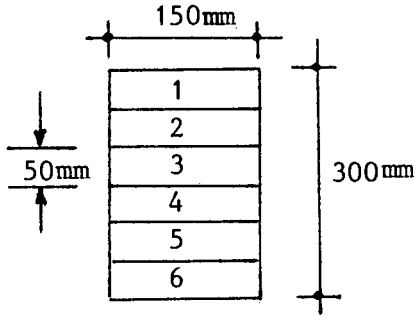

Six equal layers are used to Model the Rectangular Section.

Figure 5.8 Finite Element Model with Geometric and Elastic Material Properties, for a Simply Supported Rectangular Cross-Section Beam with a Point Load at Midspan.

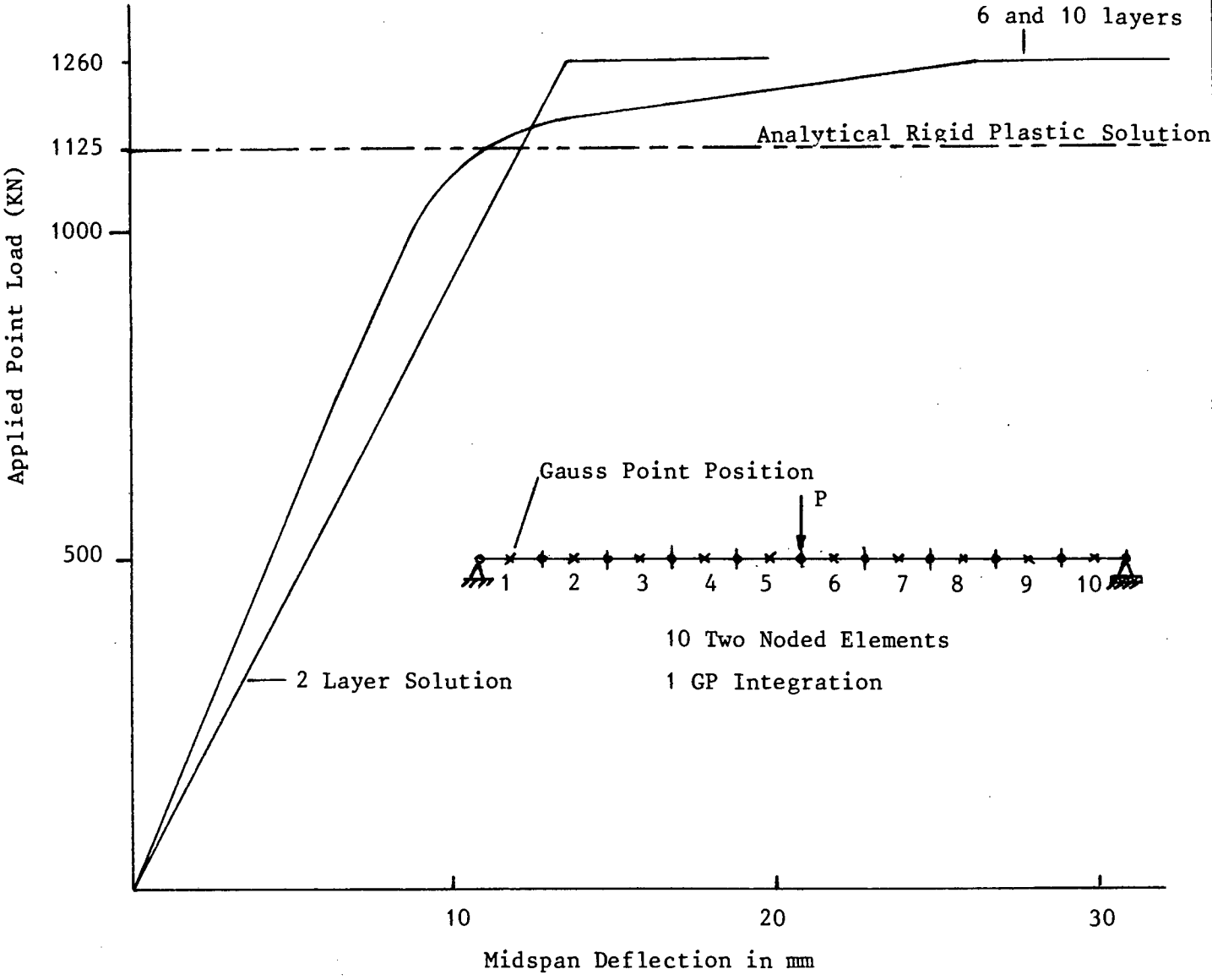

Figure 5.9(a) Load Versus Mid-Deflection Elastic-Plastic Response.

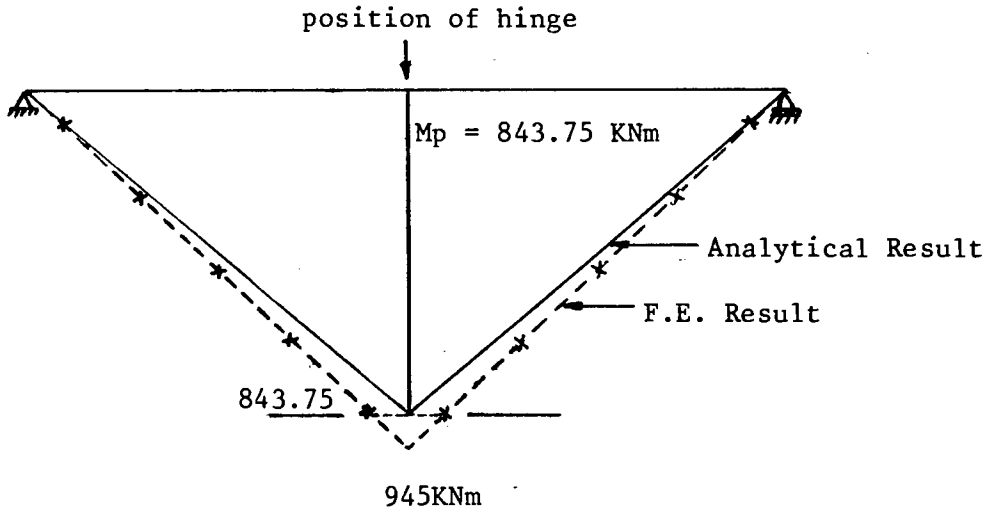

Figure 5.9(b) Bending Moment Diagram at Plastic Collapse.

Figure 5.9 Simply Supported Beam with Central Point Load.

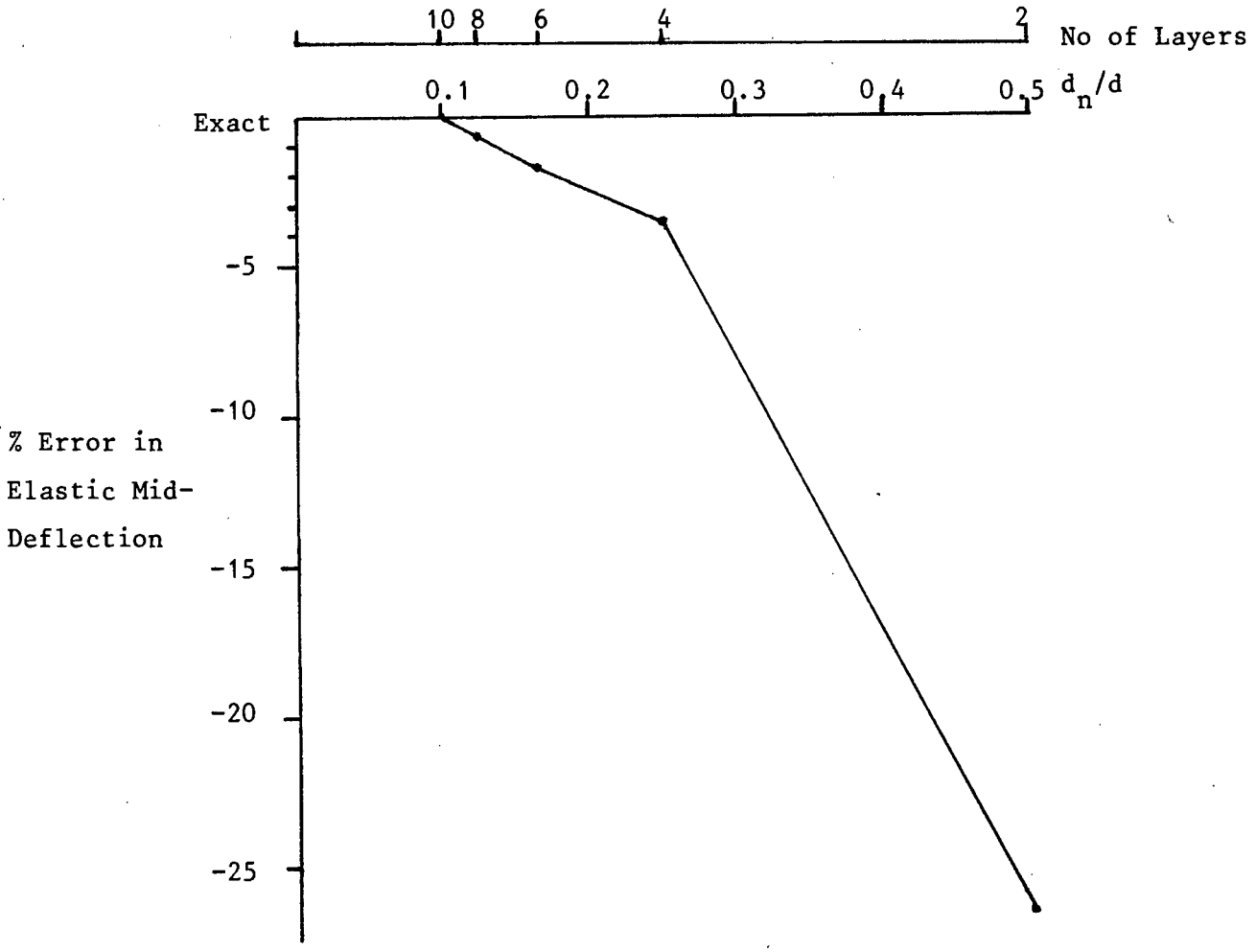

- d_n is the thickness of a layer

- d is the depth of the section

Figure 5.10 Effect of Layer Discretization of the Section on the Accuracy of the Elastic Solution.

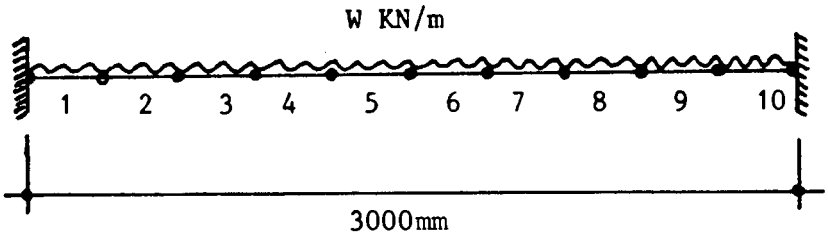

1. Ten, Two Noded Elements

2. 1GP Integration Rule used per Element

3. Material Properties

$E = 210 \times 10^{6}$ MPa

$G = 80.769 \times 10^{6}$ MPa

$I = 68.48 \times 10^{-6}$ m^4

$\nu = 0.3$

$\sigma_y = 250 \times 10^{3}$ MPa

$A = 0.0096$

$\hat{A} = A/1.5$

$\ell/d = 15$

4. Cross-Section

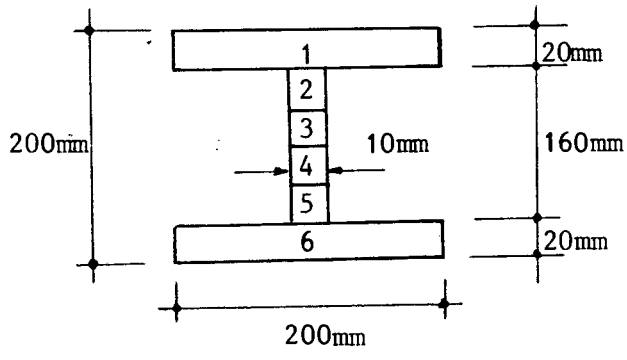

Six Layers used to Model Cross-Section, One Layer (200 x 20) for each Flange and Four Layers (10 x 40) for the Web.

Figure 5.11 Finite Element Model with Geometric and Elastic Material Properties for a Clamped I Beam with Distributed Loading.

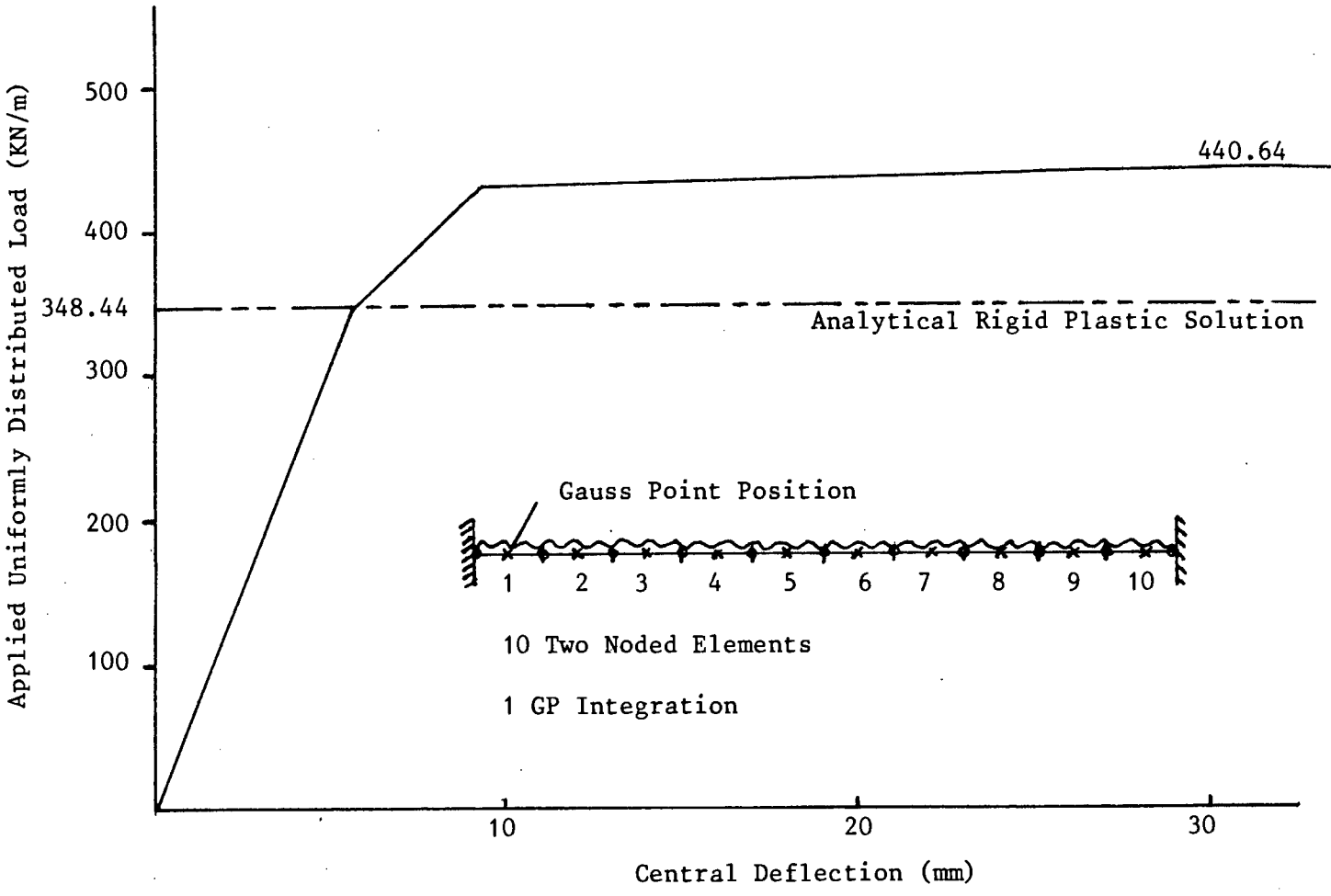

Figure 5.12(a) Load Versus Mid-Deflection Elastic-Plastic Response.

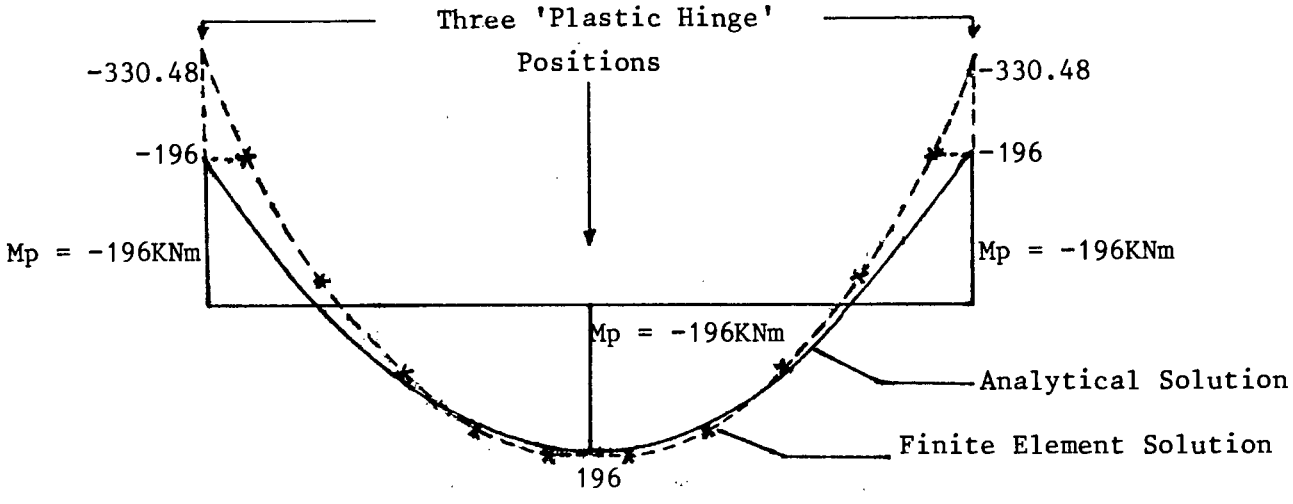

Figure 5.12(b) Bending Moment Diagram at Plastic Collapse.

Figure 5.12 Clamped I Beam with Uniformly Distributed Loading.

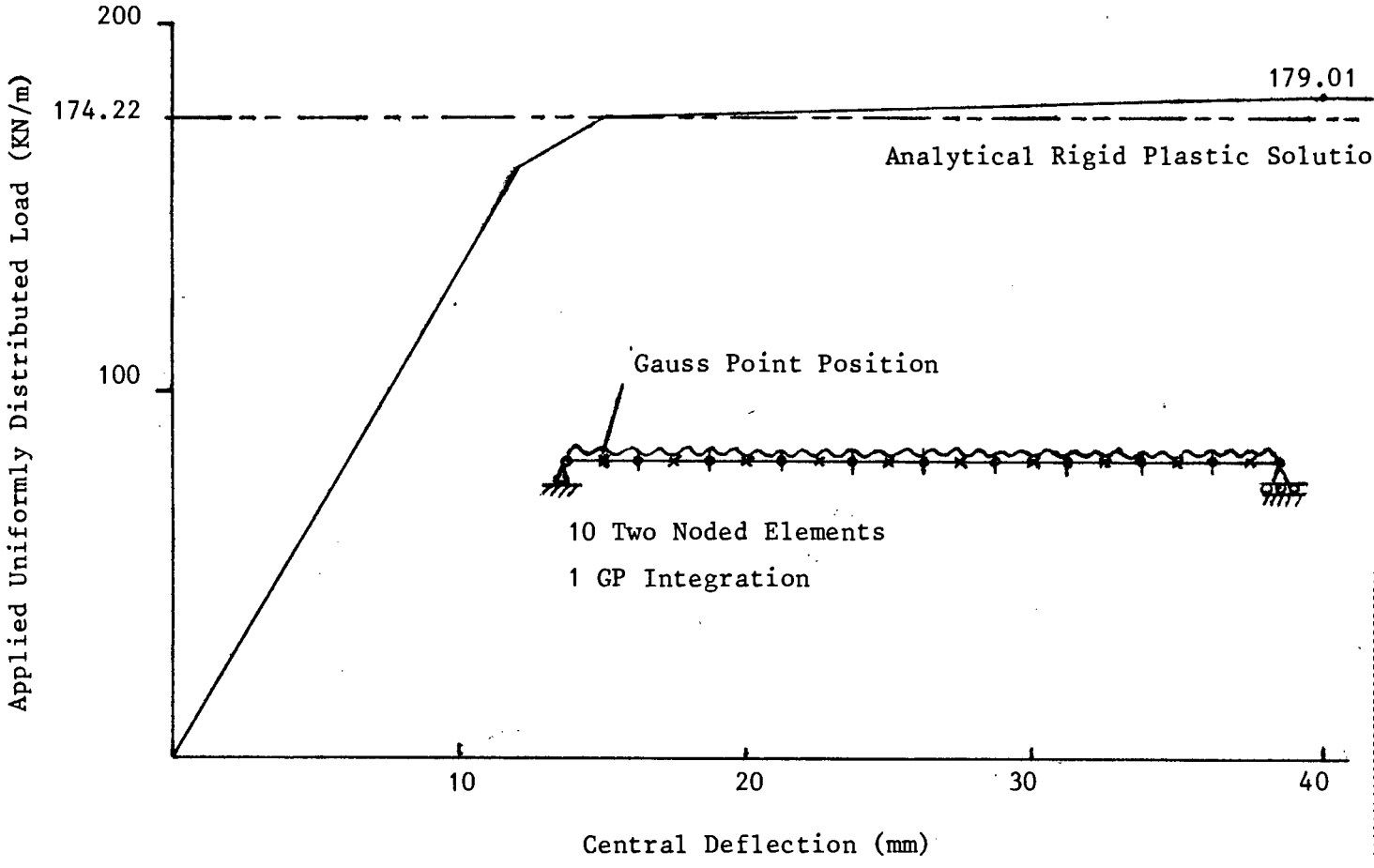

Figure 5.13(a) Load Versus Mid-Deflection Elastic-Plastic Response.

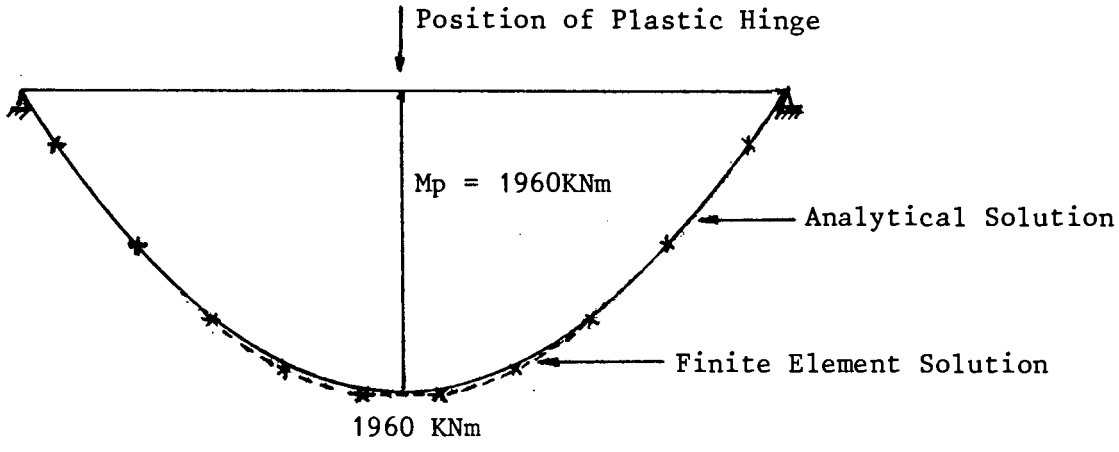

Figure 5.13(b) Bending Moment Diagram at Plastic Collapse.

Figure 5.13 Simply Supported I Beam with Uniformly Distributed Loading.

5.4 Elastic and Elastic-Plastic Large Deflection Bending and Buckling Examples

To evaluate the ability of the present simplified nonlinear geometric algorithm to model large deflection elastic and elastic-plastic problems, the four examples considered by Tang et al [18] are investigated. These examples are: elastic-bending; elastic-buckling; elastic-plastic-bending; and elastic-plastic-buckling. In each example a rectangular cross-section cantilever beam is used. The geometric and material properties as well as the finite element mesh used, are given in Figure 5.14.

Tang et al [18] use an Updated Lagrangian formulation. Their results which compare favourably with an analytical solution [19] are used as a check for the numerical solutions given in this section. The loading increments used by Tang et al [18] are adapted in this work and no further attempt is made to investigate the efficiency of the solutions obtained with different loading increments.

5.4.1 Elastic-Bending

A load increment of $\Delta P = 44.48N$, [18] , and a force tolerance of 0.5% are used in this analysis. In the present study, results could only be obtained for loads up to P = 2668N. This corresponds roughly to displacements of the order of the dimensions of the structure. For higher applied loads the solution did not converge. Smaller load steps and slacker tolerances were used in the analysis but no further convergence could be achieved. There is a close agreement between the numerical results obtained and those given in reference [18]. The elastic load-deflection response is plotted in Figure 5.15. Some of the deflected shapes of the cantilever for loads up to 2668N are illustrated in Figure 5.16.

5.4.2 Elastic-Buckling

A small transverse load of 44.8N is applied to the tip of the beam-column to trigger buckling. This load is maintained while the axial load P is increased. The plot of the elastic, buckling and post-buckling load-deflection response is given in Figure 5.17. Results were obtained for loads up to P = 38125.7N which corresponds roughly to displacements of the order of dimensions of the structure. For higher loads the solution did not converge. Smaller load steps and slacker tolerances were used in the analysis but no further convergence could be achieved. The present numerical results are similar to those obtained in [18], although at higher loads the two solutions deviate slightly. Buckling interpreted as a large increase in displacement for little or no increase in load occurs at a load similar to the small deflection theory critical buckling load, $P_{cr} = \frac{\Pi^2 EI}{4\ell^2} = 13718N$. Some of the deflected shapes of the cantilever beam-column for loads up to P = 38125.7N are shown in Figure 5.18.

5.4.3 Elastic-Plastic-Bending

The load increment, $\Delta P = 4.448N$, suggested in [18] is used again together with a force tolerance of 0.5%. Results could only be obtained for loads up to P = 3378N which corresponds roughly to displacements of the order of the dimensions of the structure. For higher loads the solution did not converge. Smaller load steps and slacker tolerances were used in the analysis but no further convergence could be obtained. There is a close agreement between the numerical results obtained in this work and those in [18] . The elastic-plastic load-deflection response is given in Figure 5.19. Some of the deflected shapes of the cantilever for loads up to P = 3378N are illustrated in Figure 5.20.

5.4.4 Elastic-Plastic-Buckling

In this example a displacement controlled solution procedure using a prescribed axial displacement increment $\Delta u = -2.54 \times 10^{-2}$ mm is used in the analysis. A small transverse load of 155.7N applied to the tip of the beam-column is used to trigger the buckling mode. The plot of the elastic-plastic-buckling and post-buckling load-deflection response is given in Figure 5.21. The elastic-plastic-buckling is indicated by a region of the response where a sharp decrease in load occurs followed by an increase in displacement with no further change in load. The peak load obtained before the onset of elastic-plastic-buckling is 1340N. This value is greater than the value of 1200N obtained for the same problem in reference [18]. Smaller increments in displacement were used and the same results were obtained.

The values obtained for the post-buckling behaviour are the same for both solutions. Some of the deformed shapes of the beam-column for various amounts of prescribed displacement are shown in Figure 5.22.

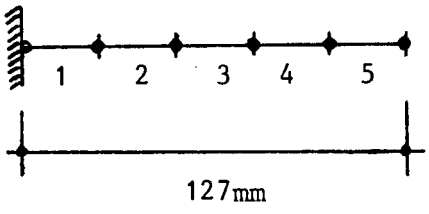

1. Five, Two Noded Element Models

2. 1 GP Integration Rule per Element

3. Material Properties

$E = 207 \times 10^3$ N/mm^2

$G = 7961.538$ N/mm^2

$H' = 7137.93$ N/mm^2

$\nu = 0.3$

$\sigma_y = 207$ N/mm^2

$A = 32.258$ mm^2

$\hat{A} = A/1.5$

$I = 433.574$ mm^4

$\ell/d = 10$

4. Cross-Section

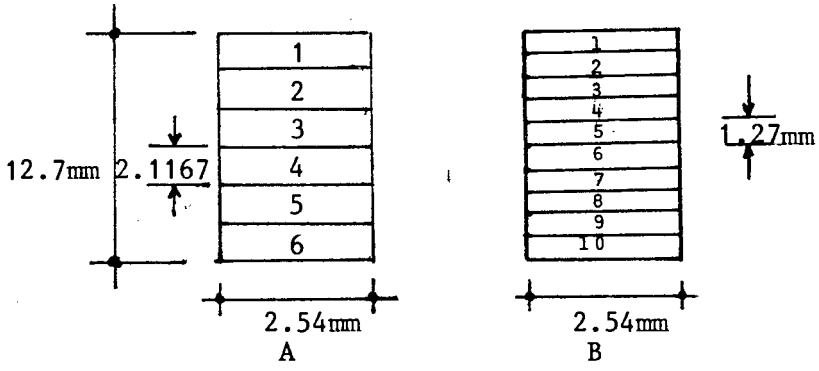

- A is used to model the cross-section for the elastic analysis.
- B is used to model the cross-section for the elastic-plastic analysis.

Figure 5.14 Geometric and Material Properties of Finite Element Cantilever Test Model for Nonlinear Geometric Behaviour.

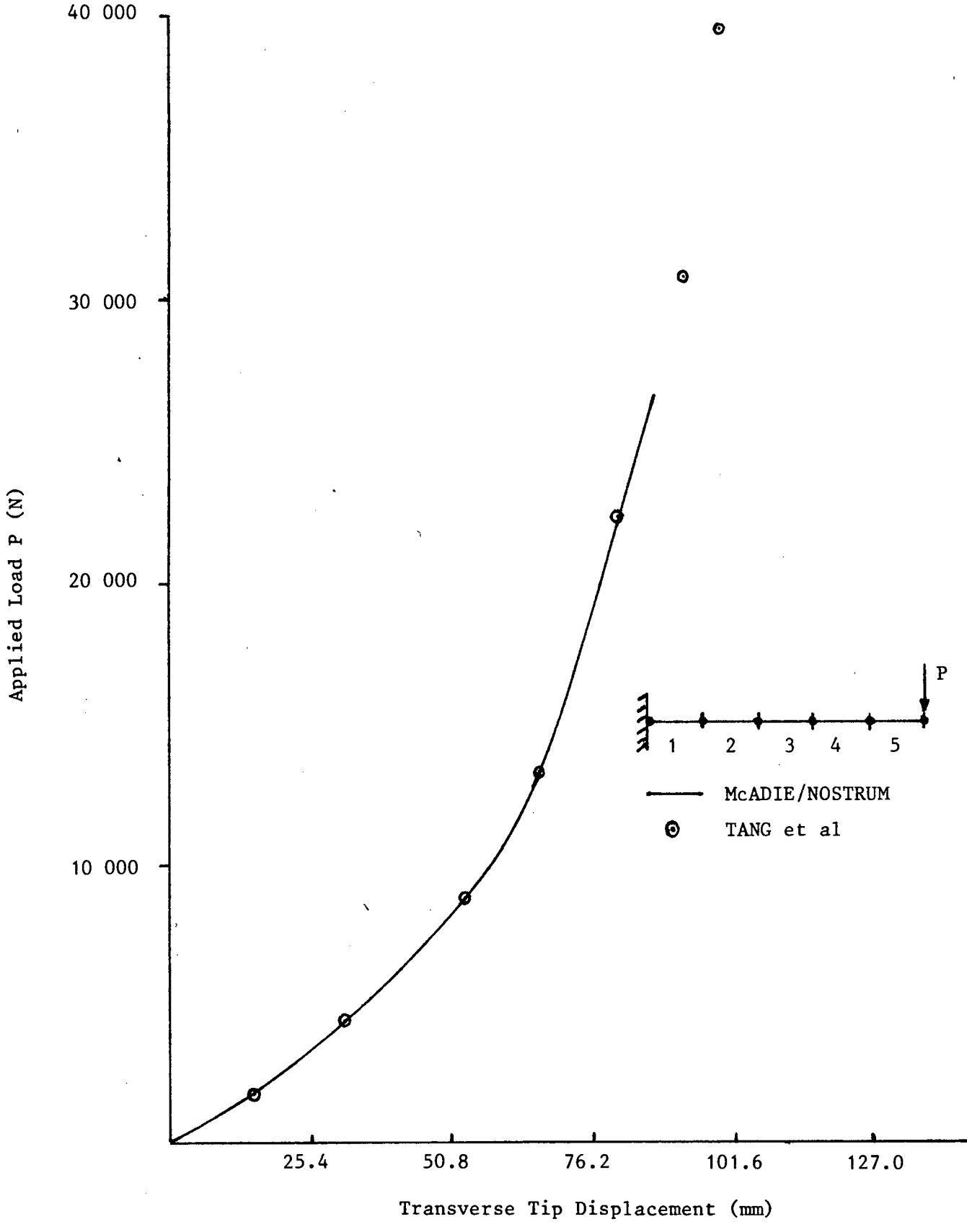

Figure 5.15 Load versus Deflection Response for an Elastic Cantilever Beam under Transverse Load.

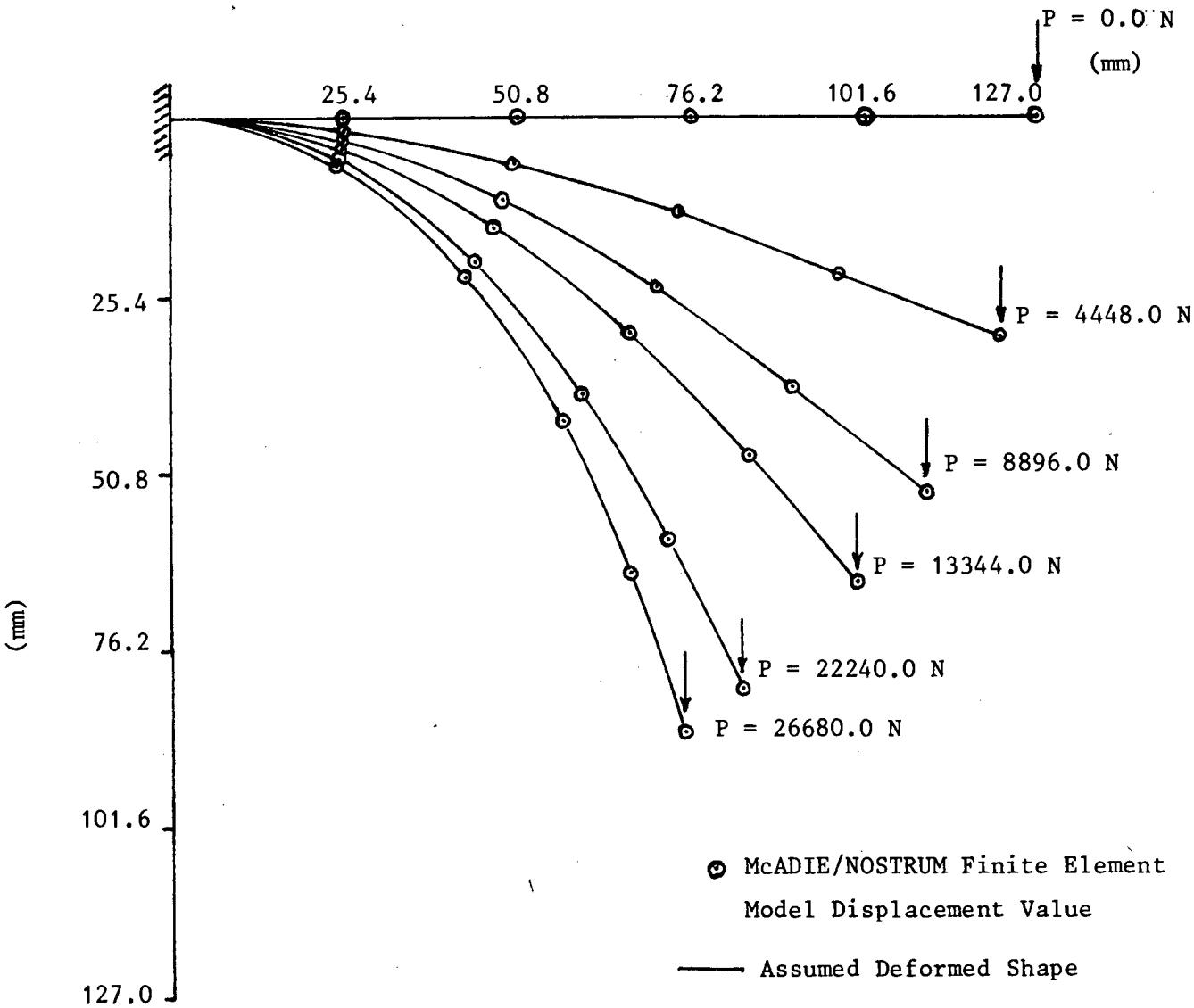

Figure 5.16 Deformed Shapes for Various Amounts of Transverse Load Acting on the Elastic Cantilever Beam.

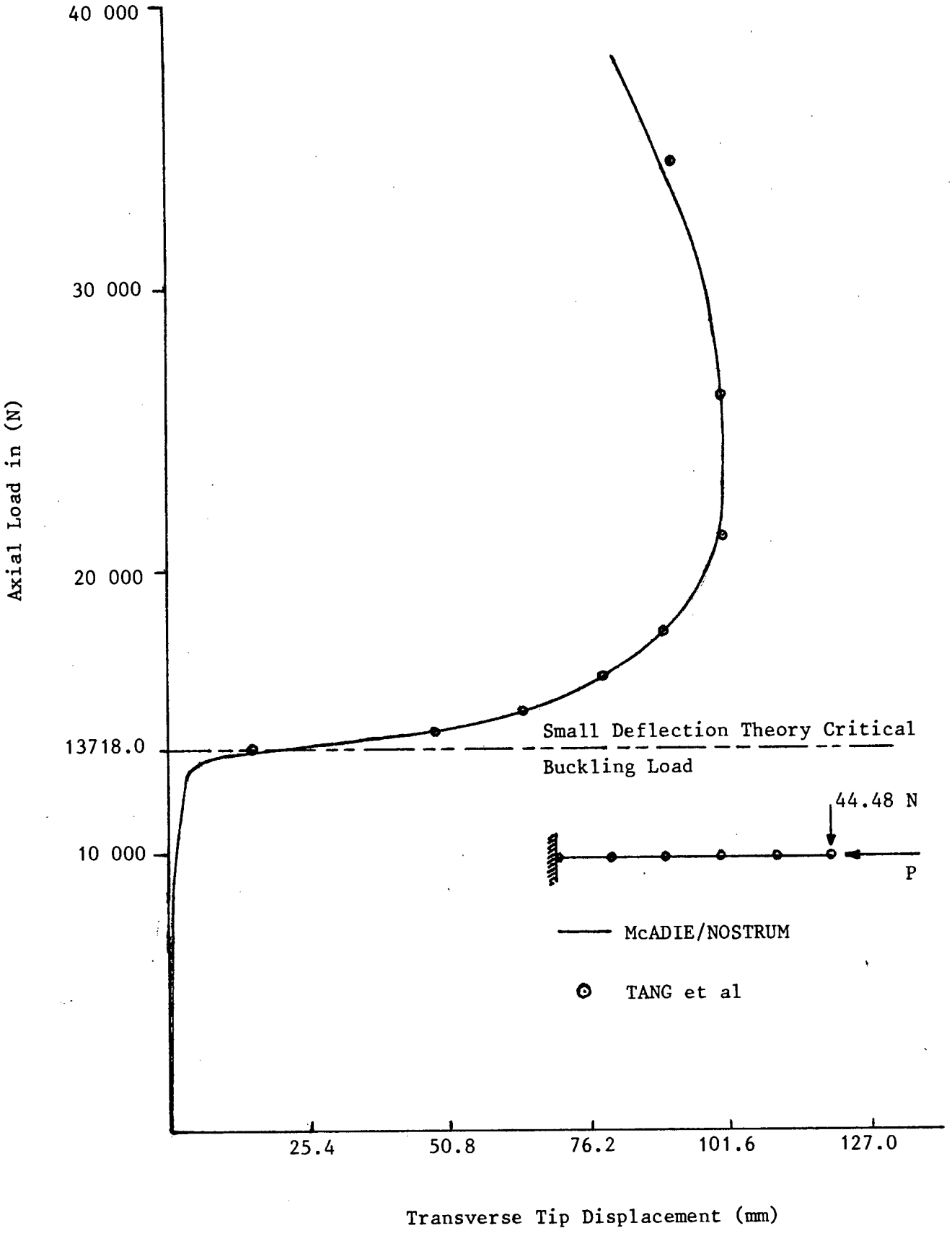

Figure 5.17 Buckling and Postbuckling Response of an Elastic Cantilever Beam.

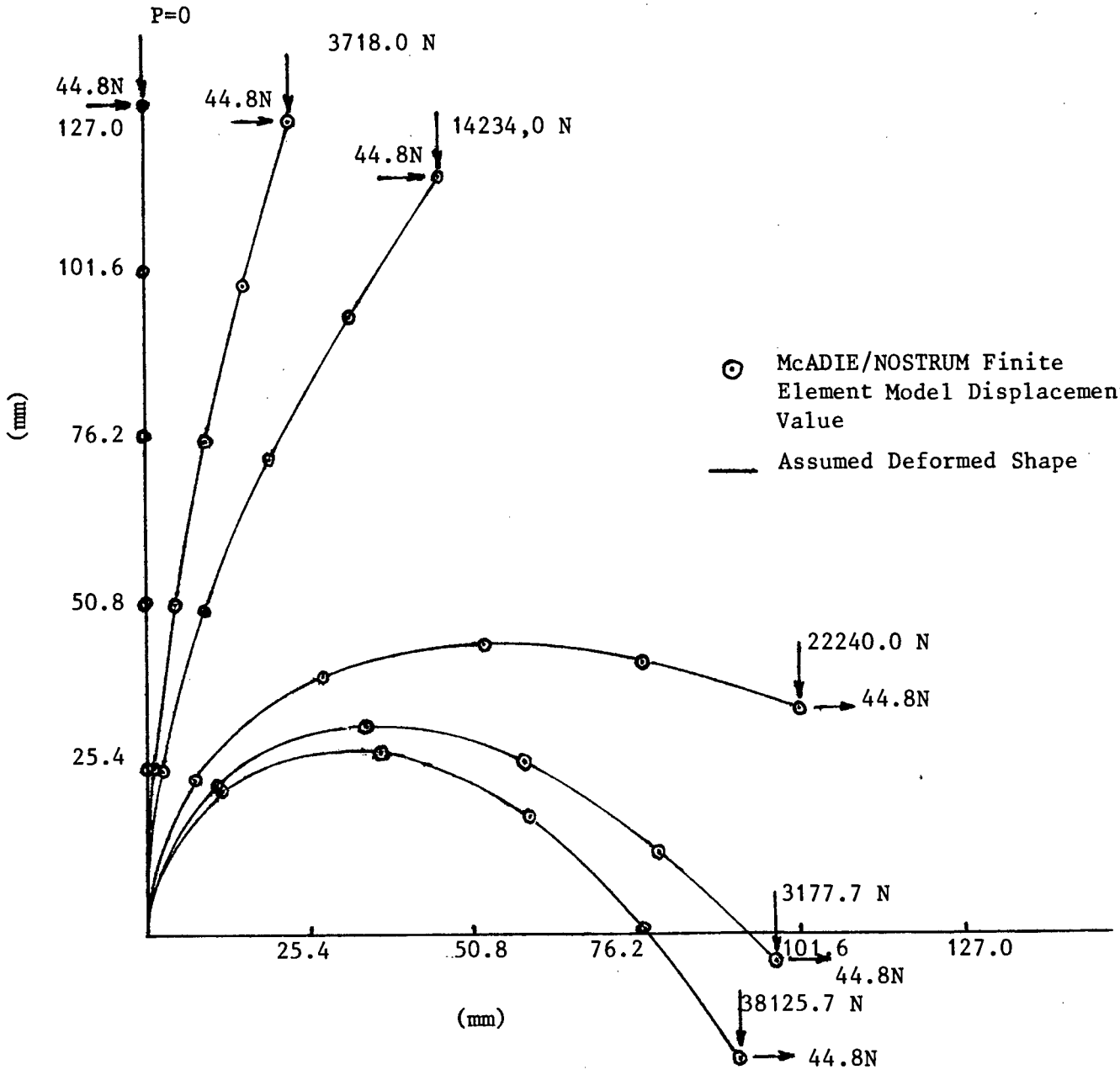

Figure 5.18 Deformed Shapes for Various Amounts of Axial Load Acting on the Elastic Cantilever Beam.

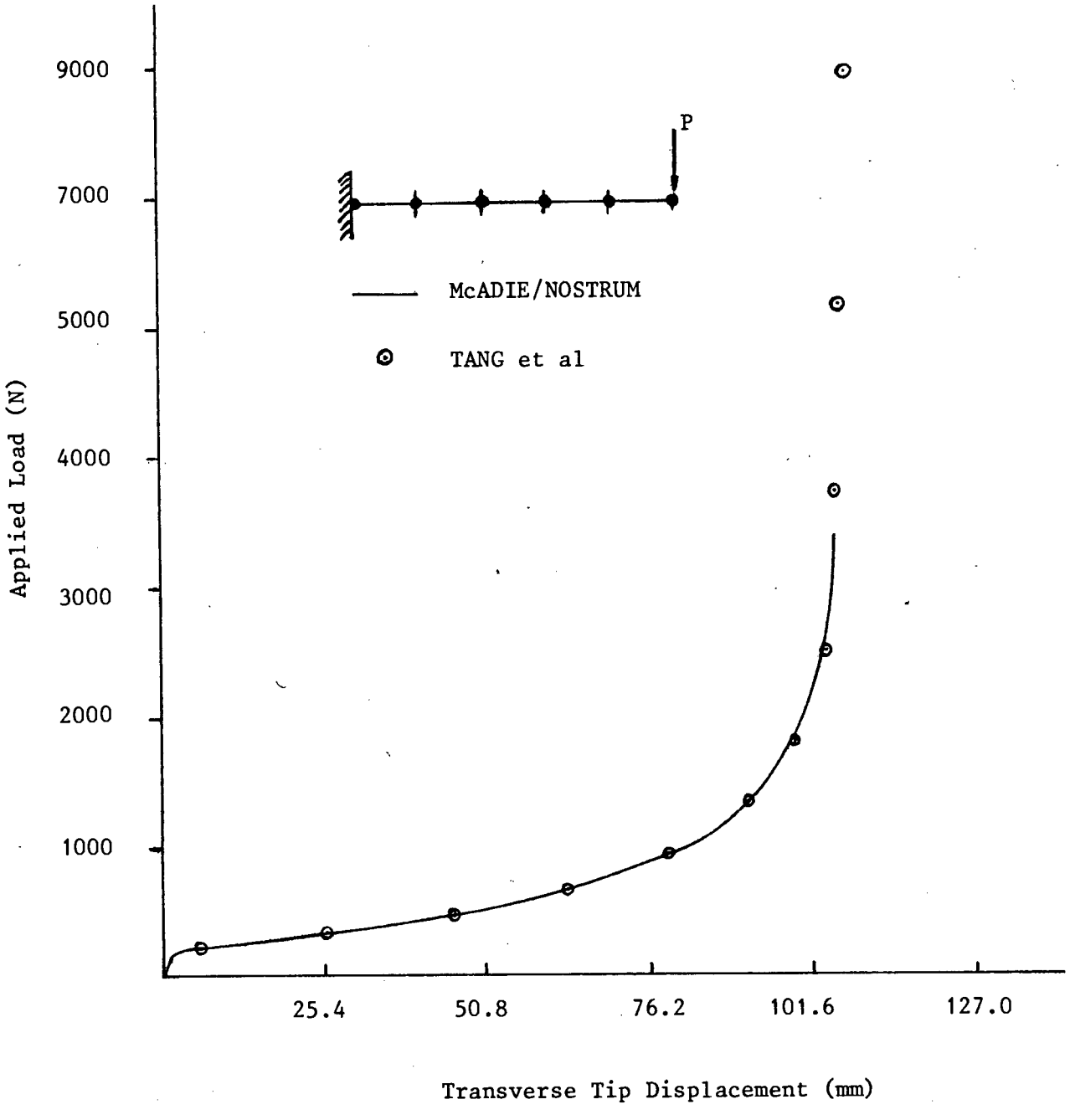

Figure 5.19 Load versus Deflection Response for an Elastic-Plastic Cantilever Beam under a Transverse Load.

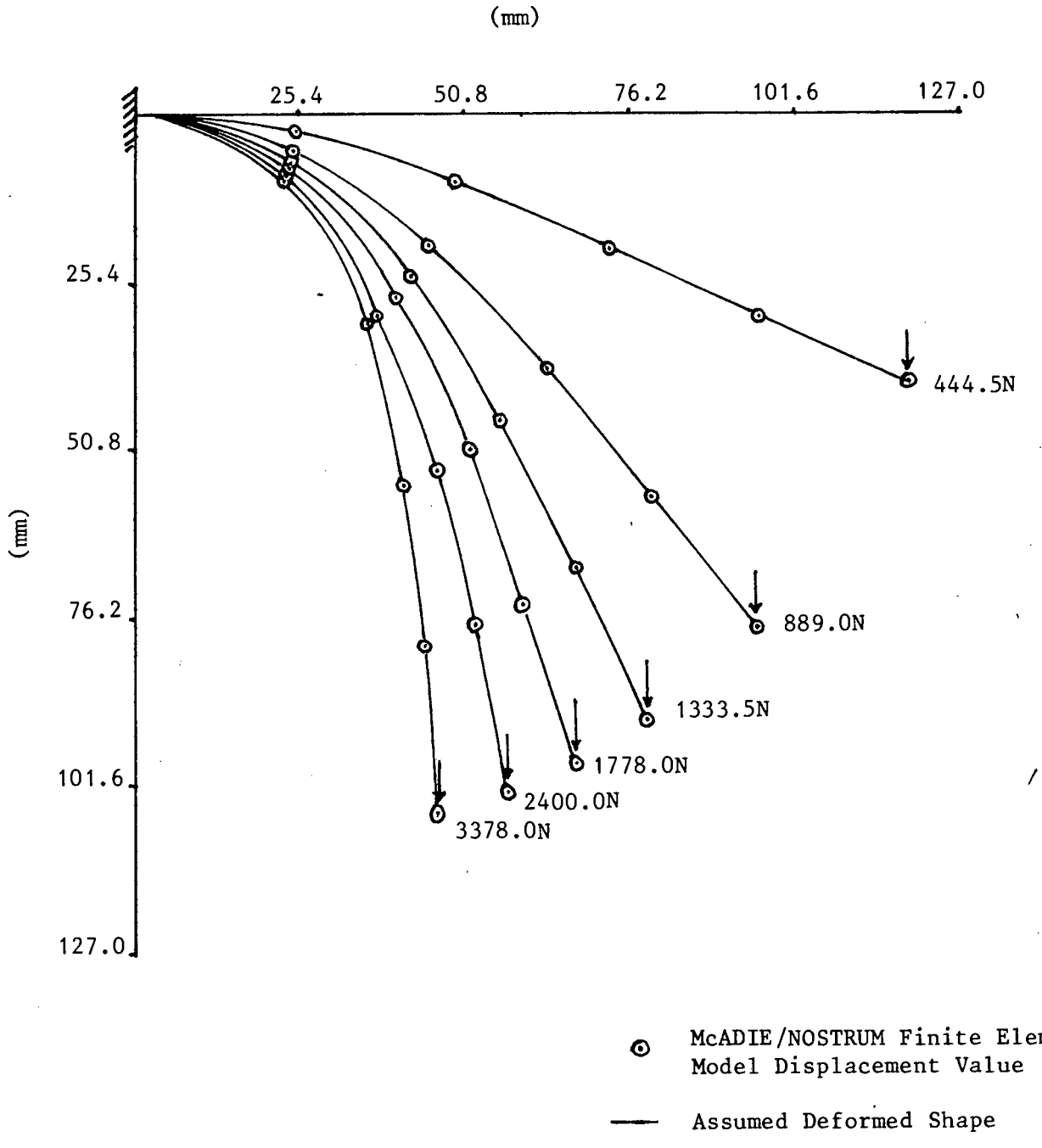

Figure 5.20 Deformed Shapes for Various Amounts of Transverse Load Acting on the Elastic-Plastic Cantilever Beam

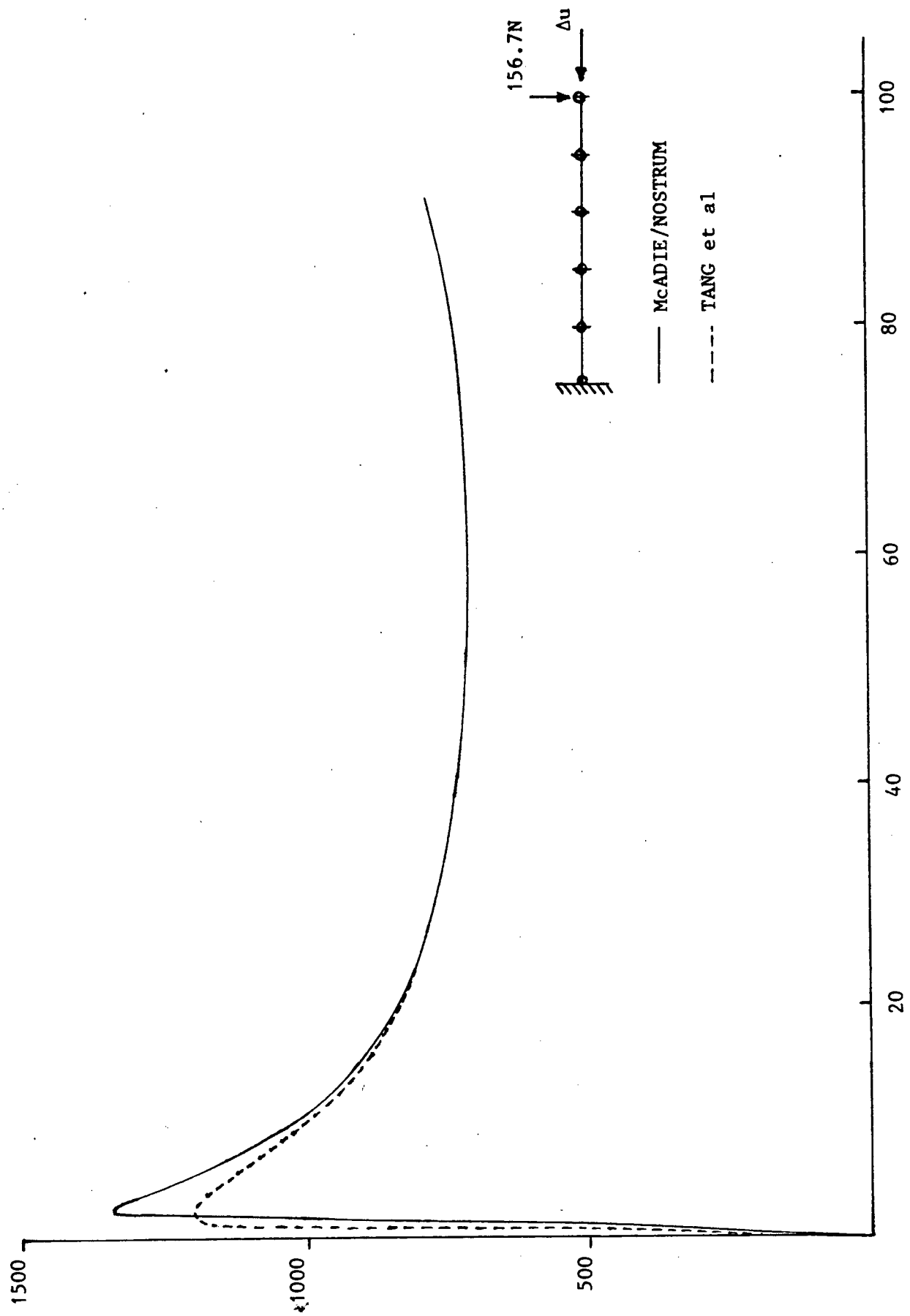

Figure 5.21 Buckling and Postbuckling Response of an Elastic-Plastic Cantilever Beam.

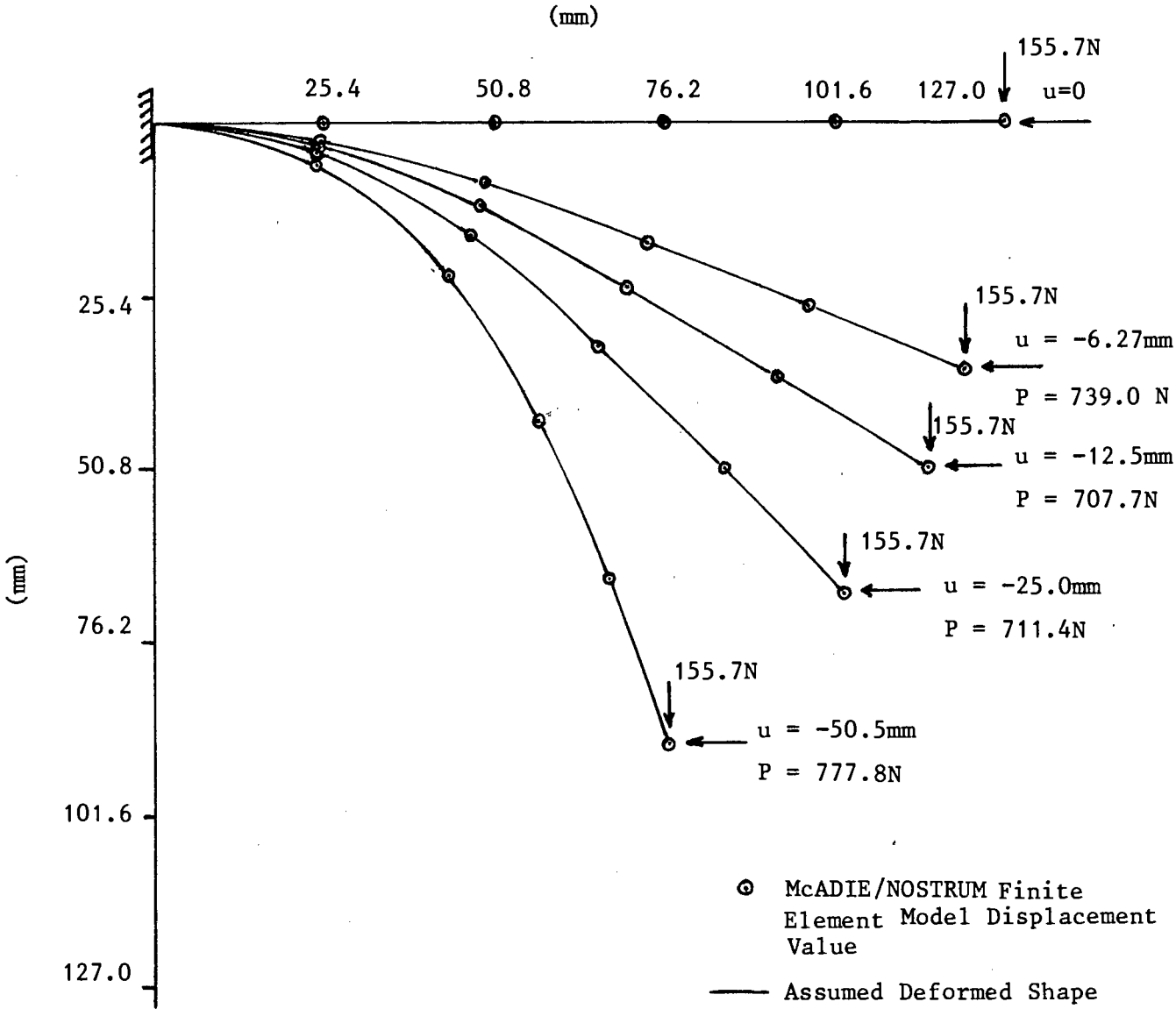

Figure 5.22 Deformed Shapes for Various Amounts of Specified Tip Displacement for the Elastic-Plastic Cantilever Beam.

5.5 Nonlinear Stability Analysis of a Two Storey Frame

The nonlinear stability analysis of the two storey frame analysed by Scholz [6] is carried out. Results obtained by Scholz from laboratory experiments and numerical analysis of the frame are used for comparison purposes. The geometric and material properties given by Scholz are shown in Figure 5.23. In addition, for this analysis it is assumed that no strain hardening occurs ($H' = 0$) and that the shear modulus (G) is calculated using a Poissons ratio of 0.3.

Scholz's numerical elastic buckling load is 1433N. This is calculated from an eigenvalue buckling analysis. His plastic collapse load is calculated as

$$P_p = 5.33 \frac{M_p}{h} ,$$

where:

h is the height of one storey.
M_p is the plastic moment of the section calculated from the plastic collapse load P_{pt} of a simply supported test specimen subject to a load at midspan. M_p is expressed as $M_p = \frac{P_{pt}\ell}{4}$.

Thus the plastic collapse load based on small deflection theory elastic rigid plastic assumption is evaluated as 565N. The inelastic stability failure load obtained in the laboratory experiment of Scholz is 458N. A plot of the experiment result showing the load versus sway response for the first and second stories is given in Figures 5.30 and 5.31 respectively.

In this work two cases are analysed: the elastic large displacement response and the elastic-plastic large displacement response.

5.5.1 Elastic Large Displacement Response

It is only possible to talk about the elastic large displacement response in terms of numerical simulation. If we were to carry out a physical test on the frame, the elastic buckling response would be pre-empted by inelastic material behaviour in the form of plastic "hinge" formation (this is considered in 5.5.2). However, it is useful to analyse the elastic large displacement response in order to validate the numerical algorithms.

The elastic buckling load of the frame given by Scholz [6] is taken as the starting point of this numerical study. Scholz's buckling load of 1433N was calculated via an eigenvalue buckling analysis and it corresponds to the first buckling mode, i.e. a sway type of deformation. In order to trigger this sway mode numerically, a small imperfection in the form of horizontal loads is applied to the frame in addition to the vertical loads shown in Figure 5.23. The applied vertical load (P) versus sway displacement responses for horizontal load imperfections of 0.1P and 0.003P are shown in Figures 5.27 and 5.28 for the first and second storey sways, respectively. Additional analysis with imperfections corresponding to horizontal loads between 0.003P and 0.1P are expected to provide responses which fall inside the envelope defined by the two analyses performed. From the 0.003P imperfection analysis response it is clear that buckling (as defined in section 5.42) occurs at a load very similar to the one given by Scholz, whereas in the 0.1P imperfection analysis the transition from the pre-buckling response to the post-buckling response is not clearly marked. It is also significant to note that the post-buckling behaviour involves an increase in load before a limit load is eventually reached. This limit load is very similar for the two imperfection cases analysed.

In the NOSTRUM calculations, the numerical solution fails to converge at a point close to the limit load which is expected since the analysis is carried out as load controlled. The ABAQUS [20] solutions, which compare very favourably with the present solutions up to the limit load, were obtained using a RIKS [21] type algorithm which considers the loading as an unknown and therefore allows us to trace the post limit load response. The ABAQUS analyses were carried out to compare the present solutions as well as to confirm that the NOSTRUM solutions fail at the limit point. It is clear that the straight line element approximations used in the present nonlinear geometric algorithm give results which compare favourably with the ABAQUS solutions where element rotations are also taken into account in the nonlinear geometric formulation.

Finally, it is worth noting that the 0.1P imperfection NOSTRUM solutions for the two different finite element meshes (twenty-four and thirty-six quadratic elements given in Figures 5.24 and 5.25) give very similar results.

5.5.2 Elastic-Plastic Large Displacement Response

For the elastic-plastic large displacement analysis a twenty-four element mesh was first used. A plot of the load versus first and second storey sway is given in Figures 5.30 and 5.31. The failure load obtained is 525N. This is in fair agreement with both the experimental and numerical solutions of Scholz. Noting the areas of plastification, a refined mesh using smaller elements to model the inelastic zones was used. The refined mesh is illustrated in Figure 5.26. The load versus first and second storey sway responses for this model are given in Figures 5.30 and 5.31 respectively. The failure load obtained using this model is 425N which is very close to the experimental result of Scholz. A plot of an exaggerated displaced shape at plastic collapse for the refined mesh is given in Figure 5.31.

In conclusion it is clear that the nonlinear stability behaviour of a frame structure can be modelled. It is possible to model the elastic-plastic large displacement response reasonably without prior knowledge of the areas of plastification. However, with this prior knowledge the frame can be modelled to give a much better estimate of the failure load.

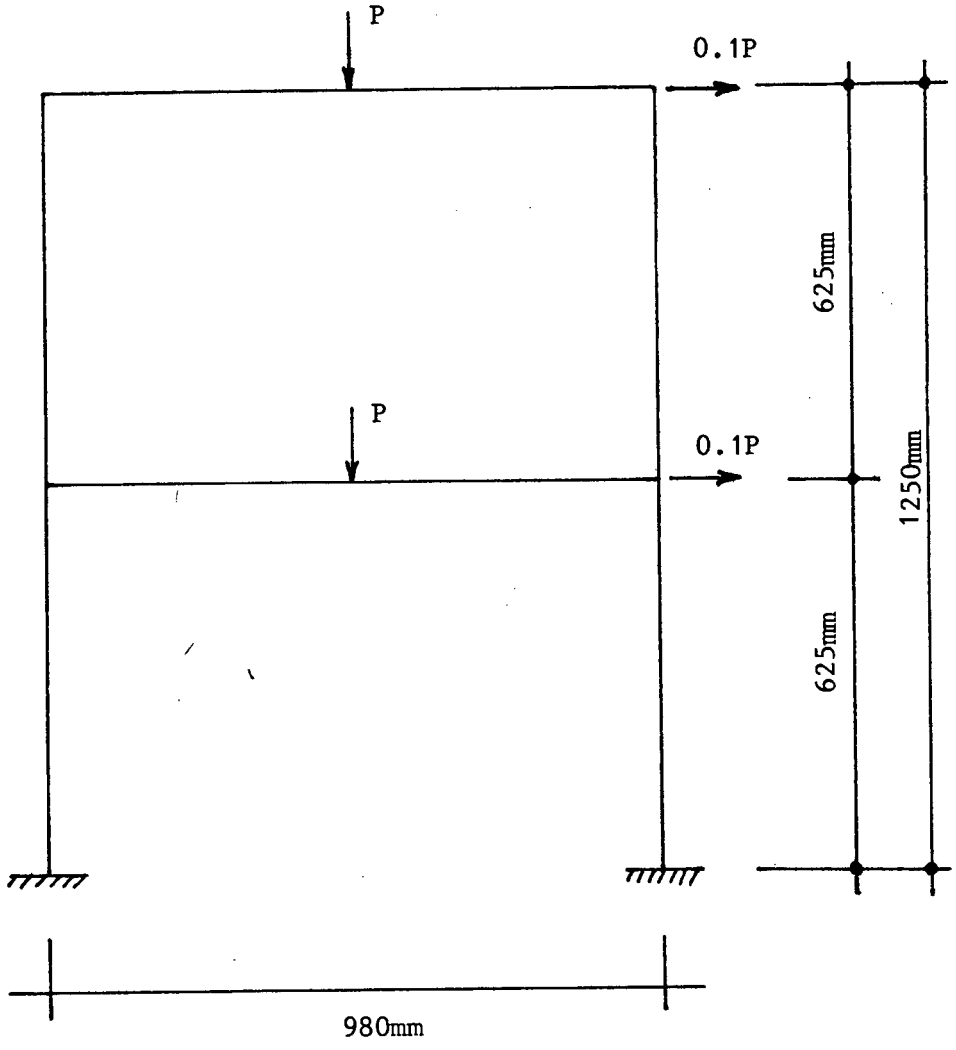

Material Properties

Given [6]:

$I = 522mm^4$

$E = 1.91 \times 10^5 \ N/mm^2$

$\sigma_y = 253.7 \ N/mm^2$

$A = 174mm^2$

Assumed:

$H' = 0$

$G = E/[2(1+\nu)]$

$= 7346.1538 \ N/mm^2$

where $\nu = 0.3$ for steel.

Cross-Section

$b = 29mm$

$d = 6mm$

The cross-section is modelled using 10 layers of equal thickness 0.6mm.

Figure 5.23 Geometric and Materials Properties of the Test Frame.

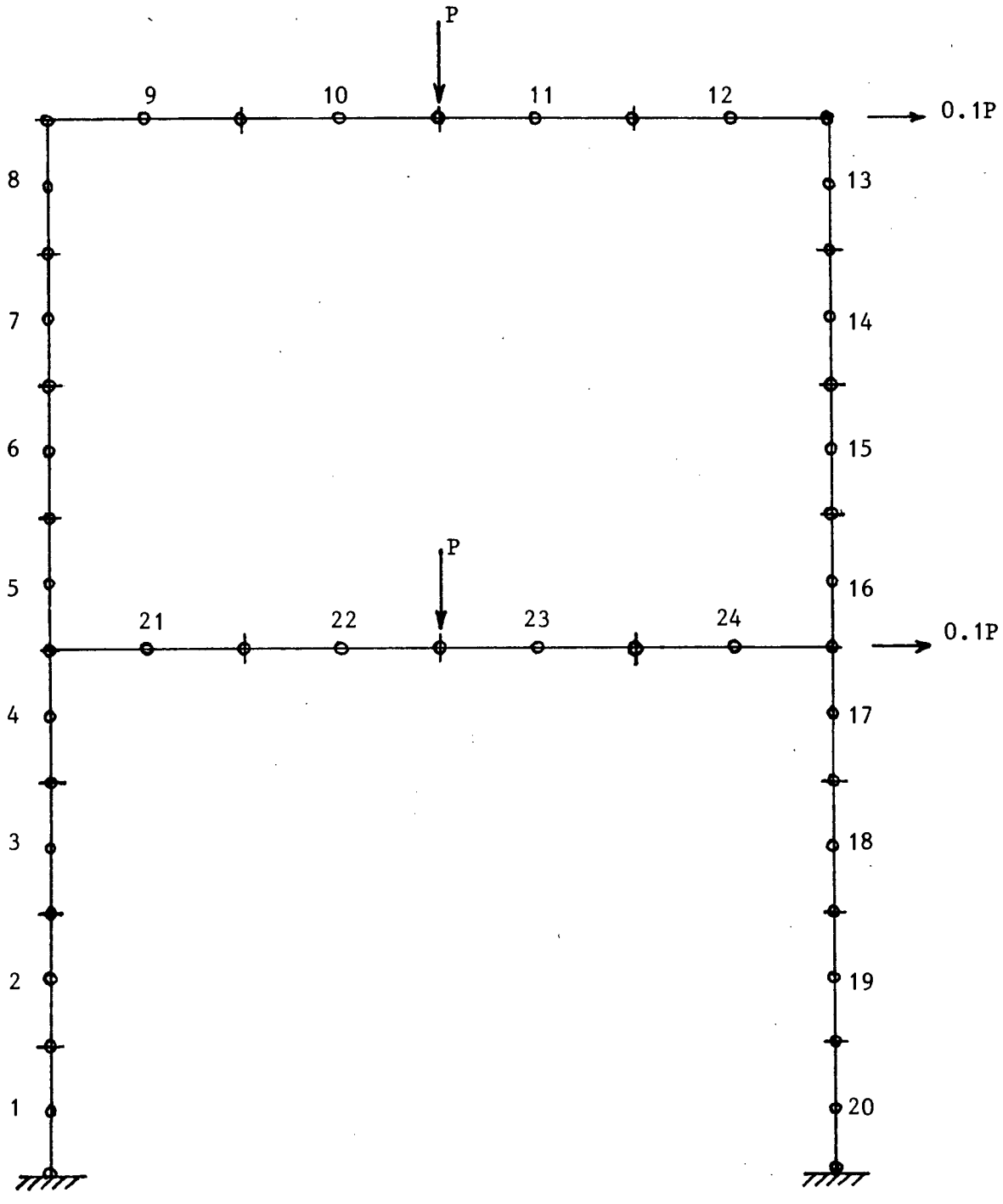

1. Total Number of Nodes in Model is 48
2. 2GP Rule is used for each Element.

MESH NO 1

Figure 5.24 Twenty-Four, Three Noded Element Model.

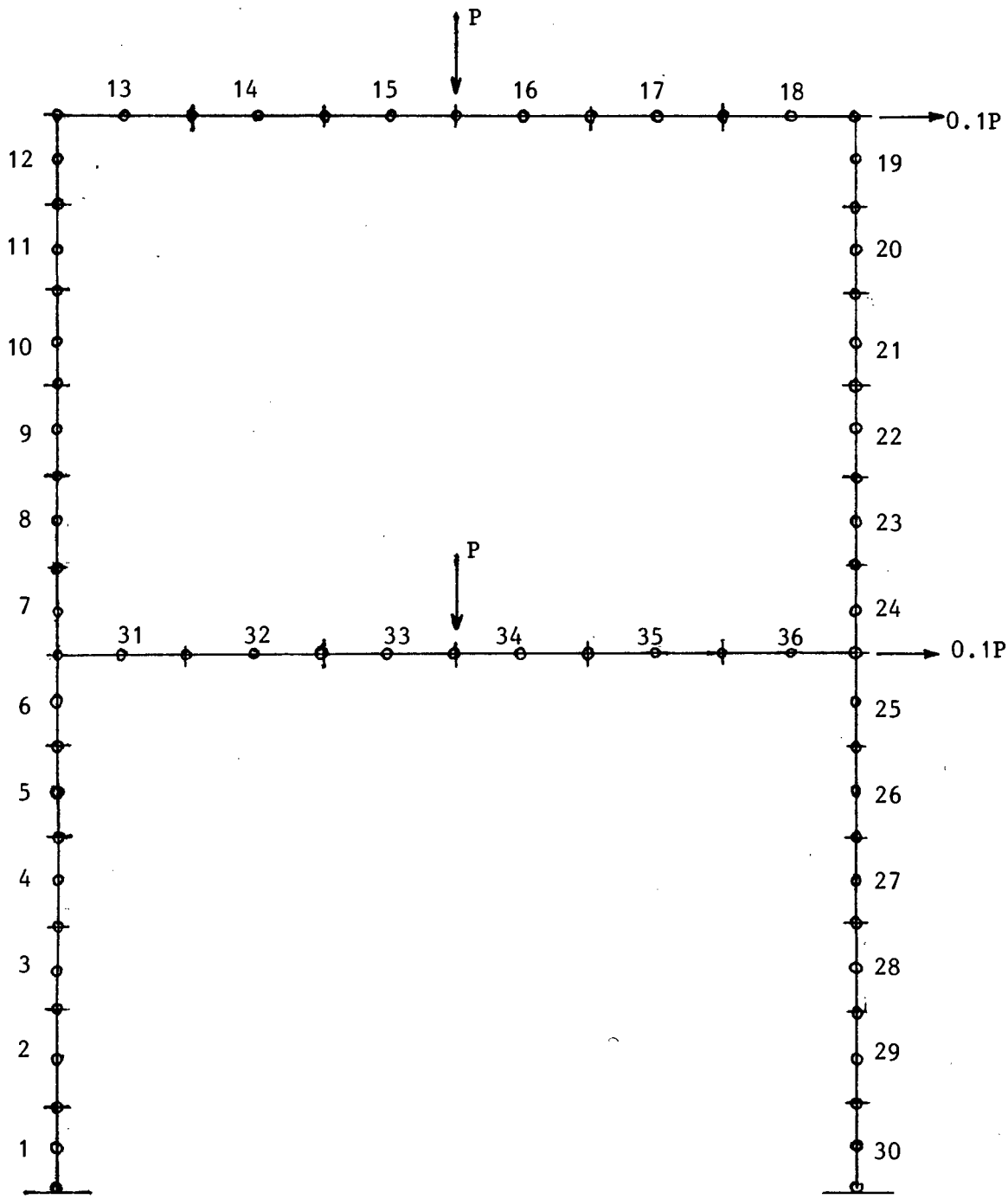

1. Total number of Nodes in Model is 72.

2. 2GP Rule is used for each Element.

MESH NO 2

Figure 5.25 Thirty-Six, Three Noded Element Model.

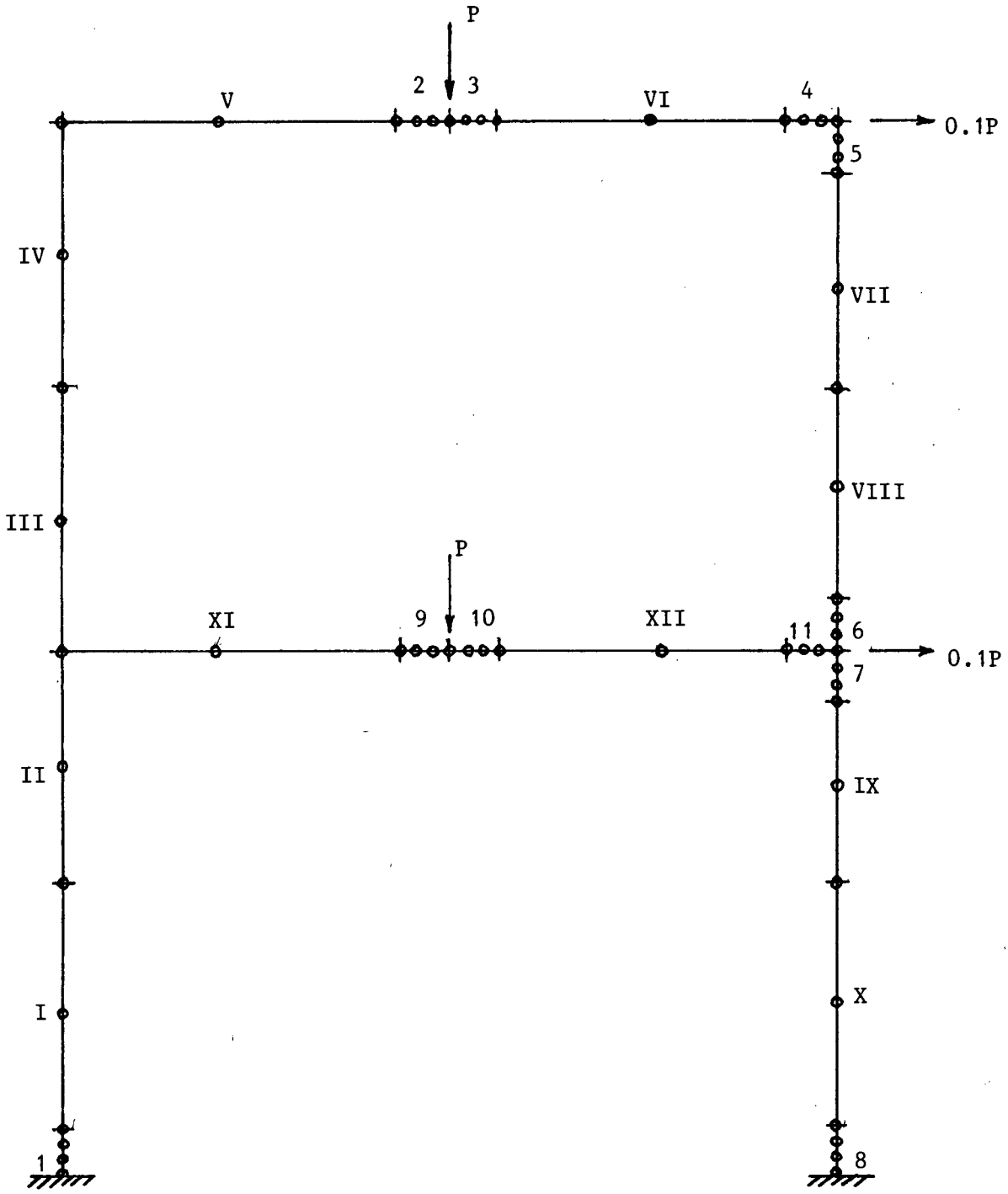

1. Total number of Nodes in 57.

2. 11, Four Noded Elements using 3GP Integration Rule.

3. XII, Three Noded Elements using 2GP Integration Rule.

MESH NO 3

Figure 5.26 Refined Mesh for Accurate Modelling of Elastic-Plastic Stability Behaviour.

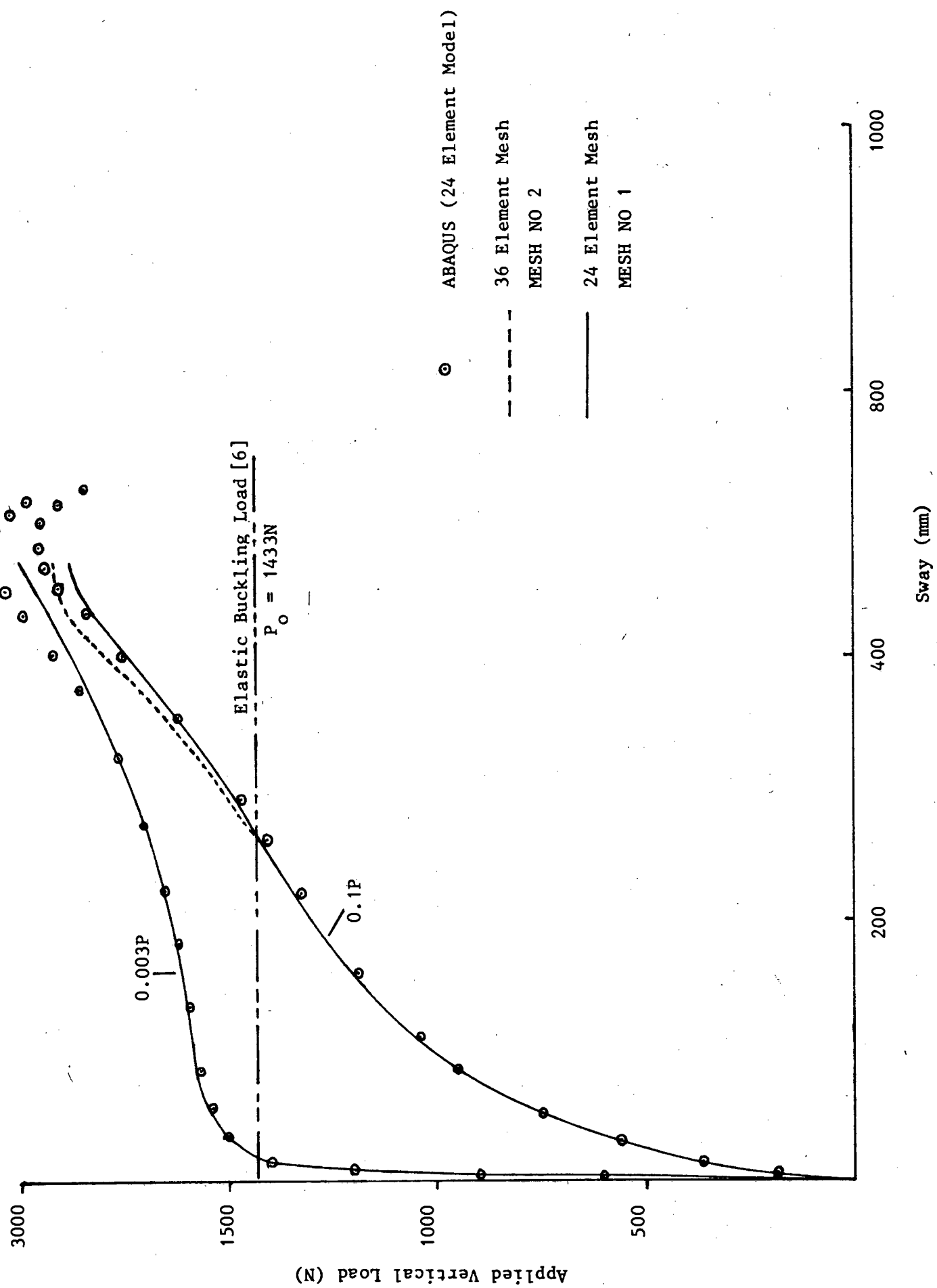

Figure 5.27 First Storey Sway for Elastic Stability Response.

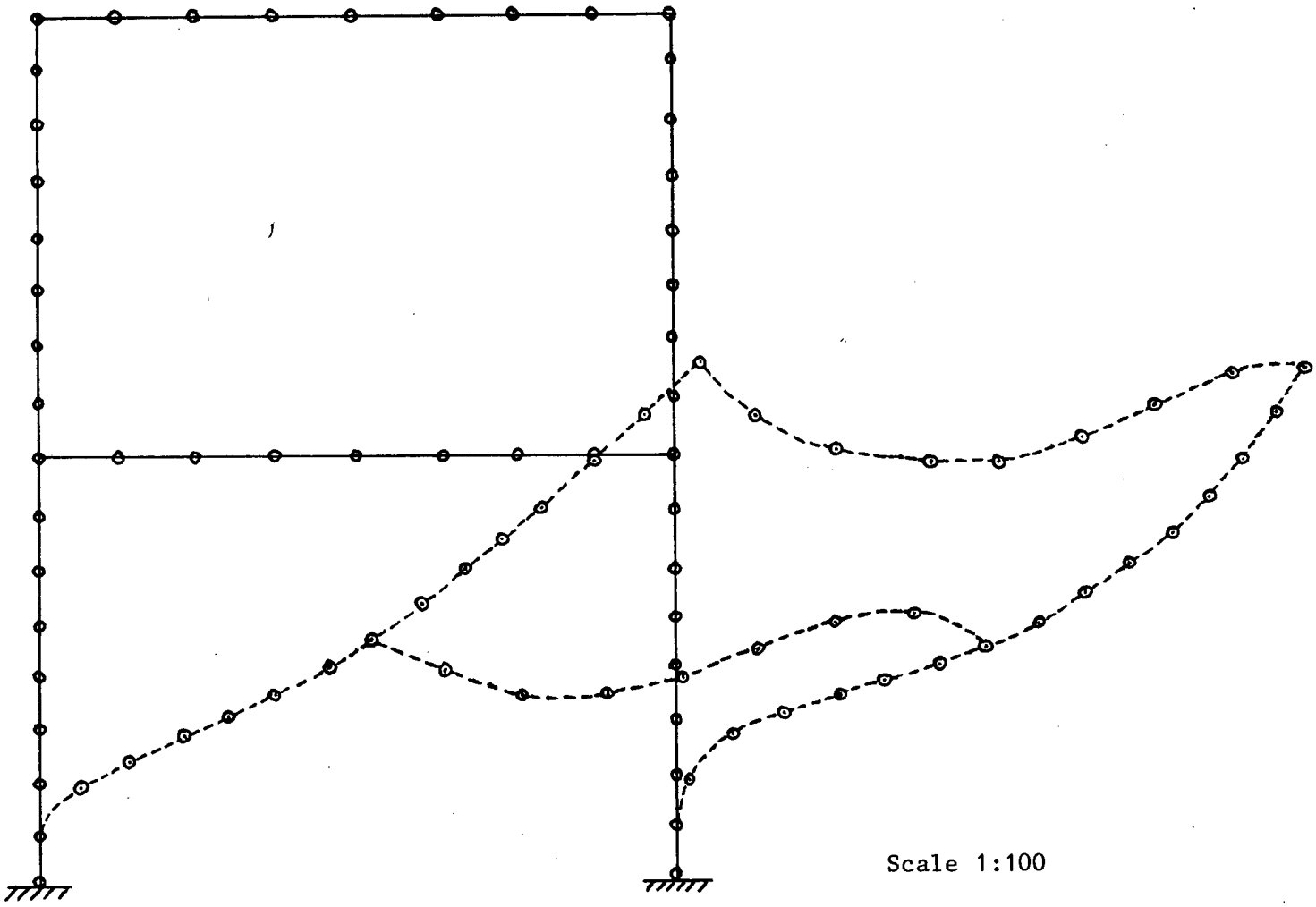

Figure 5.29 Elastic Buckling/Post-Buckling at a Load of 1863N for Mesh No. 1.

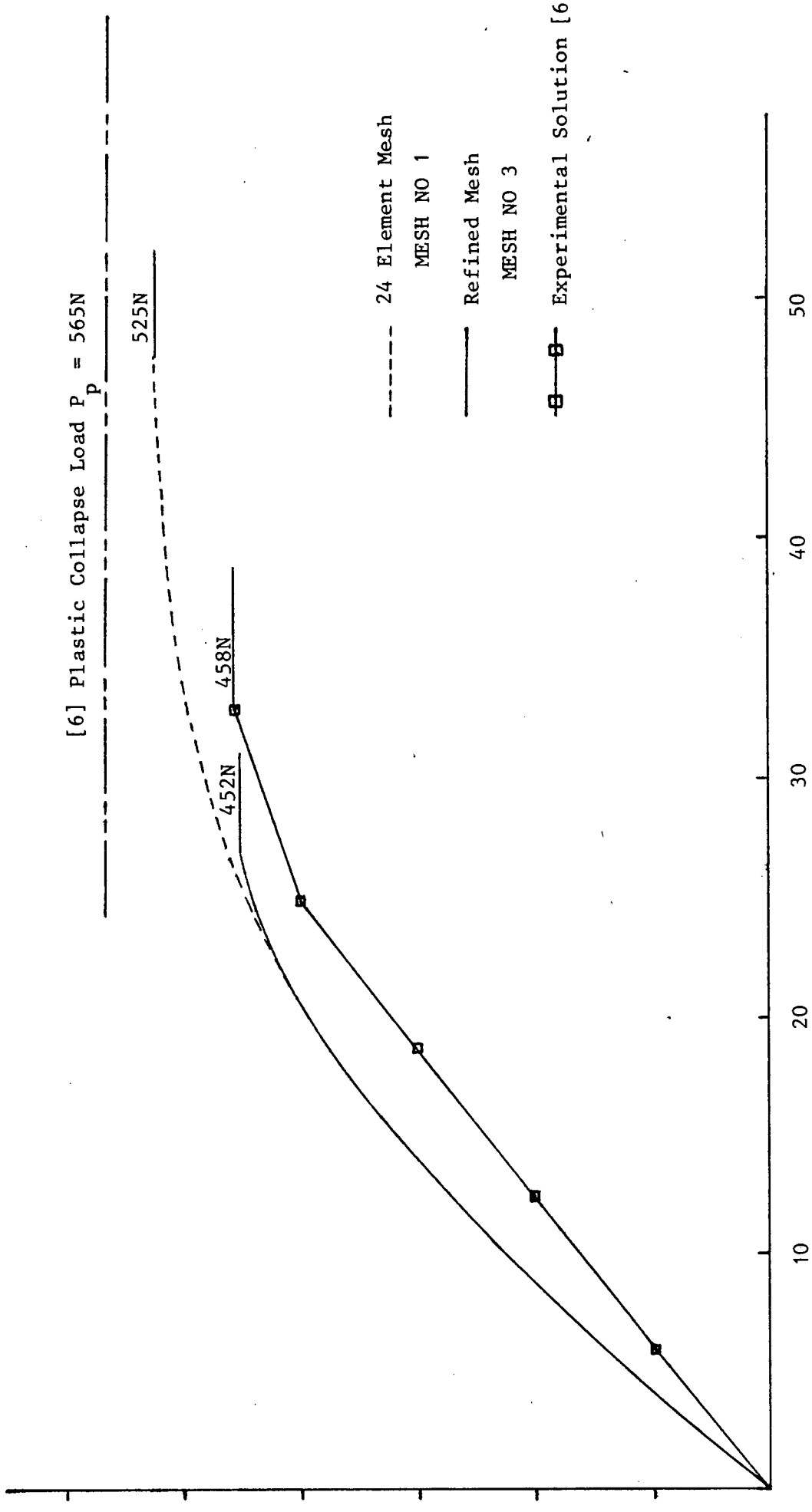

Figure 5.30 First Storey Sway for Elastic-Plastic Stability Response.

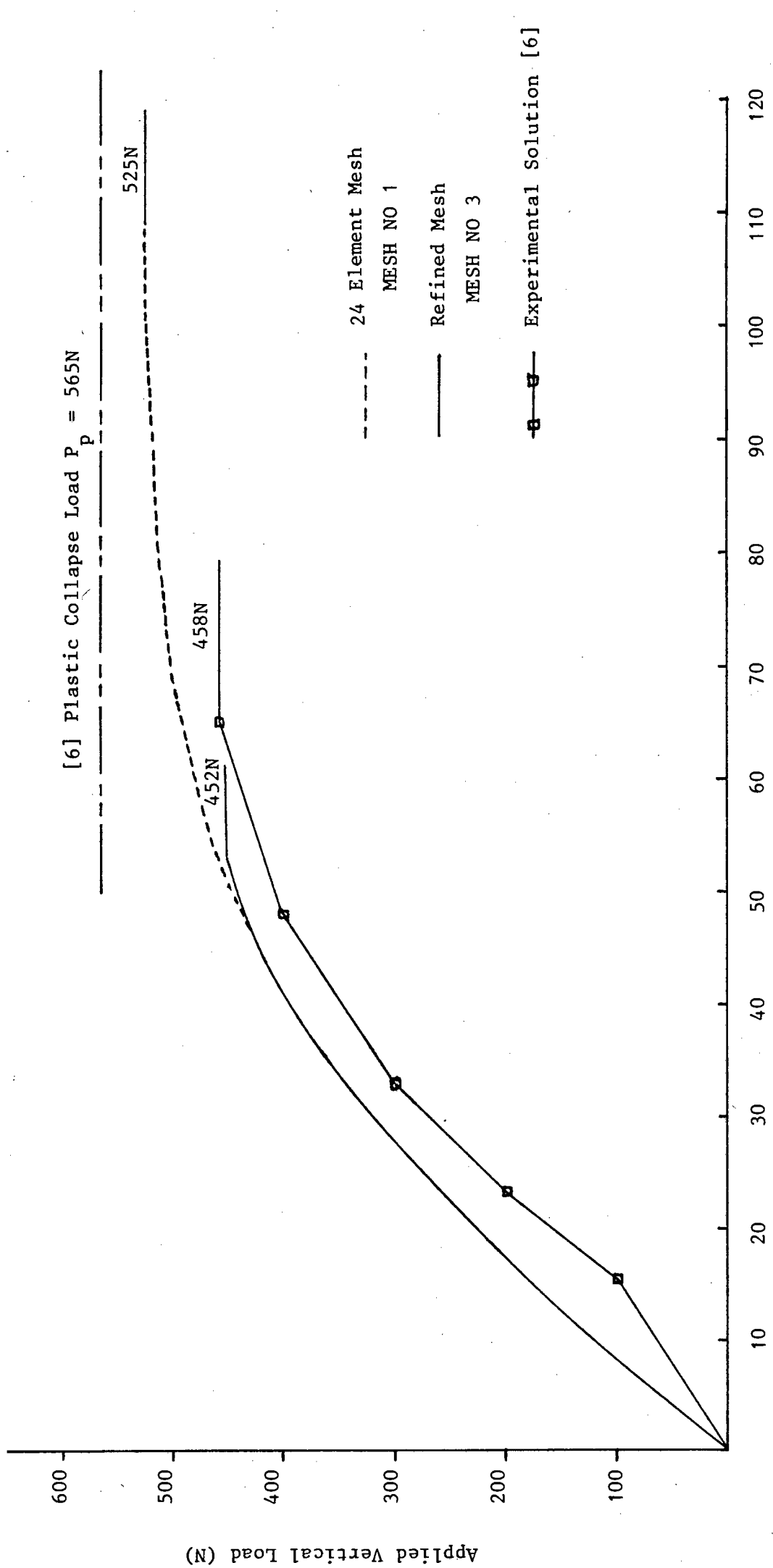

Figure 5.31 Second Storey Sway for Elastic-Plastic Stability Response.

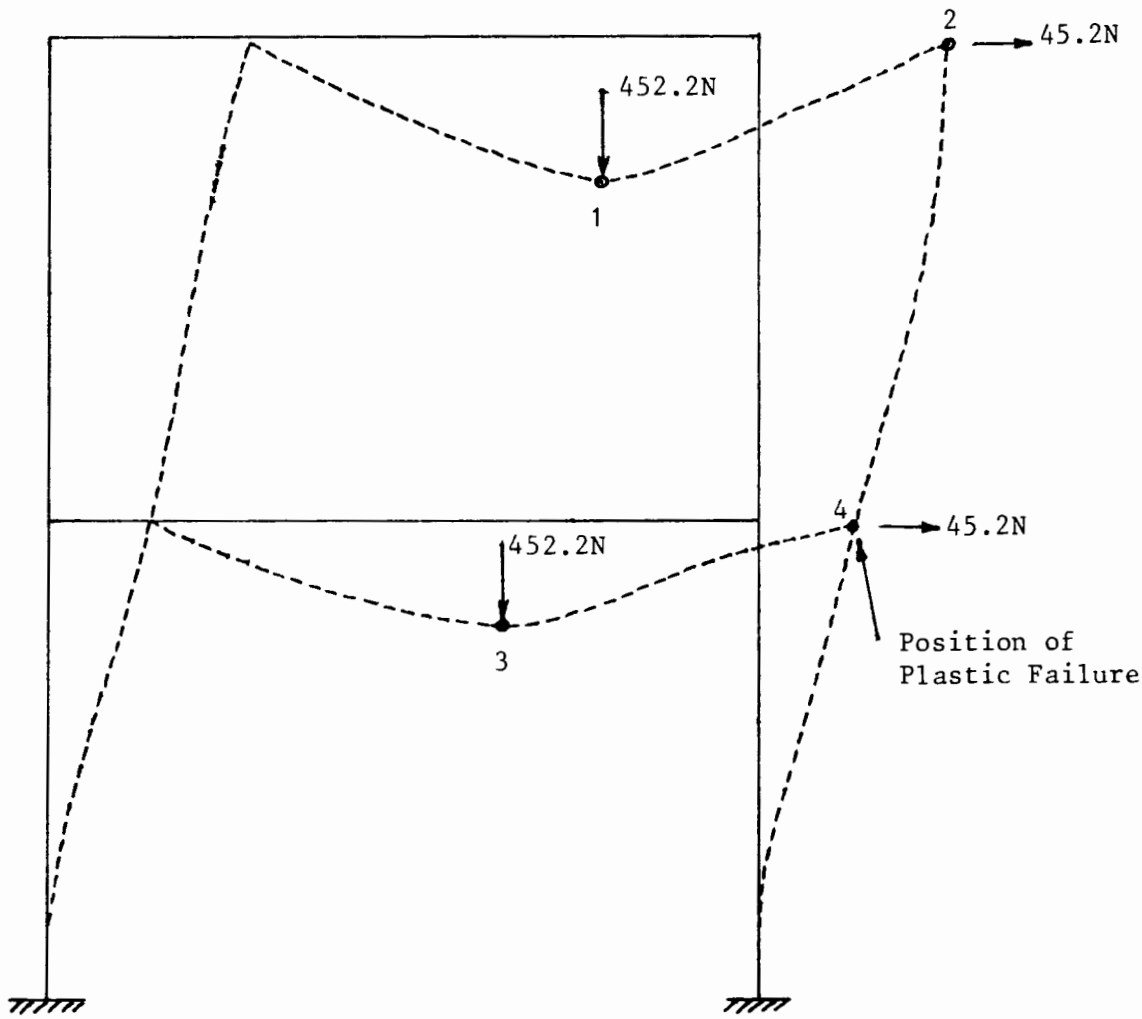

Scale 1:100 (Displacements exaggerated x 5)

1. The Section is Totally Plastic at 4
2. The Section is Partially Plastic at 1, 2 and 3

Figure 5.32 Exaggerated Displaced Shape of Frame at Plastic Collapse for Refined Mesh No. 3.

CHAPTER 6

CONCLUSIONS

The models and algorithms necessary for the nonlinear, stability analysis of frame-type structures were presented and their implementation in the finite element code NOSTRUM was discussed. They include the Timoshenko beam/frame elements with a layered representation of the cross-section, the uniaxial elastic-plastic constitutive models and a simplified updated Lagrangian algorithm to account for the relatively large deformations which take place during inelastic stability analysis.

From the validation of the software developed during the course of this work, it becomes clear that the nonlinear stability analysis of frames can be adequately carried out within the framework of the finite element method. The results obtained with the present models, in general, show good agreement with previously published results. One possible exception is the failure of the present nonlinear geometric model to cope with very large rotations, but this is not considered a limitation in the context of stability analysis for routine design purposes.

The results obtained also indicate that acceptable solutions can be obtained with relatively coarse meshes where no *a priori* knowledge of the behaviour of the structure is used to construct the mesh. On the other hand if some *a priori* knowledge of the structural behaviour is employed to construct the finite element mesh, very accurate predictions are generally attained. In terms of providing guidelines on element choice, it was found that higher order elements generally perform better and reduced Gauss Legendre integration of the element stiffness matrices should be used.

The algorithms developed in this work, together with the modelling guidelines provided, make possible the accurate analysis of nonlinear stability problems in frame structures. As further work, these techniques could be made available in micro computer software for routine frame analysis and design. The main consideration in taking this step would be to optimize the efficiency of the algorithms.

REFERENCES

1. RANKINE, W.J.M., Useful Rules and Tables, London, 1866.

2. MERCHANT, W., "The Failure Load of Rigid Jointed Frameworks as influenced by Stability", The Structural Engineer, 32, 185-190, 1954.

3. WOOD, R.H., "Effective Lengths of Columns in Multi-Storey Buildings", Building Research Establishment (BRE) - Current Paper, CP 85/74, 1974.

4. LU, L.W., "Inelastic Buckling of Steel Frames", J. of the Struct. Div. ASCE, 91, 185-214, 1965.

5. BSI, Draft Standard Specification for the Structural use of Steelwork in Buildings, British Standards Institution (BSI), London, 1977.

6. SCHOLZ, H.E., "A New Multi-Curve Interaction Method for the Plastic Analysis and Design of Unbraced and Partially-Braced Frames", Ph.d. Thesis, University of Witwatersrand, Johannesburg, 1981.

7. HANSA, C. and GRIFFIN, T.B., "Plastic Design of Portal Frames using a Micro Computer", Technical Report No. 43, UCT/CSIR Applied Mechanics Research Unit, University of Cape Town, 1984.

8. CESCOTTO, S., FREY, F. and FONDER, G., "Total and Updated Lagrangian Descriptions in Nonlinear Structural Analysis: A Unified Approach", Energy Methods in Finite Element Analysis, Chpt. 15, 1979.

9. CICHOŃ, C., "Large Displacement In-Plane Analysis of Elastic-Plastic Frames", Comp. and Struct., 19, 737-745, 1984.

10. CHEBL, C. and NEALE, K.W., "A Finite Element Method for Elastic-Plastic Beams and Columns at Large Deflections", Comp. and Struct., 18, 255-261, 1984.

11. SARAN, M., "On the Influence of the Discretization Density in the Nonlinear Analysis of Frames", Comp. Meth. in Appl. Mech. and Eng., 43, 173-180, 1984.

12. KANG, Y.-J. and SCORDELIS, A.C., "Nonlinear Analysis of Prestressed Concrete Frames", Jnl. of the Struct. Div. ASCE, 106, 445-462, 1980.

13. NOSTRUM - "A Finite Element Program for Nonlinear Structural Mechanics", Technical Report 18B, Nonlinear Structural Mechanics Research Unit, University of Cape Town, 1983.

14. OWEN, D.R.S. and HINTON, E., "Finite Elements in Plasticity - Theory and Practice", Pineridge Press, 1980.

15. BATHE, K.-J., "Finite Element Procedures in Engineering Analysis", Prentice-Hall, 1982.

16. HUGHES, T.J.R., M. COHEN and M. HAROUN, "Reduced and Selective Integration Techniques in the Finite Element Analysis of Plates", Nuclear Eng. and Design, 46, 203-222, 1978.

17. MARTIN, J.B., "Plasticity: Fundamentals and General Results", M.I.T. Press, 1975.

18. TANG, S.C., YEUNG, K.S., CHEN, C.T., "On the Tangent Stiffness Matrix in a Convected Coordinate System", Comp. & Struct., 12, 849-856, 1980.

19. BISSHOPP, K.E. and DRUCKER, D.C., "Large Deflection of Cantilever Beams", Q. Appl. Math., III (3), 272-275, 1945.

20. HIBBITT, KARLSON and SORENSEN, INC., "ABAQUS USER'S MANUAL", Version 4, Providence, Rhode Island, USA.

21. HIBBITT, KARLSON and SORENSEN, INC., "ABAQUS THEORETICAL MANUAL", Version 4, Providence, Rhode Island, USA.

APPENDIX A

Courses completed in partial fulfillment of the M.Sc. (Eng) Degree.

THE FOLLOWING COURSES WERE COMPLETED IN
PARTIAL FULFILLMENT OF THE M.Sc. (ENG) DEGREE
AT THE UNIVERSITY OF CAPE TOWN

Course		Date Credited	Credit Value
CE5B3	Structural Dynamics	1984	3
CE5B6	Frame Analysis	1984	2
CE5B7	Introduction to the Theory of Elasticity	1984	2
CE5B8	Plates and Shells	1984	2
CE5B9	Introduction to the Finite Element Method	1984	2
CE5B10	Finite Element Analysis	1984	3
AM343	Numerical Methods	1984	4
AM344	Advanced Numerical Methods	1984	4
		Total	22

Course Credits : 22
Thesis Credits : 20

Total 42

Total credit requirements for the M.Sc. (Eng) Degree : 40

A brief description of the courses are given as follows:-

CE5B3 - STRUCTURAL DYNAMICS

Principles of dynamics. Natural modes of vibration. Energy methods. Forced vibrations; differential equations, normal mode and frequency response methods. Damping. Introduction to earthquake effects.

CE5B6 - FRAME ANALYSIS

The application of the force method of analysis to framed structures of straight and curved members. The stability of equilibrium of framed structures.

CE5B7 - INTRODUCTION TO THE THEORY OF ELASTICITY

Stress, strain, equilibrium, strain displacement relations. Elastic constants. Solutions of simple boundary value problems in plane stress and plane strain.

CE5B8 - PLATES AND SHELLS

An introduction to the elastic theory of plates and shells. Generalised stresses, generalised strains, elastic constitution relations, co-ordinate systems. Analytical solutions of simple problems. Variational methods using Energy Principles. Ritz and Finite Element Methods relating to plates and shells.

CE5B9 - INTRODUCTION TO THE FINITE ELEMENT METHOD

Generalised displacement method of analysis for framed structures. Elastic energy theorems. Basic procedures of the finite element method illustrated for framed structures.

CE5B10 - FINITE ELEMENT ANALYSIS

Plane stress and plane strain elements, plate bending elements, shell elements, three-dimensional elements. Programming of the finite element displacement method. Techniques for equation solving.

AM343 - NUMERICAL METHODS

The theory and practice of numerical methods is dealt with in this course. Topics include: approximate solution of nonlinear equations, interpolation, numerical integration, numerical solution of ordinary differential equations.

AM344 - ADVANCED NUMERICAL METHODS

Solving of partial differential equations using the Galerkin Method with Finite Element approximations.